Aalto University
School of Chemical
Engineering

Pratama Istiadi Guntoro

EXPERIMENTAL INVESTIGATION OF MATTE-SLAG INTERACTIONS IN COPPER FLASH SMELTING

Master's Programme in European Mineral Engineering Course (EMEC)

Master's thesis for the degree of Master of Science in Technology submitted for inspection, Espoo, 28th of July, 2017.

Supervisor Prof. Ari Jokilaakso

Instructor Niko Hellstén, M.Sc.(tech)

Ville Naakka, M.Sc.(tech)

Aalto University
School of Chemical
Engineering

Aalto University, P.O. Box 11000, 00076 AALTO
www.aalto.fi

Abstract of master's thesis

Author: Pratama Istiadi Guntoro

Title: Experimental Investigation of Matte-Slag Interactions in Copper Flash Smelting

Date: 28.7.2017 **Language**: English **Number of pages** 118 + viii

Department: Department of Chemical and Metallurgical Engineering

Major: European Mineral Engineering Course (EMEC)

Thesis Supervisor: Prof. Ari Jokilaakso

Thesis Advisor(s): Niko Hellstén, M.Sc.(tech); Ville Naakka, M.Sc.(tech)

Abstract

Much of the studies related to copper flash smelting focuses on the burner and reaction shaft, while settler part of the furnace is not much evaluated. In the settler part, matte and slag separation take place, and it is critical in determining the final matte grade. In this thesis, a novel experimental procedure is employed to evaluate the time-dependent behavior of matte during settling process.

Copper concentrate and synthetic slag mixture of known SiO_2/Fe ratio was contacted at 1300°C in air atmosphere and inert Argon atmosphere. The ratio corresponded to the actual fluxing ratio of an industrial flash smelting furnace (SiO_2/Fe 0.7 – 1.0). The experiments were carried out at several different reaction times, and subsequently analyzed with SEM-EDS to see the progression of matte-slag interactions and reactions. Additional experiments were also conducted by introducing 5-10 mm sized crushed printed circuit boards (PCB) to the mixture. These additional experiments provide initial analysis regarding how the minor metals in the PCB behave in copper smelting.

A comprehensive and detailed information about the sequential steps leading to the matte settling from the slag are described in the present work**.** It was found that oxygen mass transport in slag is the limiting factor of the overall reaction rate. Separation and settling of matte ceased after 10 minutes, while continuous feeding of air leads to total loss of matte to the slag phase after just 5 minutes, with Cu content in the matte reaching peak level after 2-3 minutes. Precious metals in the PCB mostly distributed to the matte to create a Cu-Fe alloy phase distributed rather randomly within the matte. The novel procedure employed in the present work is generally sufficient to qualitatively elaborate the matte-slag separation process, but not quantitatively.

Keywords: matte settling, matte separation, time-dependent behaviour, PCB smelting

Acknowledgements

This Master's Thesis was conducted in the Department of Chemical and Metallurgical Engineering at Aalto University School of Chemical Engineering in Otaniemi, Espoo.

I would like to thank my supervisor Professor Ari Jokilaakso for the complete guidance and support during construction of this thesis. I would also like to thank Niko Hellstén, M.Sc. for the guidance and assistance in both experimental and literature work of my thesis. Many thanks are also addressed to Boliden Harjavalta Oy for providing financial support for this thesis, and especially to Petri Latostenmaa, M.Sc. and Ville Naakka, M.Sc. for providing guidance and feedback from the industry.

My gratitude are also extended to the people that helped me during the experimental and analysis work of this thesis; Aleksi Kekkonen for helping with the sample preparation and experiments; Dmitry Sukhomlinov, Ph.D. for helping with the slag synthesis; Lassi Klemettinen, M.Sc. and Imam Santoso, M.Sc. for helping with the SEM-EDS analysis and phase diagrams; as well as many other people in both Metallurgical Thermodynamics Modelling Research Group and Metallurgy Research Group.

Last but not least, I would like to express my highest gratitude to my family and partner for their everlasting support during my journey in this master's program.

Espoo, 28 July 2017

Pratama Istiadi Guntoro

Table of Contents

List of Figures

List of Tables

1. Introduction

Finding applications in many fields, copper is unarguably one of the most important non-ferrous metals in the world. It is used mainly in electrical equipment wirings and motors, primarily because it has high heat and electrical conductivity. Copper is primarily found in sulfide minerals such as Chalcopyrite ($CuFeS_2$) and Chalcocite (Cu_2S). Other than that, copper also exists in oxidized minerals such as Azurite {$2CuCO_3.Cu(OH)_2$} and Cuprite (Cu_2O). Several secondary copper sources, such as scrap copper and copper alloys, also exist. Additionally, the re-melting of scrap produced from copper manufacturing also adds to the number of secondary copper resources.

Around 80% of the world copper is processed through the pyrometallurgical route, where copper sulfide ores are concentrated, smelted and refined. Much work have been done in studying the smelting process, as it is the core in pyrometallurgical route of copper production. These works mainly aim to enhance the productivity and efficiency of the copper smelting; producing high quality copper matte while consuming minimum energy.

One of the most prominent technologies used in copper smelting is the flash smelting process, which accounts for around 50% of the world's primary copper production. While the burner and reaction shaft parts of the flash smelting furnace has been studied extensively, less attention has been paid to the settler part of the furnace, where the copper matte separates from the slag phase by settling.

The main focus of this thesis is the settler part, especially the area underneath the reaction shaft. In this area, most of the reactions, interactions, and separations between matte and slag take place. It holds a critical role in the flash smelting process, as it determines the grade of the matte produced. The reaction sequences and limiting factors in this process will be evaluated in this thesis, using a novel experimental procedure. Additionally, the effect of the addition of Printed Circuit Board (PCB) scrap is also evaluated. It is expected that this thesis will form a good basis for continuing research work in copper flash smelting, especially work related to the settler part of flash smelting.

1.1. Objectives

The thesis has several objectives as follows:

- Evaluate, both qualitatively and quantitatively, the employed experimental and analytical procedure in producing accurate and reliable results
- Elaborate the reaction sequences and limiting factors involved in the settling process of copper matte in slag.
- Evaluate the time-dependent behaviour of the major elements in matte during settling and separation process.
- Provide an initial idea regarding behaviour of printed circuit board scrap in contact with molten slag-matte at high temperature.

PART I: LITERATURE REVIEW

2. Overview of Copper Smelting Processes

Copper smelting process is the key part in the pyrometallurgical route of copper production. The process utilizes oxidizing agent such as O_2 to oxidize iron sulfide into iron oxides in the form of slag, leaving high concentration copper behind in the matte phase. The reaction of this process is shown in reaction (1)

$$CuFeS_2 + O_2 \rightarrow (Cu, Fe, S)_{(matte)} + FeO_{(slag)} + SO_2 \quad (1)$$

The copper matte produced is the main product of the smelting process, with slag as a secondary product. A competition exists in the oxidation reaction, as the copper can be oxidized as well to the slag phase in the form of Cu_2O. The phenomena occurs mainly because of the over-feeding of the oxygen gas. This could lead to lower recovery of copper in the smelting process, with copper ending in the slag phase through reaction (2)

$$Cu_2S_{(matte)} + 1.5O_2 \rightarrow Cu_2O_{(slag)} + SO_2 \quad (2)$$

Controlling the oxygen feed is vital to achieve a balanced matte with reasonably high grade, while also achieving good recovery of copper. Asides from that, the copper could end up in the slag due to high activity of FeO in the slag phase, leading to the following substitution reaction:

$$FeO_{(slag)} + Cu_2S_{(matte)} \leftrightarrow FeS_{(matte)} + Cu_2O_{(slag)} \quad (3)$$

High activity of FeO also leads to formation of magnetite through reaction (4)

$$FeO + 0.5O_2 \rightarrow Fe_3O_{4(s)} \quad (4)$$

The presence of unreacted solid magnetite is unwanted, since matte or metal droplets can be attached to this magnetite during the settling process, which then leads to loss of recovery (Toguri, 1992). Magnetite is also known to alter the slag fluidity, making it harder to handle.

In order to remove unreacted magnetite solids, many smelters make use of silicate flux (SiO_2), which will lower the activity of FeO in the slag through reaction (5) (Schlesinger, 2011)

$$FeO + SiO_2 \rightarrow FeO - SiO_{2(slag)} \quad (5)$$

Again, controlling the amount of the flux to the smelting process is necessary, as overfeeding may result in some unwanted phenomena to occur in the smelting process (Schlesinger, 2011). This is because SiO_2 tends to polymerize when it is melted, therefore increasing the viscosity of the slag. A highly viscous slag is absolutely unwanted as it poses challenges to slag handling processes and it will more likely entrap copper during the matte settling process. Moreover, SiO_2, as an acidic oxide, will have a lower solubility to slag compared to other acidic oxide impurity found in the matte, such as As_2O_3, Bi_2O_3, and Sb_2O_3. Therefore, most of these impurities will not dissolve into the slag and remain in the matte. Basic oxide fluxes such as CaO and MgO are often added to the smelting furnace in order to break the silicate network polymers and promote more efficient metal and silicate separation (Piatak and Scal, 2010), as well as increasing the solubility of acidic oxide impurities into slag (Mulenshi, 2015).

In general, smelting of copper is a very delicate process, requiring balanced feeding of materials to achieve good recovery of copper whilst maintaining the product grade as well. To simplify, a smelting process will have three sequences (Schlesinger, 2011):

1. Contact process of the oxygen enriched air with the copper concentrate and flux in a high temperature environment, generally ranging from 800 – 1300^{o}C (Potysz, et al. 2015). This process will lead to exothermic reaction described by equation (1), producing molten products.
2. The produced matte then settles through the silicate slag layer, as the matte is heavier than slag. During this settling process, FeS that has not been oxidized during the first sequences will further be oxidized into the slag through the reverse reaction of equation (3). This process will also decrease the amount of copper in the slag phase, increasing the copper recovery. As discussed above, the settling process is quite an intricate process, it is affected by many parameters such as slag acidity, composition, viscosity, as well as temperature. Several smelting furnaces have a dedicated settling area, so that the settling process could be enhanced with minimal interferences.

3. Periodical tapping of matte and slag is done through separate holes in the smelting furnace. This process is mostly controlled by setting height targets for slag and matte layers, respectively, so that matte and slag could be separately tapped from the tapping holes.

To this date, several matte smelting technologies have been developed around the world. Different processes have their own advantages and disadvantages, and copper smelters have their own preferences in choosing such technology.

2.1. Flash Smelting

The flash smelting is the youngest industrially established smelting technology. The technology was developed by Outokumpu, in response to the electrical energy shortage in Finland at the 1940s. About 50% of world primary copper production and 30% of world nickel production is done by the flash smelting technology (Firdu, 2009). The technology offers a better fuel efficiency and promotes an environmentally friendly process (Sridhar, 1997). The smelting furnace is shown in Figure 1.

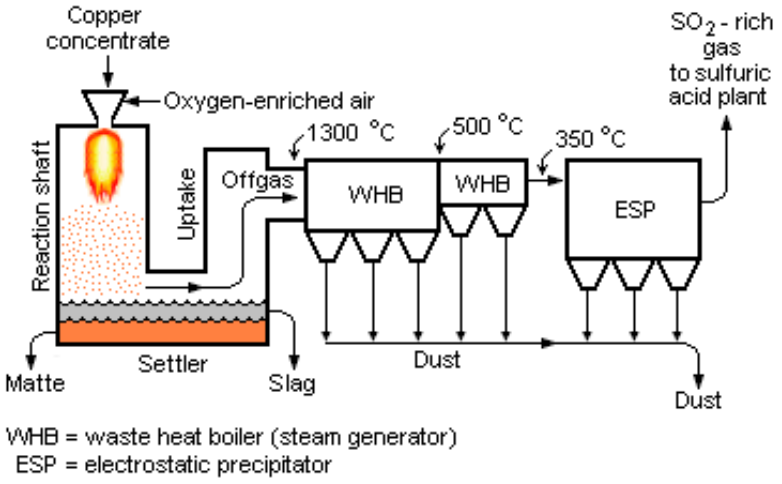

Figure 1. Outotec Copper Flash Smelting (Beychok, 2009)

The contact process between the copper concentrate, flux, and oxygen happen in the reaction shaft in a time less than second (hence the name “flash smelting”). Therefore, concentrates and gases are mixed prior injection to the reaction shaft to ensure good reaction process. Oxygen enriched air is used as well to enhance the reaction kinetics. The flash smelting process requires fine particle size, less than 100 µm (Vaarno et al., 2003). The reaction progresses rapidly and produces a substantial amount of heat that leads to the melting of the particles. These molten solid progress downward from the reaction

shaft to the settler, creating two immiscible layers of matte and slag, as shown in Figure 1. These slag and matte phases are tapped periodically through separate tap holes. The off gas, mainly consisting of SO_2 and N_2, flows through the waste heat boiler (WHB), in order to recover heat generated in the reactions in the form of steam. Due to the finer particle size, there will be around 5% of dust losses to the off gas, hence the use of electrostatic precipitator to collect the dusts and recycle them back to the furnace feed system.

Most of copper smelters use flash smelting in a high Cu grade matte, thereby sacrificing the copper recovery, mainly due to following reasons (Schlesinger *et al*, 2011):

- High matte grade production leads to increased heat generation, therefore reducing fuel consumption
- Less burden for the subsequent converting process, as the matte will contain lower amount of Fe and S
- Increased SO_2 in the off gas, thereby lowering gas treatment costs (a very dilute SO_2 containing gas will be very difficult to process)
- Nevertheless, the slag is often subjected to further slag cleaning process, which can further recover the copper from the slag.

2.2. Reverberatory Smelting

Reverberatory furnace is a fossil fuel heated hearth furnace that smelts Cu-Fe-S concentrates to produce molten matte and molten iron-silicate slag (Davenport *et al,* 2002). The technology produces slag with 0.6 to 0.8% Cu, which is subsequently discarded. This technology was dominant throughout the 20th century, however its use began to decline after the development of flash smelting and other environmentally friendly and economically better smelting technologies. Overview of this furnace is shown in Figure 2.

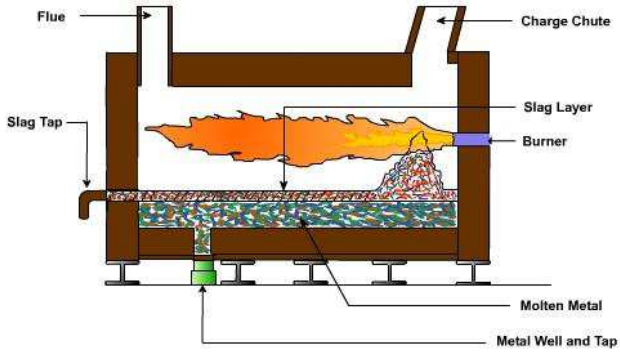

Figure 2. Reverberatory Furnace (Gupta, 2014)

Reverberatory smelting operates at continuous mode. The burner is continuously fired, molten matte and slag are also continuously tapped from the furnace. Heat of the smelting is supplied by the fossil fuel burners, as shown in Figure 2. Off gases are also continuously withdrawn from the flute, in which it then flows through waste heat boiler and electrostatic precipitator before discharging to the atmosphere. Reverberatory furnaces can be used as well to treat converter slags. In a typical operation, slag enters the furnace at 6-8% Cu, and leaves the furnace at 0.6-0.8% of Cu.

Several disadvantages of reverberatory furnace made its use to decline rapidly. Some of the main reasons are (Davenport *et al*, 2002):

- The smelting technology produces off gas with low SO_2 content, less than 2% volume. This makes an efficient SO_2 removal from the off gas unachievable and unfeasible.
- It also use a considerable amount of energy compared to its successor technologies. This is mainly because the technology mostly melts the concentrate, rather than oxidizes it, so that it makes a little use of heat generated by the exothermic oxidation reaction in equation (1). This is also the main reason why there are only a little amount of SO_2 produced in this technology, since only small amount of S is oxidized into the SO_2 gas.

2.3. Electric Smelting

The electric smelting furnace is an electrically heated hearth furnace which basically performs the same functions as the reverberatory furnace (Davenport *et al*, 2002). The electric smelting requires dried or roasted Cu-Fe-S concentrates as feed, and produces

molten matte with 50-60% of Cu, molten slag, and the off gas. Similarly with the reverberatory furnace, it can also treat converter slags.

The heat in the electrical smelting process is provided by the six self-baking carbon (Soderberg) electrodes. When the electrode is contacted with the slag layer, an electrical circuit is formed, in which an electrical current is passed through this circuit. Heat is generated due to the resistance provided by the slag, which is then used for the smelting process. The dry roasted concentrate will first spread out as a layer on top of the slag, then it heats up and melts. The melt then starts to settle through the slag layer, forming two separate layers of matte and slag, which then can be tapped periodically.

Electric furnaces have their own advantages and disadvantages. Their advantages over the previous reverberatory furnace are:

- Smaller amount of off gas, mainly due to practically no combustion in the furnace (heat is provided by electricity)
- Reasonable amount of SO_2 content in the off gas (5% volume of SO_2), which all and all combined with the first point makes the technology cheaper in terms of the gas handling
- Electricity is seen as more reliable energy source than the fossil fuel.

Still, compared to the flash smelting, electric furnace does not perform well, as it has several disadvantages:

- The technology does not use much of the heat generated from the oxidation reaction of Fe and S.
- Compared to the flash smelting, the technology produces less SO_2 in the off gas. This leads to preference of flash smelting over the electric smelting

3. Matte – Slag Interactions and Formations during Settling Process

The formation reactions of matte from chalcopyrite oxidation, and its separation from slag comprises of several steps, which are (Fagerlund, 2000):

1. Copper concentrate is introduced into the burner, where the fine particles heat and ignite immediately. This makes fast reactions possible. Chalcopyrite will lose its labile sulfur, and transform into an intermediate solid solution of bornite (Cu_5FeS_4) through reaction 6 and finally into Cu_2S chalcocite through reaction 7 (Ahokainen and Jokilaakso, 1998). It is observed that bigger particles will fragment into smaller particles because of the explosive discharge caused by the pressure exerted by the molten sulfidic core to the outer solid oxide crust of the particles (Jokilaakso *et al,* 1991).

$$5CuFeS_2 \rightarrow Cu_5FeS_4 + 4Fe_{1-x}S + 4\,x\,Fe + 2S \quad (6)$$

$$2Cu_5FeS_4 + O_2 \rightarrow 5Cu_2S + 2FeS + SO_2 \quad (7)$$

2. During the oxidation, sulfur and iron will be preferentially oxidized. Sulfur will be oxidized into SO_2 gas, while iron will be oxidized into iron oxide in the slag phase. Some part of the iron oxide that is insoluble in the molten sulfide phase will precipitate into magnetite (Fe_3O_4) particles. Magnetite particles can also be formed due to the oxidation of the iron oxide through reaction (4). Ahokainen and Jokilaakso (1998) also proposed several reaction mechanisms of magnetite formation, described in reactions 8 and 9.

$$3Fe + 2O_2 \rightarrow Fe_3O_4 \quad (8)$$

$$3FeS + 5O_2 \rightarrow Fe_3O_4 + 3SO_2 \quad (9)$$

3. The process continues in the settler region, whereas suspended particles are collected onto the molten slag. This process will mix together reaction products and the silica flux, and further desulfurization reaction of the concentrate as well as magnetite reduction is done, through the following reaction :

$$3Fe_3O_{4(s)} + FeS_{(matte)} + 5SiO_{2(s)} \rightarrow 5(Fe_2SiO_4)_{slag} + SO_{2(g)} \quad (10)$$

and/or

$$3Fe_3O_{4(s)} + FeS_{(matte)} \rightarrow 10(FeO)_{slag} + SO_{2(g)} \quad (11)$$

If the sulfur activity is at high level, reaction (12) must also be taken into consideration

$$2Fe_3O_{4(s)} + S_{(matte)} + 3SiO_{2(s)} \rightarrow 3(Fe_2SiO_4)_{slag} + SO_{2(g)} \quad (12)$$

4. The resulting Cu_2S from step one can be oxidized into Cu_2O through reaction (2), in which it is dissolved into the slag. Taking this into account, further reactions between matte and slag may proceed, which are described in the following reactions:

$$FeS_{(matte)} + Cu_2O_{(slag)} + 0.5SiO_{2(s)} \leftrightarrow Cu_2S_{(matte)} + 0.5(Fe_2SiO_4)_{slag} \quad (13)$$

$$FeS_{(matte)} + 3Cu_2O_{(slag)} + 0.5SiO_{2(s)} \leftrightarrow 6Cu_{(l)} + 0.5(Fe_2SiO_4)_{slag} + SO_{2(g)} \quad (14)$$

$$Cu_2S_{(matte)} + 2Cu_2O_{(slag)} \leftrightarrow 6Cu_{(l)} + SO_{2(g)} \quad (15)$$

5. The formed matte droplets will go through a coagulation process, where the coagulated matte droplets will settle to the bottom of the furnace through the slag layer, mainly driven by gravitational force.

Taking a closer look to the aforementioned steps in the settling process, it can be concluded that a matte droplet can be chemically dissolved into the slag phase by matte slag interaction reactions in the fourth step, or become mechanically entrained in the slag phase (primarily during the last step).

3.1. Experimental Studies Related to Matte-Slag Reactions and Interactions

Early work aiming to better understand the whole matte formation, settling and separation from slag was done by Fagerlund (2000). Laboratory scale experiments were done in order to analyze the effect of matte copper content to the matte forming reactions, as well as matte droplet's coagulation and settling through the slag layer. Various degrees of oxidized chalcopyrite (OCHP), industrial Cu Matte (MGIM), and saturated cuprous sulphide (SHM) were used, alongside with iron silicate slag and silicate sand. The silicate sand was charged to bring the slag close to and above silica saturation point. The smelting reaction was conducted in a crucible placed in a fused quartz ampoule,

shown in Figure 3. He used three different methods, each method corresponding to different analysis of the smelting process.

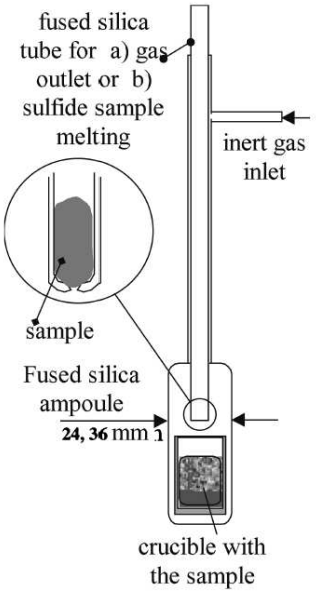

Figure 3. Fused Quartz Ampoule (Fagerlund, 2000)

The first method involved introducing the mixture of various slags and chalcopyrite in a crucible placed in the quartz ampoule to the furnace at 1325°C in an inert N_2 or Ar atmosphere, and evaluating the reaction progression through time. The sampling was done by dipping copper rod onto the surface of the samples, or quenching the whole ampoule with water. The specimen was then analyzed with Scanning Electron Microscope – Energy Dispersive X-ray Spectroscopy (SEM-EDS) and Light Optical Microscope (LOM). Second method was slightly different: matte powder was placed in a fused silica tube above the slag containing crucible. The fused silica tube had a small orifice around 1 mm at the bottom. The system was heated in the furnace so that both the matte inside the fused silica tube and the slag inside the crucible were melted. The idea behind this method was that surface tension would hold the matte inside the fused silica tube, and only after pressurized gas was charged through the silica tube, the matte was introduced onto the slag and the subsequent reaction was started. After a certain time lapse, the whole ampoule was taken out and quenched, after which the specimens were studied using LOM and SEM-EDS. The third method is practically the same with the second one, differing only so that samples are not taken out periodically, rather analyzed visually using x-ray

transmission image system, similar to that of Toguri (1992), is shown in Figure 4. Only after the reaction approached equilibrium, the samples were taken out and studied.

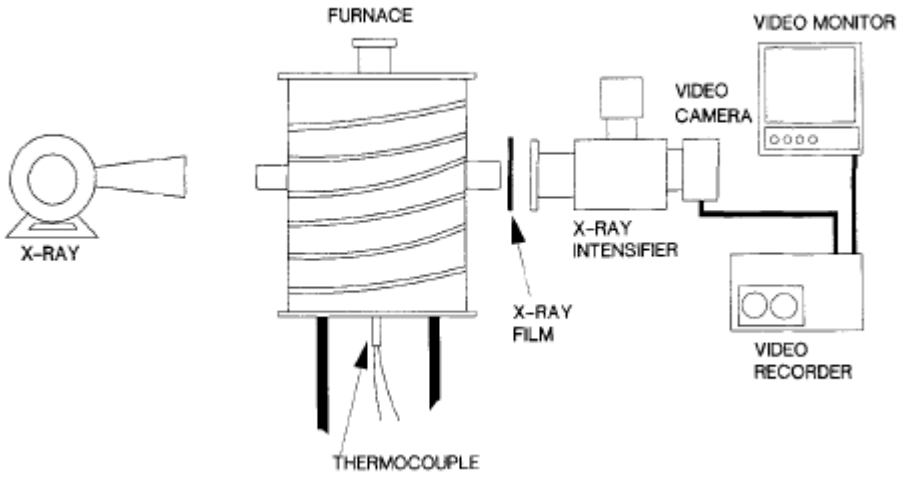

Figure 4. X-ray Image Transmission System (Toguri, 1992)

A comprehensive explanation regarding matte and slag formation, alongside with the matte-slag reactions was proposed in his work (cited in present work at Chapter 3). Fagerlund found out that most of the desulfurization and deironization of the matte occurred due to magnetite interacting with iron sulfides in the matte, primarily due to reactions (10) and (11). Ultimately, most of the slag and matte has already separated into two distinctive phases after 15 minutes, whereas after 30 minutes the final copper content of the slag and matte can already be concluded, as shown in Figure 5 and 6.

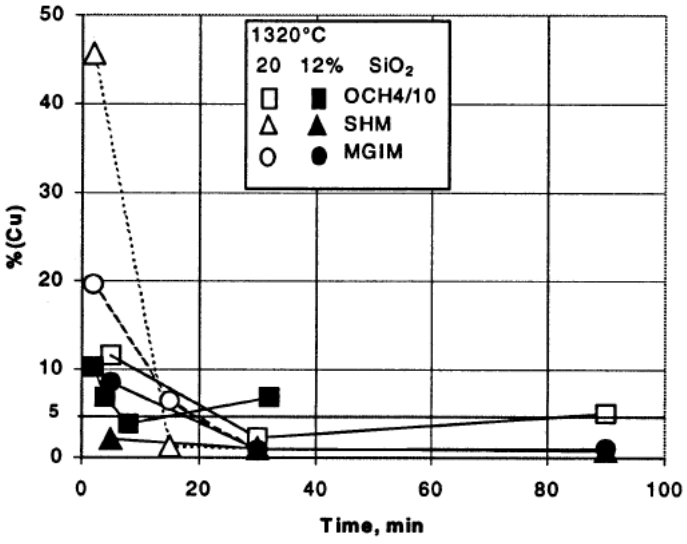

Figure 5. Superficial Copper Content in Slag as a Function of Settling Time (Fagerlund, 2000)

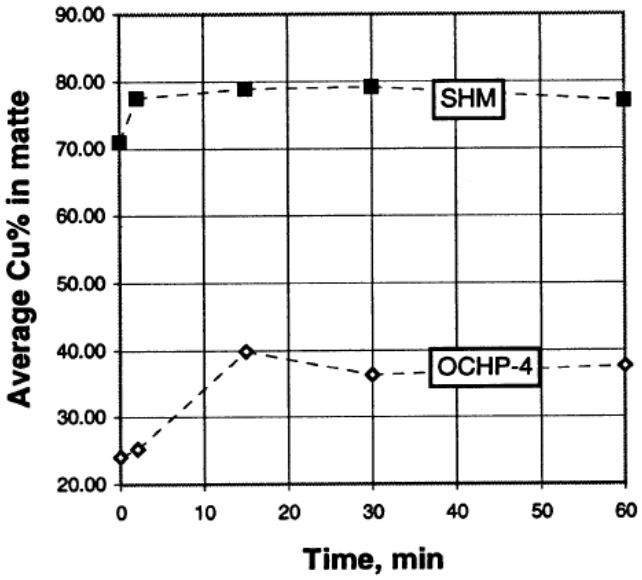

Figure 6. Average Copper Content in Matte during Settling Time (Fagerlund, 2000)

It can be seen from Figure 5, that as the silica charge is increased above the saturation point (20 wt%), the matte settling rate would subsequently decrease. Above the saturation point, silica would only increase the viscosity of slag, therefore hindering the matte settling rate. The matte settling rate is lower in the low-grade copper matte and oxidized chalcopyrite, due to the mutual solubility effect, iron oxide and silica remain in the matte phase. This is shown in Figure 6, whereas in SHM, the matte-slag separation ceased faster than in OCHP.

Using the X-ray image transmission system, Fagerlund evaluated the settling phenomena of matte through the slag layer. Added with periodical sampling and SEM-EDS analysis, Fagerlund was able to explain further the effects of droplet properties (size and copper content) to the settling phenomena in general. These micrographs are shown in Figure 7.

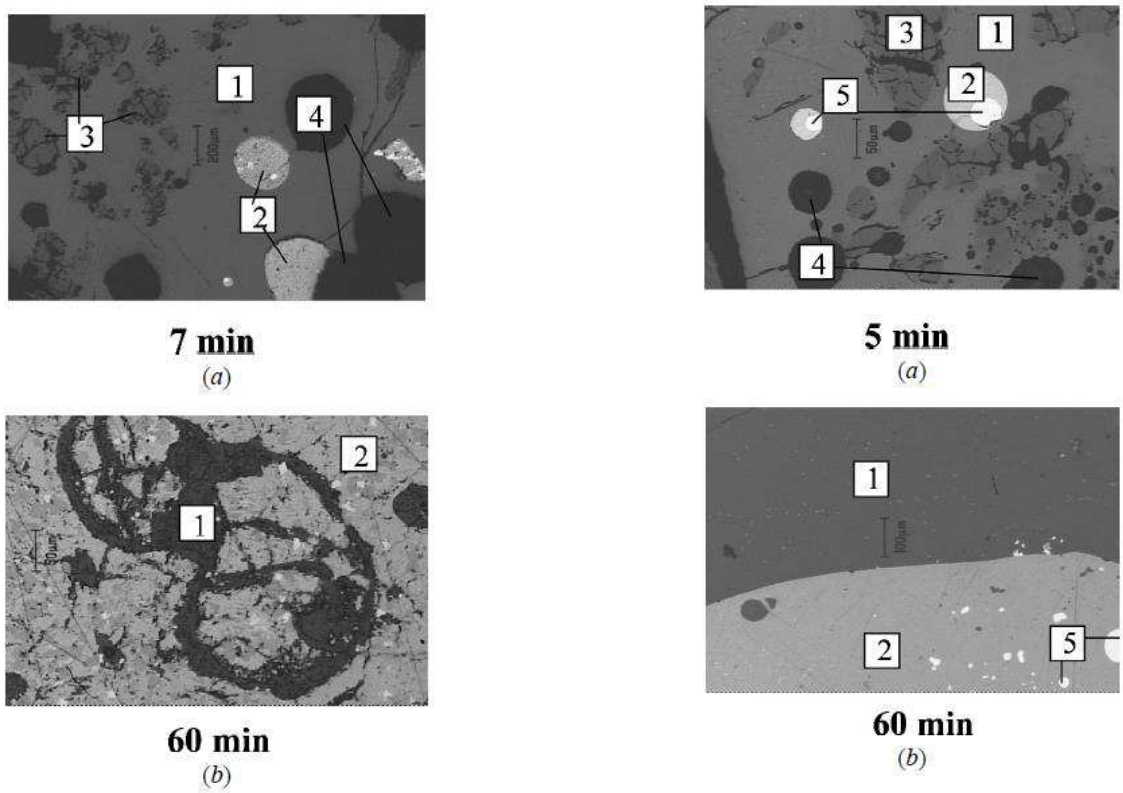

Figure 7. Micrographs of OCHP Settling (left) and SHM (right), showing (1) slag, (2) matte, (3) silica sand, (4) gas bubbles, and (5) Cu (Fagerlund, 2000)

Reaction between slag and matte tend to proceed vigorously, as gas bubbles were observed in the micrographs of the samples, shown in Figure 7. This gas evolution is the key property in the desulphurization reaction during matte settling, in which it releases SO_2 gases. Copper content in the matte is also found not to have any correlation to the matte droplet flotation by the SO_2 gas formed at matte slag interphase, whereas this phenomena is known to increase the settling rate of matte droplets by enhancing mixing process in the system. However, some adverse effect is observed in relation to this phenomena, due to the vigorous gas evolutions, in which it would break the matte droplets, promoting emulsification of the matte in the slag, therefore hindering the matte settling.

Tahmasebi (2013) conducted a similar study regarding reaction between copper sulphide (Cu_2S) matte droplets and slag phase. He analysed the effect of matte droplet size (mass and surface area) and temperature (1400, 1425, 1450, 1475 ^oC) on the desulphurization rate of the matte, as well as proposed the rate controlling mechanism of the desulphurization of matte droplets.

A furnace equipped with X-ray fluoroscopy apparatus and pressure transducer was used in his study, shown in Figure 8. Experiments were conducted in an inert atmosphere. Similarly with Fagerlund's second method, the matte pellet was placed in an alumina dispensing tube placed 9 cm above the alumina crucible. This configuration allows matte to melt prior entering the slag as droplets. The settling process was observed using the X-ray fluoroscopy imaging system.

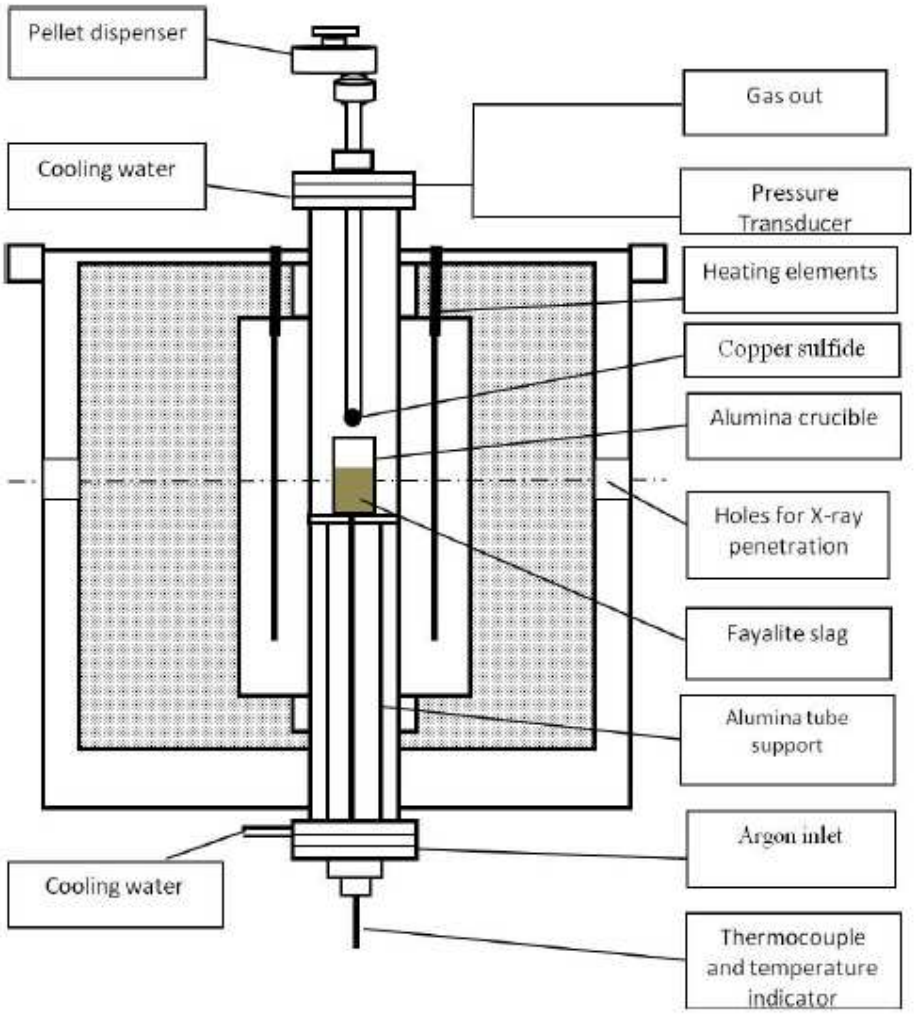

Figure 8. Experimental Setup of Tahmasebi (2013)

As volume and temperature inside the furnace is regarded as constant, the release of SO_2 gas during desulphurization reaction would increase the furnace pressure. The increase was detected by the pressure transducer installed in the furnace. This technique is commonly referred as CVPI (Constant Volume Pressure Increase) Technique.

Having known the furnace volume and the principal reaction of matte desulphurization (Reaction 16), the molar amount of SO_2 released could be calculated, which would be valuable in determining the reaction rate.

$$Cu_2S_{(matte)} + 2O_{(slag)} \leftrightarrow 2Cu_{(l)} + SO_{2(g)} \quad (16)$$

Tahmasebi found that the rate of desulphurization reaction tends to increase with increasing mass of matte droplets, however no linear correlations were observed. Had it been linear, it meant that the rate had a linear correlation with droplet volume, indicating an internal gas nucleation (droplet swelling) or subsurface nucleation. The rate also increase exponentially with temperature, indicating agreement with the Arrhenius law.

Having known the droplet mass, density of Cu_2S, and assuming a perfect sphere shape for the droplets, Tahmasebi then proceeded to estimate the surface area of the droplet. However, the results from the X-ray imaging system showed that the droplet would tend to fall not in one piece, but several pieces. During the settling process, only parts of the droplet came in contact with slag to initiate the desulphurization reaction, so not all the surface area of the droplet is effective in the reaction interphase. These considerations were taken into account in Tahmasebi's work.

It was found out that the reaction rate linearly increases with the droplet surface area. This indicated that the reaction took place on the surface of the matte droplet. However, it was also discovered that the fitted experimental data does not extend to the origin. This indicated that as the droplets get smaller, the reaction rate was limited by something other than the droplet surface area

Results from both the microscopy and X-ray imaging system showed that there was a gas halo observed around the matte droplet. This gas halo was thought to be the resulting SO_2 gas from reaction (16). The observation of gas halo also gives an idea of the reaction mechanism for kinetic model formulation. A couple of these micrographs are shown in Figure 9.

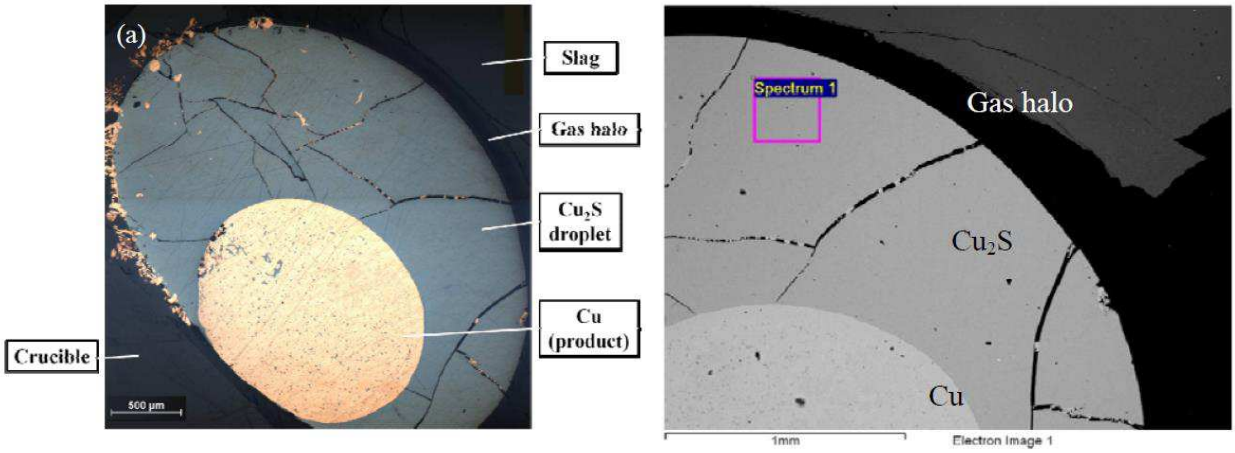

Figure 9. Micrographs of Matte-Slag Sample after Quenching from 1400°C (Tahmasebi, 2013)

To further understand the matte settling and separation process, Zhou and Chen (2016) conducted investigations of an industrial scale Outokumpu-Kennecott Flash Converting Furnace. A different approach was taken, whereas the study consists of sampling in different parts of the settler (mainly varying in distance from the reaction shaft and to the slag tap hole), and analyzing these samples with SEM EDS to understand what happened during an actual matte settling process.

In their work, Zhou and Chen presented some important findings regarding the flash smelting process, which are:

- The reactions occurred rapidly in the shaft, with all process sequences in the smelting (including agglomeration and separation of slag and matte, as well as declining copper in slag) going almost to completion already in the area under the shaft. Consequently, most of the settling zone was primarily used only for storing the matte and slag, as there are no significant composition changes of matte and slag from the settling zone to the slag tap holes.

- Magnetite content in the slag tap hole does not differ greatly to the one underneath the reaction shaft. This means the magnetite content will not be decreased purely by the settling process. An effective way to decrease the magnetite content would be to improve reactions in the shaft

- Large matte droplets in the slag settle rapidly to the matte layer, as copper level in slag rapidly drops to the final level. This means that the reduction of copper loss in the slag would not be done purely by extending settling time.

4. Thermodynamics of Copper Matte-Slag System

In general, evaluating a chemical phenomenon taking place in a system requires understanding of both kinetic and thermodynamic aspects of the system. Kinetic aspects provide the information of the process sequences and rate towards the equilibrium stage, while thermodynamic aspects provide information regarding what the equilibrium stage should be, given the known conditions of the process (temperature and pressure). Prevalent studies have been done in terms of thermodynamics and phase equilibrium of the copper matte-slag system. These thermodynamic studies will be briefly discussed in this chapter, especially the ones which are related to the present work.

Yazawa and Kameda (1954) were among the first to study the thermodynamics of iron silicate slag. They managed to generate the phase diagram for mixture of FeO, FeS, and SiO_2, heated at 1200^oC, part of which is shown in Figure 10.

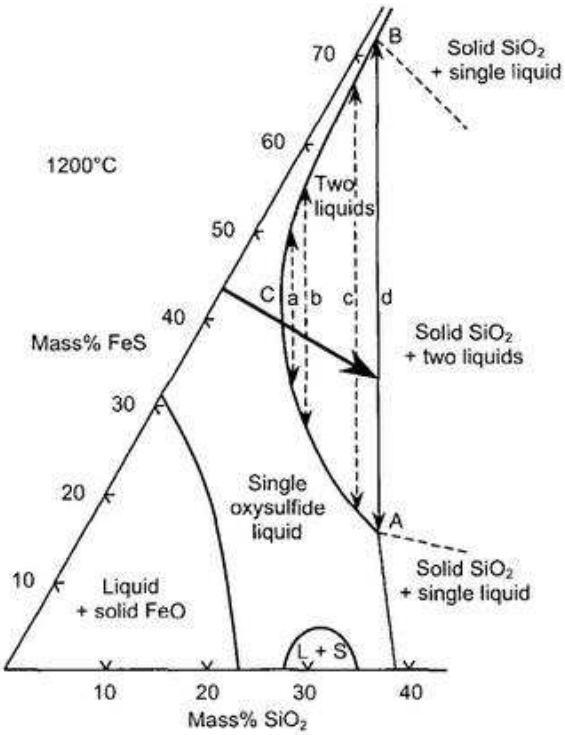

Figure 10. Simplified Phase Diagram of FeO, FeS, and SiO_2 System (Yazawa and Kameda, 1952)

Figure 10 illustrates a simple way to understand a slag-matte equilibrium in regards to the iron element. Without any addition of silica (for FeS concentration above 31% mass), a single oxysulfide melt would be produced at the equilibrium stage. If enough silica is added, a miscibility gap appears, and the equilibrium compositions follow the phase

boundary C-A and C-B, as shown in lines a, b, c, and d. The sulphide rich melt would represent matte, while the oxide would represent slag. The compositions of both phases in silica saturation (saturation line is pointed with an arrow) are given in point A for slag and B for matte.

In terms of copper smelting, Cu-S phase diagram and thermodynamics have also been studied by several researchers such as Cook (1972), and Chakrabarti and Laughlin (1983). Phase diagram of the system is given in Figure 11.

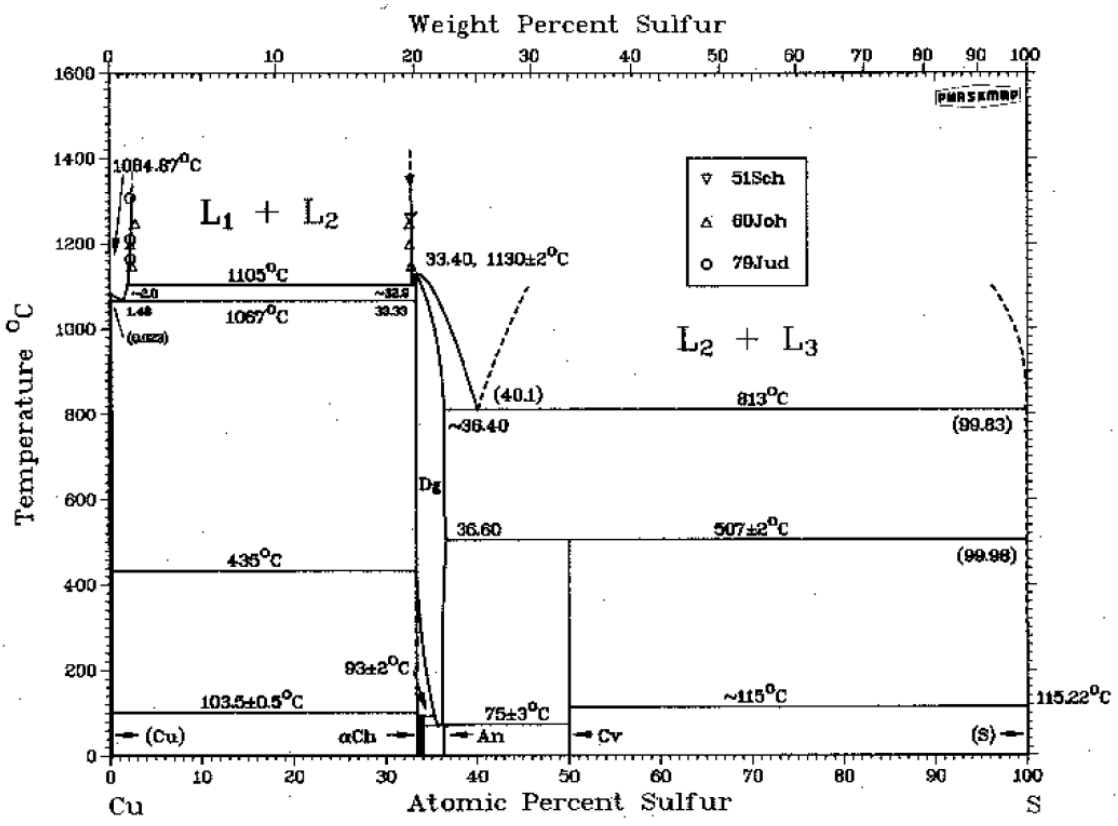

Figure 11. Cu-S Binary Phase Diagram (Chakrabarti and Laughlin, 1983)

In relation to the matte converting of Cu_2S, it can be seen that a miscibility gap appears at the temperature of 1105°C from 1.2 wt% to 19.5 wt% S. Two liquids coexist in this region: liquid 1 which represent the copper metal phase (having a limited sulphur solubility of around 1 wt%) and liquid 2 which represents the sulphide melt of Cu_2S, having sulphur solubility of 20-22 wt%.

Schlegel and Schuller (1952), have studied the phase diagram of Cu_2S-FeS system, which corresponds well with matte smelting of chalcopyrite ($CuFeS_2$) concentrate. This phase diagram is shown in Figure 12.

As shown in Figure 12 at temperatures above 1200°C, all phases are molten, which would be defined as the matte. In industrial operation, smelting furnaces use temperature of 1250°C to produce a molten slag and superheated matte. This way it is ensured that the matte and slag are in liquid phase during tapping and transferring.

From Figure 12 it could be concluded as well, that without addition of silica, the industrial copper smelting would not be feasible, as the product would consist only of one homogenous liquid which would be difficult to separate between the copper and iron. The use of silica, as shown in Figure 10, would enables the formation of an oxide melt, separating iron from the sulphide rich matte to the oxide rich slag.

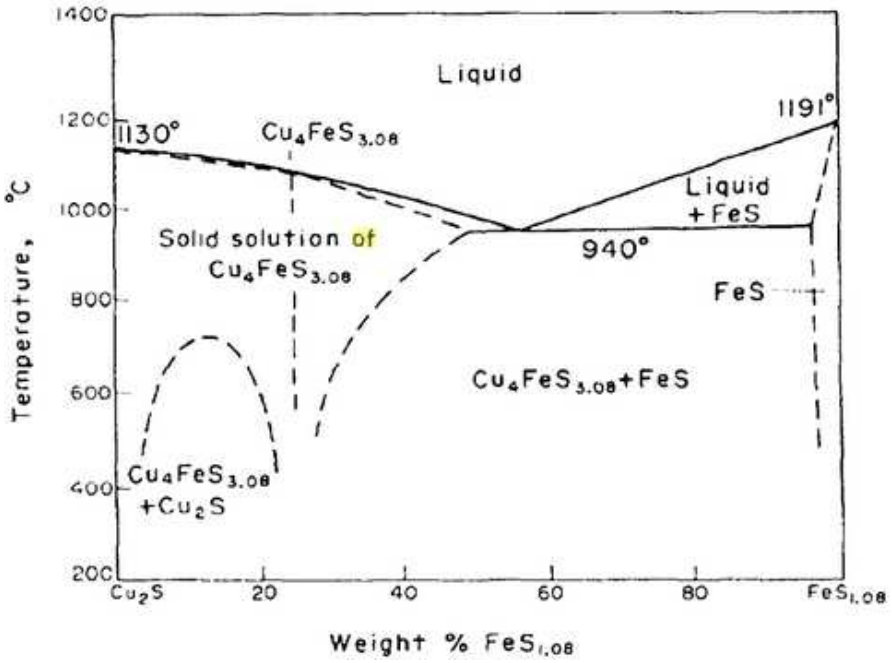

Figure 12. Phase Diagram of Cu_2S-FeS System (Schlegel and Schuller, 1952)

Hidayat, et al. (2012) as well as Devia and Sanchez (2011) have done more thorough thermodynamic studies of Cu-Fe-O-Si system. These studies give an idea regarding phase equilibria of typical slag that contains Si, O, Cu, and Fe. A stability diagram in this quaternary system is presented in Figure 13.

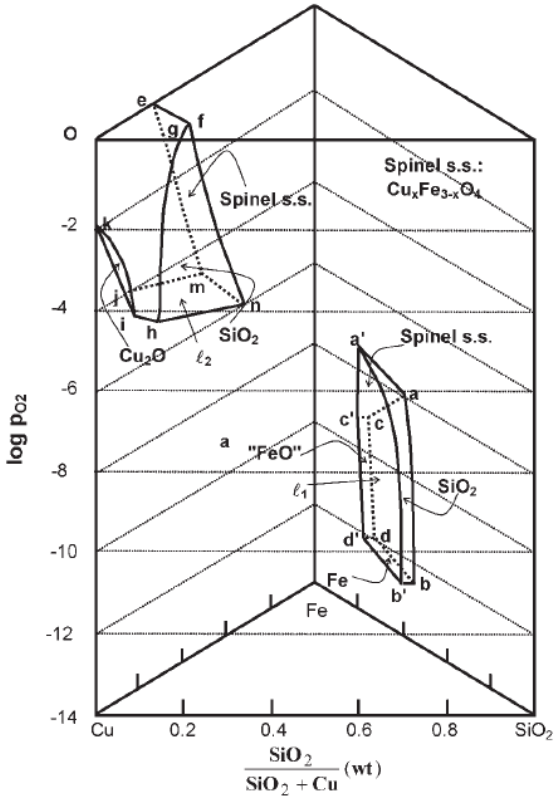

Figure 13. Stability Diagrams of Quaternary System Cu-Fe-O-SiO2 at 1200°C (Devia and Sanchez, 2011)

The area l_2 on the top left of the Figure 13 shows the stability area of the liquid oxide based on Cu_2O and the slag. The other surfaces of the volume represent the following:

- surface ijk represents the saturation with Cu_2O
- surface fghn represents the saturation with SiO_2
- surface efnm represents the saturation with solid spinel solution
- surface hjmn represents the saturation with l_2.
- surface efgO represents 1 atm partial pressure of O_2

Different ternary systems would be formed in a lower oxygen partial pressure atmosphere, whereas the substance Cu_2O would not be formed. This set of ternary systems is shown on the lower right of Figure 13. These surfaces represents the following:

- aa'b'b for the saturation with silica
- bb'dd' for the saturation with Fe_γ
- d'dcc' for the saturation with FeO
- acc'a' for the saturation with spinel solid solution.

Point a' represent the lowest partial pressure of oxygen where slag could exist in equilibrium, which would be around 10^{-7} atm.

A compositional space of the Cu-Fe-O-Si system has also been constructed, as shown in Figure 14, presenting an overview of the Cu-Fe-Si phase equilibrium at different pO_2 atmospheres.

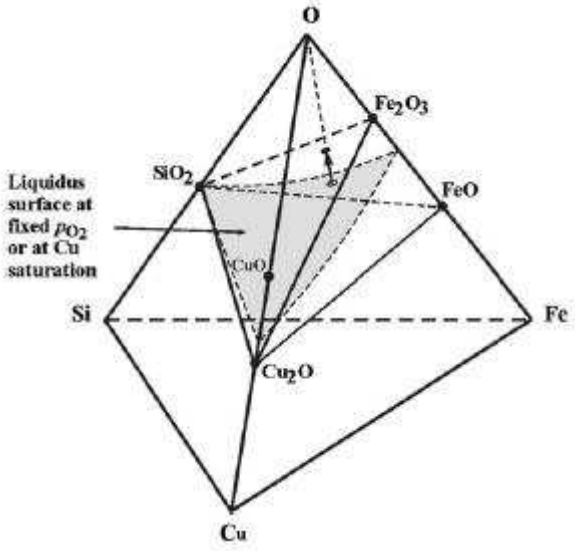

Figure 14. Compositional Space of the Cu-Fe-Si-O System (Devia and Sanchez, 2011)

The partial ternary phase diagram for this system in air is shown in Figure 15. It shows clearly that fayalite slag would not be formed in equilibrium stage in an air atmosphere. Oxides of the iron and copper in the form of cuprite, delafossite, as well as spinel and tridymite would be formed as well. With this diagram the expected final product of experimental smelting in air could be known.

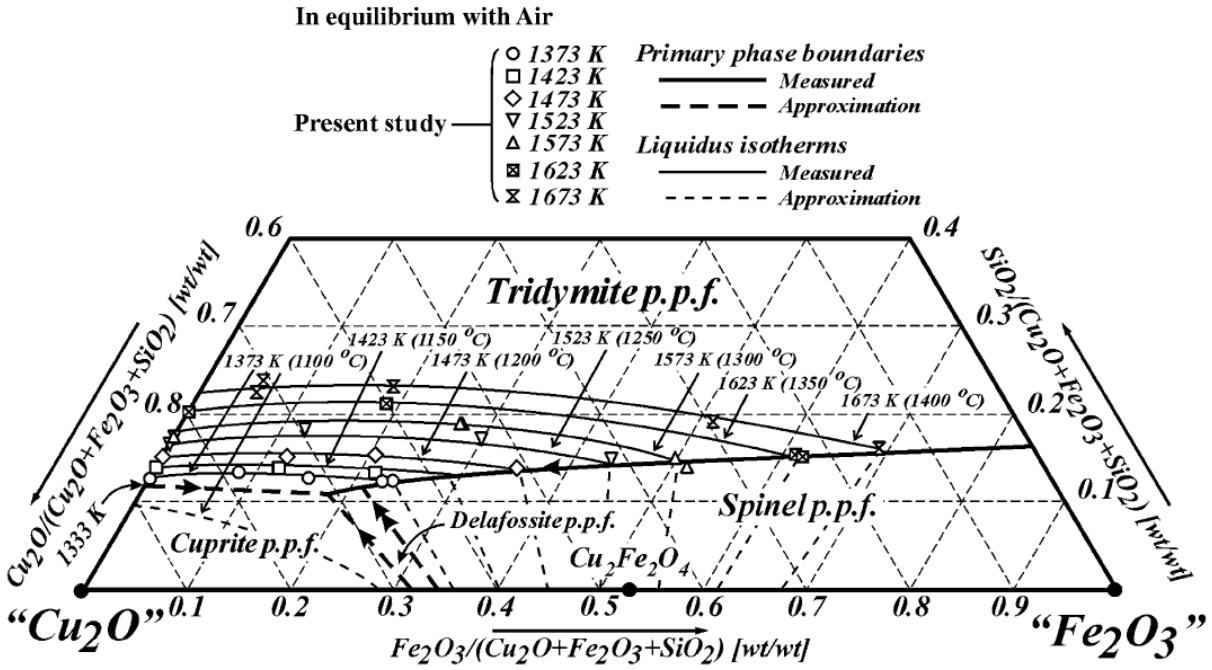

Figure 15. Ternary Phase Diagrams in Cu_2O-Fe_2O_3-SiO_2 System with Liquidus Isotherms (Hidayat et al, 2012)

Hidayat *et al* (2012), extended the study of Cu-Fe-O-Si system by analysing its equilibrium with metallic copper in inert argon atmosphere. This study was later expanded more to equilibrium of matte-slag system (Hidayat *et al,* 2016) and evaluation of Ag distribution between the matte and slag phase. This recent study by Hidayat would be the closest system to the present work, bearing the CuS-FeS matte as well as FeO-SiO_2 slag.

Details of the experimental technique used by Hidayat, and results regarding the Ag metal distribution between the phases has been elaborated elsewhere in the present work (chapter 2.2.1). In regards to the equilibration and thermodynamics, they evaluated two different systems in equilibrium, which are gas-slag-matte-spinel and gas-slag-matte-tridymite. They evaluated the system with fixed SO_2 gas pressure of 0.25 atm. Micrographs of their system after equilibration are shown in Figure 16.

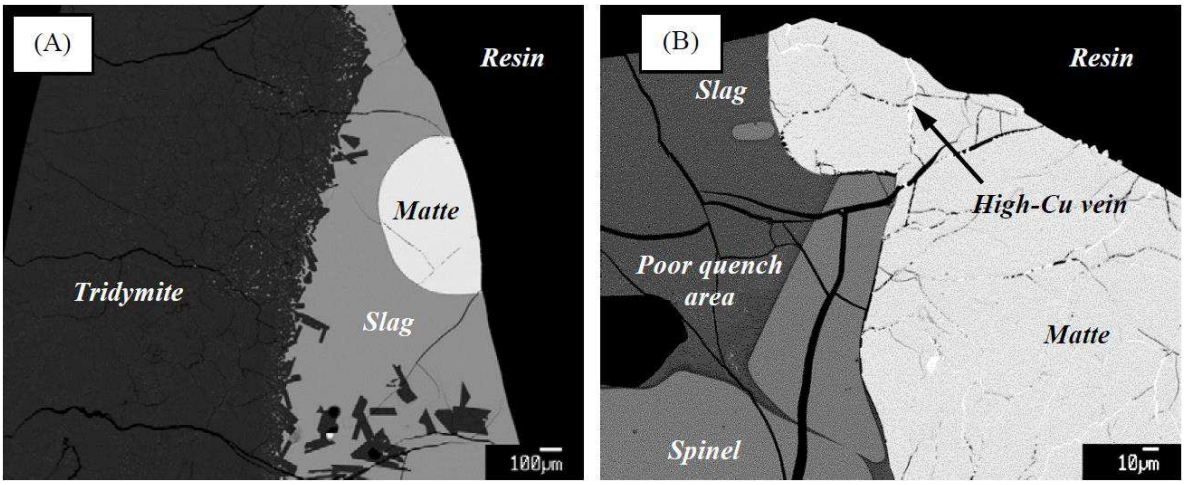

Figure 16. Micrographs of Equilibrated Samples of Cu-Fe-Si-O-S System. (A) gas-slag-matte-tridymite. (B) gas-slag-matte-spinel (Hidayat et al, 2016)

Copper veins observed in the matte phase, as seen in the micrographs, were associated with cracks formed during cooling of the samples. At the given condition (1200^{o}C temperature and 0.25 atm SO_2 partial pressure) it appears that both systems are in equilibrium at oxygen partial pressure around 10^{-8} atm. This explains the presence of matte and slag after 24hrs equilibration time, whereas in Figure 13 and 15, no matte or slag phase were to be found at equilibrium with air, as these phases would be oxidized to their respective oxide phases.

Many other thermodynamic studies have been done regarding copper smelting. Several studies include CaO, Al_2O_3, as well as MgO in their systems (Henao *et al,* 2010. Zhao *et al,* 2013) whereas these compounds are regularly added to the smelting furnace to alter the slag properties. Other studies focuses on the distribution of minor elements such as Ag and Au between the matte and slag (Nagamori *et al,* 1975. Roghani *et al,* 2000. Kim and Sohn, 1998). This topic has been discussed quite well, as it gives an idea of the feasibility in recovering certain kind of element from the slag.

It is important to note that phase diagram in the present work would have to be used very carefully, as the present work deals mostly with systems that are not in equilibrium. The phase diagram could be used to confirm that the system is not in equilibrium, but it could not be used directly to prove that the system is in equilibrium by the presence of similar phases to that shown in phase diagram. However, it could give an idea of what the equilibrium stage should be.

5. Kinetics of Copper Matte-Slag System

In evaluating a rate of a chemical process, two main phenomena must be considered. These two are the physical transport of the reactants, as well as the chemical reaction between these reactants. In general, three basic stages happen in any given chemical reaction interphase (Ajersch and Toguri, 1972):

1. Diffusion of the reactants to the reaction interphase (the boundary layer between the phases)
2. The reaction takes place at this interphase. The reaction may include absorption, adsorption, dissociation or activated complex mechanism that could determine the overall chemical rate
3. Diffusion of products away from the reaction interphase.

With an appropriate experimental technique, the rate controlling step from these aforementioned stages could be determined. The knowledge of the controlling step would give a better idea of the overall rate of the chemical reactions.

To this date, little is known about the kinetics of the reactions proceeding in the settling part of the copper flash smelting. Ahokainen and Jokilaakso (1998) have studied extensively the reactions proceeding in the reaction shaft, while an attempt to study the reaction sequences in the area underneath the reaction shaft has been done by Fagerlund (2000).

Several workers, such as Alyaser and Brimacombe (1995), Rottmann and Wuth (1975), Jalkanen (1981), as well as Ajersch and Toguri (1972) already extensively studied oxidation kinetics of molten Cu_2S. Similar to that reaction (16) used by Tahmasebi (2013), oxidation of molten Cu_2S could be explained by reaction (19)

$$Cu_2S_{(l)} + O_2 \leftrightarrow 2Cu_{(l)} + SO_2 \qquad (19)$$

This time, the oxygen would come from air, instead of slag. Reaction (19) could be broken down into two steps, which is the combination of reaction (2) by Mulenshi (2015) and reaction (15) by Fagerlund (2000).

$$Cu_2S_{(matte)} + 1.5O_2 \leftrightarrow Cu_2O_{(slag)} + SO_2 \qquad (2)$$

$$Cu_2S_{(matte)} + 2Cu_2O_{(slag)} \leftrightarrow 6Cu_{(l)} + SO_{2(g)} \quad (15)$$

Peretti (1948) suggested that the matte oxidation would follow a primary stage prior to reaction (19), in which the melt is partially desulfurized until the sulphur content is lowered to about 19.4%. This sulphur deficient phase is also known as white metal. This primary stage is presented in reaction (20)

$$Cu_2S_{(l)} + x(O_2) \leftrightarrow 2Cu_2S_{1-x} + x(SO_2) \quad (20)$$

In most cases, fitting a rate equation / model to a chemical reaction could be done by analysing the ratio of the products and reactants. In terms of Cu_2S oxidation, this would correspond to the molar ratio of reacted oxygen to the formed sulphur dioxide (α). The molar amount of these components throughout the reaction could be obtained by gravimetric measurements, CVPI (Constant Volume Pressure Increase), or gas analysis based measurement. This molar amount as a function of time could be differentiated to obtain the molar consumption/production rate.

The results from Rottmann and Wuth suggested that during reaction (19), α is calculated to be greater than unity (approximately 1.2), while during reaction (20), α is less then unity (approximately 0.9). This result would contradict the primary-secondary stage theory of copper sulphide oxidation through reaction (20) and (19). Moreover, although the value of α is 3/2 for reaction (2), formation of Cu_2O would not proceed before the complete oxidation of Cu_2S. This practically means the reaction (2) would only proceed if there is unlimited amount of oxygen in the system, so that the Cu_2S could be completely oxidized. Ajersch and Toguri (1972) further added that any intermediate stages in reaction (19) would be expected to occur rapidly. Many studies end up assuming that reaction (19) would take place as an overall reaction in molten Cu_2S oxidation, as the value of α is close to unity.

Ajersch and Toguri (1972) found out that gas diffusion would be the rate controlling step in Cu_2S oxidation. This result corresponds well with findings from Rottmann and Wuth (1975), Jalkanen (1981), as well as Alyaser and Brimacombe (1995).

Those aforementioned studies have different opinions regarding the steps of reaction. Ajersch and Toguri (1972) as well as Rottmann and Wuth (1975) conclude that reaction

(19) was the main overall step in the reaction. Jalkanen proposed two primary-secondary stages in the reaction, presented in reactions (21) and (22)

$$[S] + 1.5O_2 \leftrightarrow [O] + SO_2 \quad (21)$$

$$[Cu_{2+\Delta}S] + O_2 \leftrightarrow (2+\Delta)Cu + SO_2 \quad (22)$$

Alyaser and Brimacombe (1995) take the study further by addressing the fact that these elements and reactants are present in the melt in the form of ions, instead of neutral elements. Taking this into account, they proposed the reaction steps as follows:

1. The primary stage, where α is calculated to be greater than unity. This means that part of oxygen consumed is dissolved in the melt, while the other react with sulphur to form SO_2. This stage proceeds through reaction (23)

$$[S^{2-}] + 1.5(O_2) \leftrightarrow [O^{2-}] + SO_2 \quad (23)$$

2. The secondary stage, where α is calculated to be slightly less than unity. This means that the amount of sulphur removed is slightly more than the oxygen consumed. It indicates that the reaction takes place at the bath surface between dissolved oxygen and dissolved sulphur through reaction (24)

$$[S^{2-}] + 2[O^{2-}] + 6\,[Cu^{+}] \leftrightarrow 6Cu + SO_2 \quad (24)$$

Should the value of α be unity, then reaction (25) would proceed

$$[S^{2-}] + (O_2) + 2\,[Cu^{+}] \leftrightarrow 2Cu + SO_2 \quad (25)$$

During this stage, while copper and SO_2 are generated within the melt through reaction (24), surface reaction with oxygen gas also continues to take place. The overall limiting step for molten Cu_2S oxidation was determined to be the gas phase mass transfer of oxygen to the melt surface.

On the other hand, the kinetics of molten copper matte oxidation has been analyzed by Asaki *et al.* (1988). This study would resemble the converting process, whereas matte from smelting are converted into blister at this stage. The matte oxidation process would

also take place in the lower area of the reaction shaft of the Outukumpu flash furnace, where matte droplets come into contact with oxygen and are oxidized.

In Asaki's work, copper matte was considered as a ternary melt of Cu_2S-FeS-Fe. The experiments were conducted in a quartz reaction tube, heated inside a furnace. Gravimetric based measurements were used, in which quartz crucible containing the sample was suspended using automatic microbalance, so that the mass change could be observed throughout the experiment. Inert masking with Ar gas was done, until O_2 gas was introduced when the furnace reached the set point temperature. Oxygen partial pressure of the oxidizing gas was pre-determined. Silica gel was placed after each gas tube, so that the gas flow to the furnace was water-free. The product gas was sent to cooling section, and analyzed using infrared gas analyzer, so the SO_2 content of the gas can be monitored. Schematic of this experimental apparatus is shown in Figure 17.

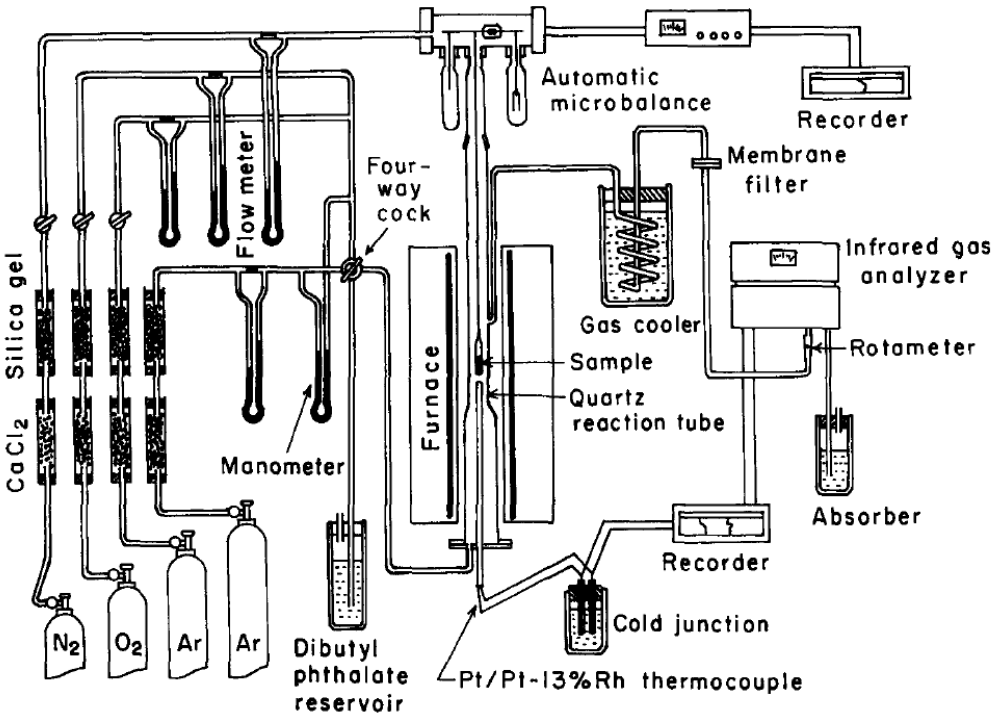

Figure 17. Experimental Apparatus of Asaki, et al. (1988)

Based on the experiment, proposed mechanism of matte oxidation reaction were as follows:

- Due to the presence of FeS and Fe, these substances would be preferentially oxidized first through the following reactions:

$$FeS_{(l)} + \frac{3}{2}O_2 \leftrightarrow FeO_{(l)} + SO_2 \quad (26)$$

$$Fe_{(l)} + \frac{1}{2}O_2 \leftrightarrow FeO_{(l)} \quad (27)$$

It is well known that reaction (27) is preferred thermodynamically. This was confirmed in the experiment, in which mass increase was observed in the first stage of the oxidation without any SO_2 gas detected. Upon applying the model, described in equation (28), with the respective experimental results, Asaki *et al*, obtained matching results.

$$\frac{dm}{dt} = \frac{\pi}{4} d^2 N_{O2} Mr_{O2} \quad (28)$$

In (28) N_i is the diffusion rate of gaseous component (i), and Mr_i is the molecular mass of gaseous component (i). It was observed that the diffusion of oxygen gas (N_{O2}) was the controlling parameter of the reaction rate, meaning the chemical reaction rate of reaction (27) was quite fast. In order to confirm this, in several runs of experiments, the oxygen gas was switched to argon, and samples were cooled for XRD analysis. Four species were identified, Cu_2S, FeS, FeO, and $Cu_{5.6}FeS_{4.4}$. The latter was thought to be formed during cooling of the sample.

- In the next stage, there was mass decrease and SO_2 gas detected. Reaction (26) is expected to happen in this stage, alongside with reaction (9)

$$FeS + \frac{5}{3}O_2 \leftrightarrow \frac{1}{3}Fe_3O_4 + SO_2 \quad (9)$$

The progress of reactions (26) and (9) was compared to the diffusion rate of the O_2 and SO_2 gases. Equation (29) was developed to predict the mass decrease at this stage:

$$\frac{dm}{dt} = \frac{\pi}{4} d^2 (N_{O2} Mr_{O2} + N_{SO2} Mr_{SO2}) \quad (29)$$

Two *k* values (3/2 and 5/3), corresponding to both reaction (26) and (9) were used in Equation (29) to describe the mass change in the experiment. This *k* value is equivalent to α value used in Rottmann and Wuth (1975), which is described as the molar ratio of oxygen consumed to the sulphur dioxides

formed. This *k* value is incorporated in the Stefan-Maxwell equation in explaining the diffusion of oxygen(N_{O_2}), details of which have been described in Asaki's work. Using *k* = 3/2, Equation (29) described the mass change measurements accurately, indicating that reaction (26) proceeded in the second stage. Furthermore, since Equation (29) could accurately describe the measured mass change in the experiment, it indicates that this stage is controlled by the gas diffusion as well. Should it be controlled by the chemical reaction, Equation (29) would not include any gas diffusion terms (N_i).

Some amount of FeS still remained in the sample after the second stage, and formation of magnetite and Cu were observed, primarily through reaction (9) for magnetite and (30) for Cu.

$$Cu_2S_{(l)} + O_2 \leftrightarrow 2Cu_{(l)} + SO_2 \qquad (30)$$

To compare the feasibilities of reaction (30) and (9), both reactions are combined to produce reaction (31)

$$5Cu_2S_{(l)} + Fe_3O_{4(s)} \leftrightarrow 10Cu_{(l)} + 10FeS_{(l)} + 2SO_2 \qquad (31)$$

Equilibrium constant of reaction (31) was calculated from thermodynamic data to be K = 4.53 x 10^{-13} at 1503 K and 1.33 x 10^{-12} at 1533 K. This means that FeS is preferentially oxidized rather than Cu_2S, as long as FeS remains in the system.

- The amount of FeS decreased considerably at the third stage, and the amount of Cu increased. Furthermore, most of the FeO resulting from reaction (27) has been further oxidized into magnetite. All of the Cu_2S formed has been oxidized into metallic copper, and portion of the copper formed has been oxidized into Cu_2O, as well as $CuFeO_2$. In this stage, reaction (30) was thought to be the main reaction, in which *k* is equal to unity. Using equation (29), the model describes the measurements quite closely, meaning that at this stage gaseous diffusion still controls the rate of reaction.

- The metallic copper from reaction (30) was further oxidized into Cu_2O, as well as $CuFeO_2$. Since no sulphide is still present, only diffusion of O_2 gas through Ar is considered, which corresponds to $k=\infty$. Using this k and applying the model

equation with the measurement, Asaki obtained a matching result, indicating the relatively faster oxide formation rate compared to the gas diffusion. After the end of this stage, mass increase of the sample was very low, which means that all the reactions have almost reached the equilibrium and progress slower.

The work by Asaki *et al* was mainly concluding that all of the species formed in the experiment were having quite fast reaction rate, comparable to that of gas diffusion. Great consideration regarding formation of these substances must be taken in modelling study of the flash smelting.

Using different approach, Tahmasebi (2013) analysed the kinetics of Cu_2S droplet in an oxidizing slag. Details of his experimental technique has been described elsewhere in this chapter, in which CVPI technique was used in his work. The main aim of his work was to evaluate the copper sulphide oxidation reaction in slag, described in equation (16)

$$Cu_2S_{(matte)} + 2O_{(slag)} \leftrightarrow 2Cu_{(l)} + SO_{2(g)} \qquad (16)$$

The reaction rate throughout the experiment was evaluated by the gas pressure change inside the furnace, detected by the installed pressure transducer. This gas pressure change in the furnace was caused due to gas producing reactions such as Reaction (16). Such pressure reading is shown in Figure 18.

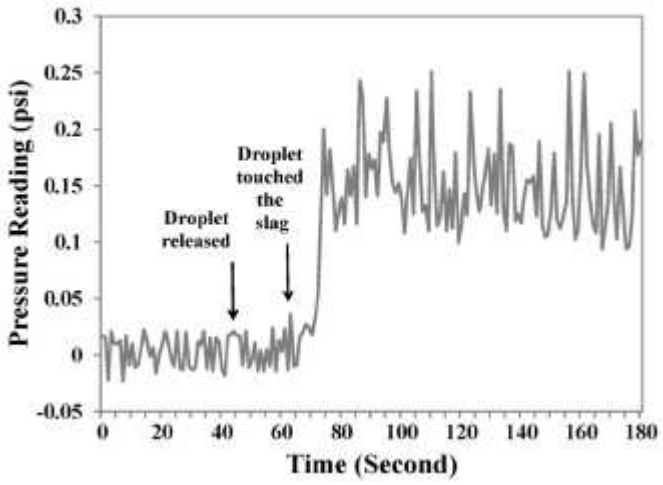

Figure 18. Pressure Reading during Copper Sulphide Droplets Contacting with Slag (Tahmasebi, 2013)

A sudden spike in pressure reading indicated the contacting between oxidising slag and the droplets, which triggered reaction (16). The actual contacting time between slag and the droplet was also noted. There existed a short delay between the droplet-slag contact and the pressure increase, indicating a mass transfer process existed before both reactants came to reaction interface and reacted. This was known as incubation period, which in this case includes:

- Diffusion of O^{2-} from the slag to the matte/slag interface
- Desulphurization reaction at the interface, SO_2 nucleation and gas evolution

After evaluating the effects of different variables in the droplet settling, Tahmasebi proposed the following steps in matte droplet reactions with oxidizing slag, shown in Figure 19.

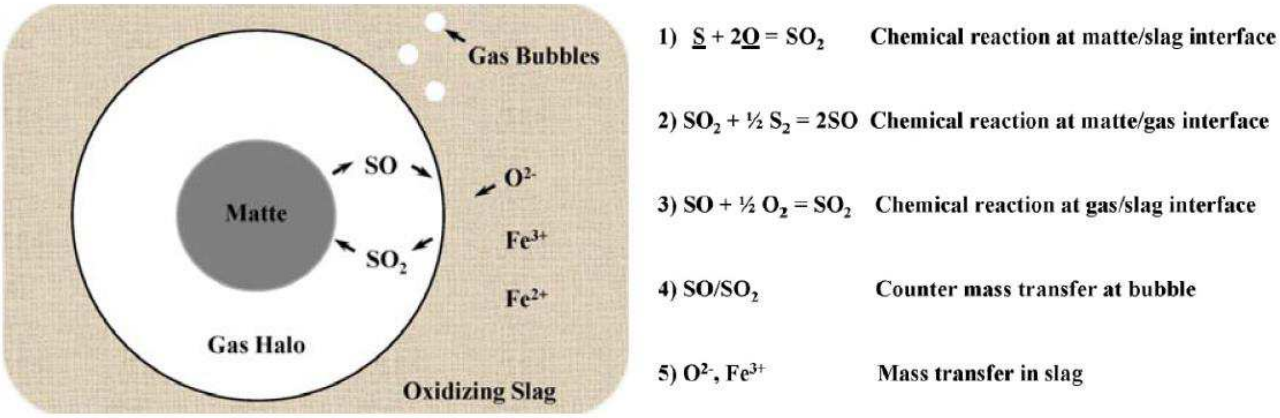

Figure 19. Matte Droplet Oxidation Sequences in Slag (Tahmasebi, 2013)

Reaction (16) takes place at the matte/slag interface, in which oxygen comes from the slag. Oxygen potential of the slag is an important factor, as well as the mass transfer in slag. After the SO_2 gas is released, gas halo was formed around the matte droplet, as shown in Figure 19. Afterwards, reactions between gaseous species in the gas halo may be required for the overall desulphurization reaction to proceed. Using thermodynamic calculation it was found that SO/SO_2 gases are dominant in this system, so that reactions (2) and (3) in Figure 19 would take place. In principle, two stages of reactions took place, the one prior to gas halo formation, and the other after the gas halo formation. Tahmasebi analysed these two stages separately, and found the rate limiting step for each stage.

Assuming that the mass transfer in the slag was the rate controlling step prior to gas halo formation, it can be deduced that the chemical reaction (16) is in equilibrium. Subsequently, the oxygen partial pressure could be calculated using simple equilibrium constant calculation, having known the temperature and assuming the activity of Cu_2S and Cu as unity (both liquids are in their standard state). Partial pressure of SO_2 is regarded as unity as well. Such calculation makes use of the relation between Gibbs free energy (available from literature) and equilibrium constant, shown in Equation (32)

$$K = \exp\left(\frac{-\Delta G^{\circ}}{RT}\right) = \frac{\alpha_{Cu} x P_{SO2}}{\alpha_{Cu2S}\, x P_{O2}} \tag{32}$$

The oxygen partial pressure is controlled by the Fe^{3+}/Fe^{2+} (ferrous to ferric) ratio in the slag, in which it is correlated through Equation (33) by Matousek (1994).

$$\log P_{O2}(atm) = 16.1 + 3.92 \log\left(\frac{Fe^{3+}}{Fe^{2+}}\right) - 1.05\, \frac{pct(Fe)}{pct(SiO_2)} - \frac{29500}{T} \tag{33}$$

In principle, Matousek stated that the oxygen potential of an iron silicate slag would be controlled by the redox reaction between Fe^{2+} and Fe^{3+} ions through reaction (34)

$$\mathrm{FeO} + \tfrac{1}{4}\mathrm{O_2} \leftrightarrow \mathrm{FeO_{1.5}} \tag{34}$$

Having known the oxygen partial pressure from Equation (32), Tahmasebi then determined the ferrous to ferric ratio. As the total Fe in slag is known, the Fe^{3+} could be determined.

Note that now it is known that the reduction of four moles of Fe^{3+} ions would produce two moles of O^{2-} in the slag. These two moles of O^{2-} in the slag then would produce one mole of SO_2 when reacted with the available S^{4+} in the reaction interface, so that the ratio of reduced Fe^{3+} to produced SO_2 is 4 to 1. The flux (J_i) of the Fe^{3+} could be written in Equation (35)

$$J_{Fe^{3+}} = \frac{k_s . A . \rho_s}{100\, MW_{Fe}} (Fe_B^{3+} - Fe_i^{3+}) = 4 J_{SO_2} \tag{35}$$

When k_s is the mass transfer coefficient, A is the matte droplet-slag interfacial area, ρ_s is the measured density of the slag, and MW_{Fe} is the molecular weight of Fe. Equation (35)

makes use of the boundary layer theory, assuming a uniform bulk composition, and composition profile only exists at the vicinity of the reaction interface.

The value of k_s could be calculated, having known the flux of SO_2 through measurement. Note that based on Matousek's equation, it could only determine the Fe^{3+} that are readily available for the reaction (34), which means that it determines the amount of Fe^{3+} ions in the interface, or Fe_i^{3+}. The amount of Fe^{3+} in the bulk phase (Fe_b^{3+}) was determined separately using titration analysis.

With the known k_s values in different temperatures, the value of activation energy of the reaction could be determined straightforwardly using Arrhenius law, presented in Equation (36). The activation energy could indicate the potential rate-limiting step in this reaction.

$$k_s = k_0 . e^{\left(-Q/RT\right)} \tag{36}$$

k_0 is the frequency constant, Q is the activation energy, R is the gas constant, and T is the temperature in Kelvin.

Tahmasebi (2013) found that the activation energies of the matte droplet desulphurization was in the range of 14.7 to 64.9 kJ/mole, which would resemble a mass transfer limited reaction. Had it been controlled by the chemical reaction or adsorption/desorption, the activation energy would be higher (in the range of 400-600 kJ/mole). Therefore, it was concluded that the initial controlling step (prior to gas halo formation) would be mass transfer in the slag.

As it can be seen from Figure 18 after the gas halo formation (sudden spike in pressure reading), pressure in the furnace remained constant, indicating a deferred gas evolution rate. This indicates that the rate-limiting step might have changed into gas-gas phenomena. Tahmasebi evaluated this by analysing the SO/SO_2 counter mass transfer in the gas halo. Similar flux equation was used, shown in Equation (37),

$$J_{SO_2} = \frac{D_{SO-SO2} . P}{\delta RT}\left(P_{SO2}^{s/g} - P_{SO2}^{m/g}\right) = -J_{SO} \tag{37}$$

in which $D_{SO\text{-}SO2}$ is the diffusion coefficient, P is total pressure, δ is the thickness of the gas halo, $P_{SO2}^{s/g}$ and $P_{SO2}^{m/g}$ corresponds to the equilibrium partial pressure of SO_2 at the slag/gas and matte/gas interface respectively.

Again, assuming this gas mass transfer is the rate-limiting step, other reactions in Figure 19 could be considered to be in equilibrium, therefore $P_{SO2}^{s/g}$ and $P_{SO2}^{m/g}$ both could be calculated at different temperatures. The thickness of gas halo (δ) was estimated using the microscopy images. The obtained value of the flux of SO_2 in the gas halo was in the order of 10^{-6} mole/s, which is much lower for the experimental values obtained for the SO_2 gas evolution rate, meaning the gas mass transfer limits the whole reaction rate after the formation of gas halo.

Summary of the kinetic studies related to matte-slag reactions are presented in Table 1.

Table 1. Kinetic Studies Related to Copper Matte-Slag Reactions

Authors	**Investigated System**	**Major Findings**
Alyaser and Brimacombe (1995) Jalkanen (1981)	Cu_2S oxidation with O_2 gas	Gas diffusion limited reaction rate Two stage reaction steps, oxidation of sulphur followed by oxidation of copper
Ajersch and Toguri (1972) Rottmann and Wuth (1975)	Cu_2S oxidation with O_2 gas	Gas diffusion limited reaction rate One stage reaction, both oxidation of S and Cu proceed simultaneously
Asaki *et al.* (1988)	Cu_2S-FeS-Fe oxidation with O_2 gas	Gas diffusion limited reaction rate

		Multistage reaction steps, Fe oxidation followed by FeS, and eventually Cu_2S
Tahmasebi (2013)	Cu_2S droplet oxidation with oxidising slag	Controlled by the mass transfer in slag prior to gas formation, and counter diffusion of SO/SO_2 after gas formation around the droplet

Although the present work will not cover kinetic studies nor rate equation formulation, it aims to give an overview of what happens during matte-slag interactions in flash smelting. The present work used an industrial chalcopyrite concentrate with an oxidizing fayalite slag, a system whose kinetics have never been studied extensively until now. The present work is similar to that of Fagerlund (2000), in which he experimentally simulated the settling and separation of matte-slag in flash smelting.

6. Miscellaneous Experimental Studies of Various Metal / Ore Systems

As the experimental procedure employed in the present work is new, in this subchapter, various other experimental studies in producing time-dependent data (kinetic data) are evaluated. Producing accurate time-dependent data is generally challenging, as an accurate control of reaction time must be achieved. Moreover, data collection in different time intervals or continuous time dependent data collection is also needed. With the high temperature and closed system, these two tasks often pose major challenge to the investigator. Different approaches in collection of such data has been employed by various investigators.

6.1. Gas-Solid and Gas-Melt Reaction Systems

Most prominent examples of a gas-solid system are oxidation or reduction kinetics of a solid in controlled atmosphere, such as oxidation of MoO_2 in air (Wang *et al,* 2016), pyrite oxidation in O_2-N_2 atmosphere (Aracena *et al*, 2016), as well as reduction of SiMn ore using CO gas, (Kawamoto, 2016). Similar to gas-solid reactions, gas-melt reaction only differs in phase of the specimen, which in this case is liquid. Examples of gas-melt system such as molten Cu_2S oxidation and molten Cu matte oxidation are already presented in previous chapter. Typically, a gas-solid and gas-melt overall reaction rate could be controlled either by the chemical reaction rate itself, or the mass transfer phenomena (diffusion of gas between the bulk solid or liquid film).

These kinds of studies mainly involve a furnace heating of solid/molten ore specimen in a controlled gas atmosphere. As the specimen decomposes to gas due to the oxidation/reduction mechanism, weight loss of the specimen (due to gas formation) is exploited for data collection. Typically, the experimental apparatus include a weighing microbalance so weight loss during heating can be observed, indicating how far the reaction has progressed. This technique is the basis of the Thermogravimetric Analysis (TGA) that is widely used in laboratories. Prior to the experiment, inert gas is purged to the furnace to ensure no reaction takes place. Reaction time is started when this inert gas is switched to the reducing / oxidizing gas, so that the reactions will start immediately.

Some experimental arrangements include gas analyzer (Asaki *et al,* 1988), presented in Figure 17, so that the gas formed during the reaction can be analyzed. Analysis of the gas

in the experiment is vital in order to correctly conclude what reactions take place in the furnace. However, in order for this to work, gas flow to the system must be adequate, so that the gas outflow can be meaningfully analyzed. In Asaki's work, gas flowrate was set at 60 mL/min, so a reasonable amount of gas flow can be analyzed using the installed infrared analyzer. Experimental apparatus of Kawamoto (2016), presented in Figure 20, does not include such gas analyzer, mainly due to the low gas flowrate used (0.5 mL/min).

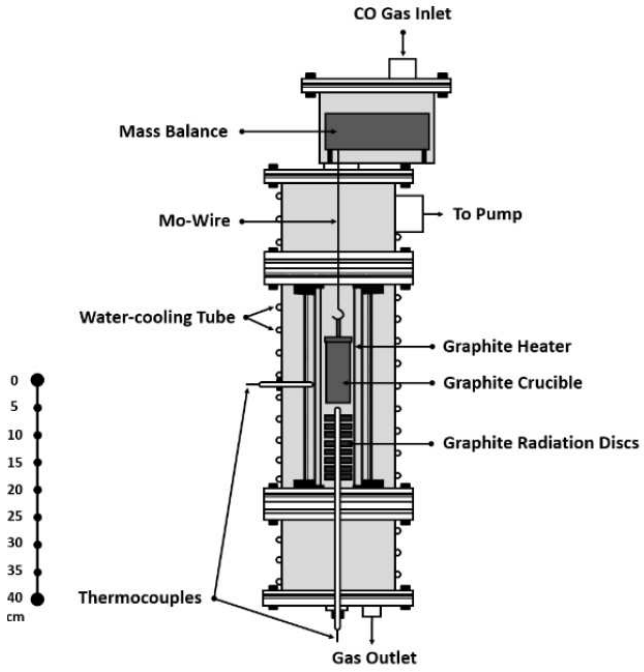

Figure 20. Experimental Apparatus of that Kawamoto (2016)

In his work, Kawamoto stated that since the gas was more or less used as a static atmosphere, recording of gas outlet was considered irrelevant. Therefore, he opted for the gravimetric analysis instead to collect the required kinetic data. Kawamoto assumed that only SiO_2 and MnO reduction reactions will take place, therefore the outlet gas consists only of CO gas resulting from the reduction reactions. Due to this assumption the need of gas analyzer is indifferent.

6.2. Multiphase Reaction Systems (Melt-Melt, Melt-Solid, and combinations thereof)

Another different reaction system includes gas flow and a multiphase specimen (solid-melt, melt-slag, and combinations thereof). In some cases the reaction system would not be affected by the gas flow (the gas flow is inert), nor it would produce any gas. These kinds of systems could be limited by the chemical reaction rate or the interfacial mass transfer between the different phases. Example of this kind of system is spinel inclusion

formation in molten steel-slag system, whose kinetics have been studied by Shin *et al* (2016). In the experiment, Shin used an inert argon gas, so the reaction would take place in an inert atmosphere. Experimental apparatus of Shin is presented in Figure 21.

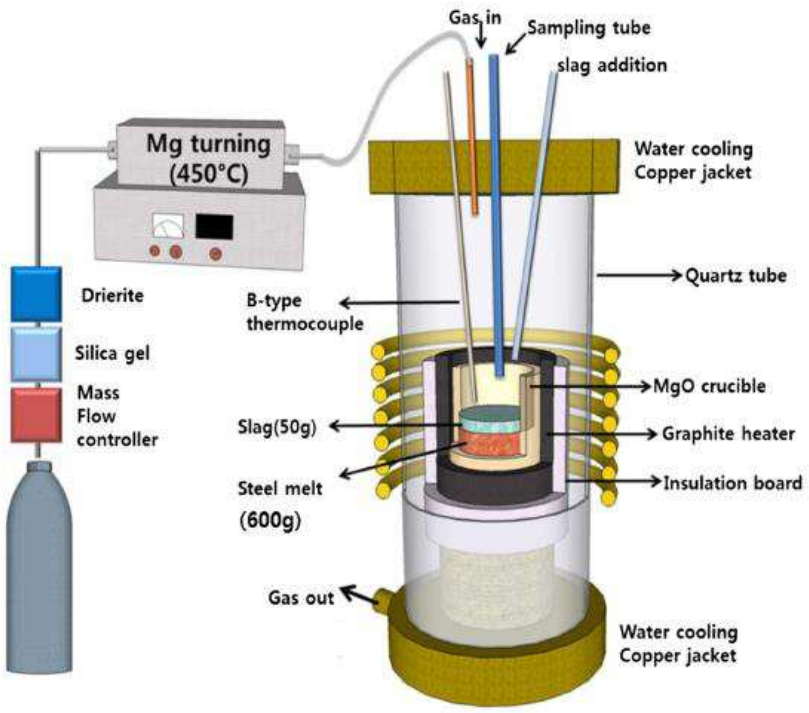

Figure 21. Experimental Apparatus of that Shin et al. (2016)

On the technical side, kinetic experiments for these multiphase systems often pose challenges, mainly due to controlling the time of the reaction. As both phases will immediately react if mixed together, a sample addition mechanism must be developed, in order to control exactly when the phases start to contact with each other and the reaction starts to proceed. Moreover, since the reaction that takes place would not change the mass (no gas formation is expected), evaluating how the reaction progressed through time is not straightforward. A sampling procedure must be done at certain periods of time, in order to analyze how the reaction progressed. The fact that both of these procedures (sample addition and sampling) must be done in a hot furnace makes this experiment more complicated.

In the experimental apparatus of Shin, showed in Figure 21, the steel melt was first placed in MgO crucible and heated in the furnace with an inert Ar atmosphere. After a certain period of time, when the steel was completely molten, pre-melted slag was introduced through a guiding quartz tube. The idea is that as soon as the slag is fed through this tube,

subsequently contacting the slag and molten steel, the reaction time was started. Additional quartz tube, filled with steel rod, was inserted to the furnace for sampling mechanism. Sampling was done after certain reaction periods by dipping the steel rod to the molten samples, then quenching it by immersion into brine.

Similar arrangement was also used by Park *et al* (2014), shown in Figure 22, in his study regarding SiO_2 reduction kinetic in SiO_2-Al_2O_3-CaO slag using Aluminum in Fe-Al melts. Mixtures of Fe-Al were melted initially in the furnace in an MgO crucible under argon atmosphere. The difference is that the slag was introduced to the liquid metal in the form of pellets, instead of molten slag like Shin *et al.* Although this technique is easier, it would take time for the slag pellet to melt while inside the crucible, therefore the exact reaction start time when both melts come into contact could not be determined. However, with reasonable pellet size, it can be assumed that the melting happens rapidly so it does not affect the overall reaction rate, and reaction start time could be taken when the slag pellet is fed to the reaction chamber.

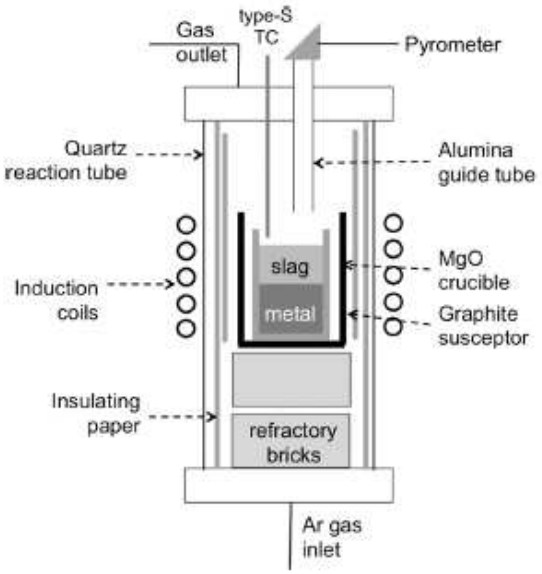

Figure 22. Experimental Apparatus of that Park et al. (2014)

In theory, melting time of a solid particle with constant size (such as slag pellets) can be determined by several trial experiments. This technique was adopted by Deng *et al.* (2014) in his study regarding lime dissolution in synthetic slags of FeO-SiO_2 and CaO-FeO-SiO_2 where pre-experiments were conducted to correctly determine the melting time of the slag particles. The pre-experiments consisted of heating the slag sample in the hot zone

of the furnace for different length of periods, and it was found that the slag sample would be completely molten after 10 seconds. Experimental apparatus of Deng *et al.* is shown in Figure 23.

As shown in Figure 23 (a), slag particles of around 2-3 mm in size were placed around the lime (CaO) particles in a platinum crucible, hung on a platinum wire. The reaction chamber was purged with inert Ar gas, and heated to the desired temperature of 1873 K. During this heating period, the crucible containing the lime and slag particles was hung outside the furnace hot zone, in order to prevent premature melting. Only after the desired temperature is reached, then the samples in the crucible was lowered to the hot zone, and kept there for 30 seconds. The idea was that the reaction would only start after the slag was molten, and subsequently brought in contact with the lime particles. Therefore, since the melting time of the slag is known to be 10 seconds, lime dissolution reaction time was taken after 10 seconds after the crucible was lowered to the furnace hot zone.

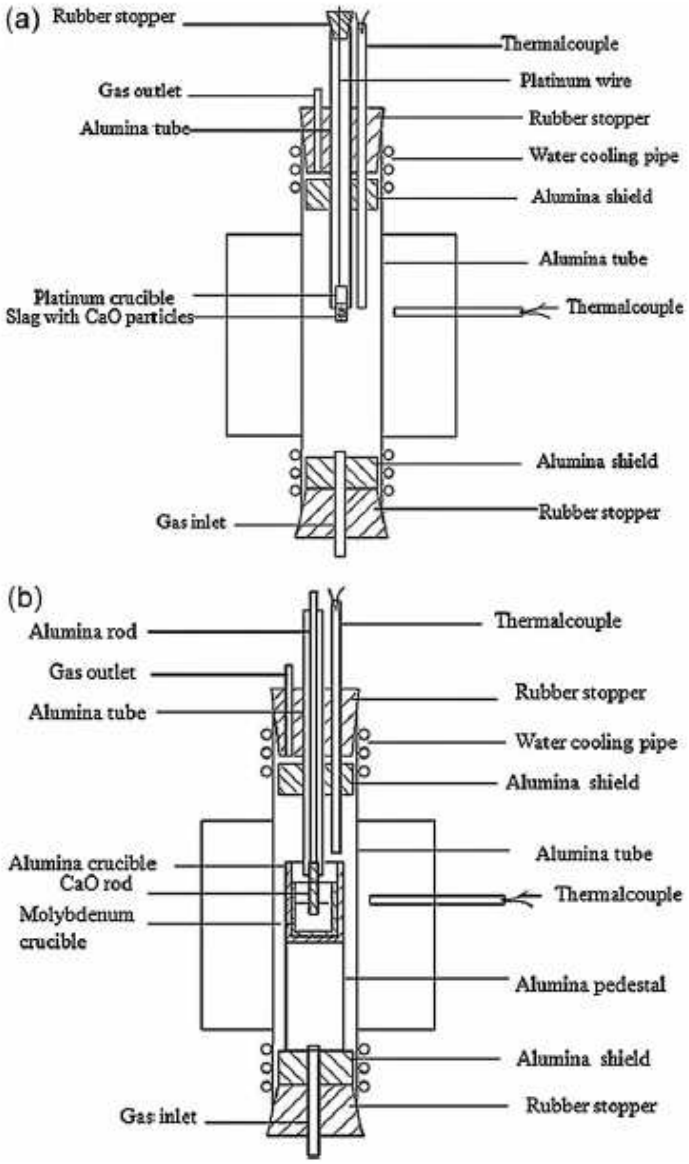

Figure 23. Experimental Apparatus of Deng et al (2014)

For comparison, Deng et al. also did another type of experimental setup, shown in Figure 23(b). In this type of setup, solid lime rods were used (10 mm x 10 mm cross section) instead of lime particles. Pre-melted slag was placed in the crucible, and heated in the hot zone of the furnace until it stabilized to 1873 K. After it reached its desired temperature, the lime rod was then lowered to just above the slag, and kept there for several minutes until it reach similar temperature with the slag. The lime rod was then introduced into the slag, and reaction time was started. After pre-determined reaction times, the lime rod was taken out and quenched in cold air. With these datasets after different reaction times, kinetic model was then derived for lime dissolution in slag.

Similar experimental technique to that of Figure 23(b) was utilized by Vardar and Eric (2008), in their studies regarding iron ore smelting in Fe-Cr-C-Si Melts, showed in Figure 24.

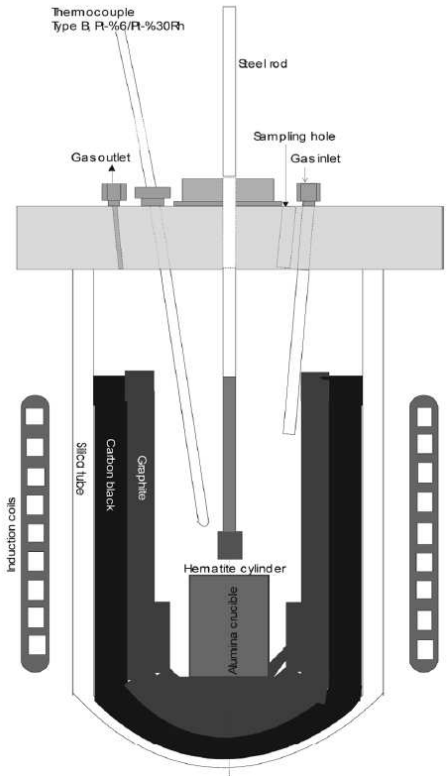

Figure 24. Experimental Arrangements of Vardar and Eric (2008)

Iron ore in the form of hematite powder was pressed (without using any binders) to form a briquetted hematite cylinder (L x D = 17.5mm x 15.5mm). This hematite cylinder is then sintered in air for 12 hours in a muffle furnace. To ensure no chemical change has happened due to the sintering, XRD analysis was conducted before and after sintering, and virtually identical diffractograms were obtained. The hematite cylinder was drilled from its top to about 5 mm deep, and alumina rod was inserted and fixed there using alumina cement.

The Fe-Cr-C-Si alloy was placed first in the alumina crucible into the reaction chamber, as shown in Figure 24. The hematite cylinder and its alumina rod were positioned around three cm above the alumina crucible. The furnace was then turned on and heated up to desired temperature of 1600^{o}C under argon gas flow, so that the alloy melted. Since the hematite cylinder was positioned around 3 cm above the crucible, the hematite cylinder was expected not to melt, as it was located outside of the furnace hot zone. Thermocouple

was placed near the hematite cylinder surface to ensure that the temperature does not exceed 1400^{o} C so that it is not going to melt.

After the desired temperature was reached, the hematite cylinder was lowered into the Fe-Cr-C-Si melt. Sampling was done by sucking the melt through a fused silica tube inserted through the sampling hole followed by quenching. Aside from that, the decrease of the hematite cylinder diameter was monitored as well to indicate the reaction progression. This was achieved by turning off the induction furnace, lifting off the hematite cylinder and leaving it cooled under the argon gas. The diameter of the cylinder was then measured and compared to the initial diameter. Melt samples were analyzed using SEM-EDS, while the hematite cylinders were sent to the SEM and XRD analysis.

In some other multiphase system modelling experiments, stirring mechanism was used to promote the contact between each phase. In their continuation study, Deng *et al.* (2012) used this stirring mechanism to study the mechanism of lime dissolution in slag, shown in Figure 25.

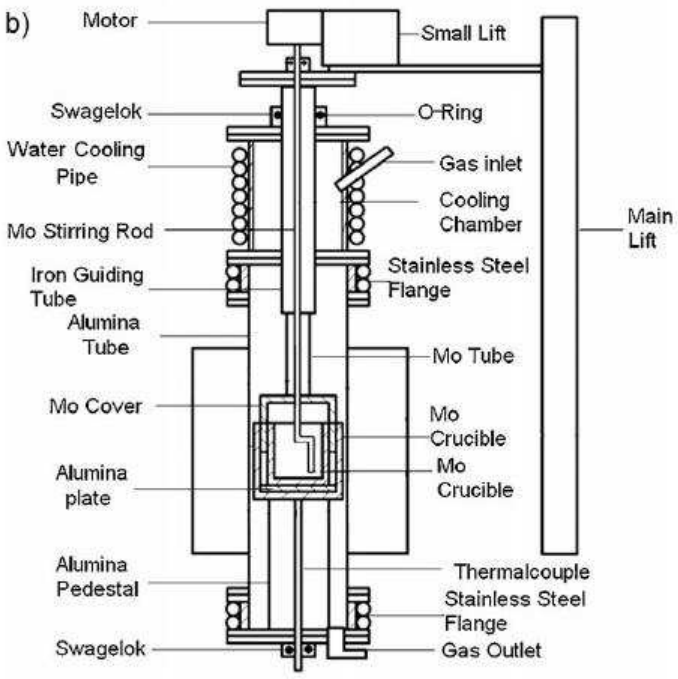

Figure 25. Experimental Apparatus of Deng et al (2012)

Experimental apparatus shown in Figure 25 is a development from their previous experimental setup shown in Figure 23. As shown in Figure 25, a quenching chamber cooled with water was integrated on the top side of the furnace. A stirrer made out of molybdenum was used, and it was connected to a small precision lift up top, so that the stirrer can be moved up and down vertically. The molybdenum crucible was placed in another Mo crucible holder and cover, so the sample could be stabilized during stirring. The main lift was also installed so that the crucible could be moved up to the quenching chamber as well as down to the different zone of the furnace.

In a normal experiment, lime particles were placed inside a crucible with slag particles surrounding them. The furnace was then heated up to desired temperature of 1873 K, whereas during this period, crucible containing the sample was suspended outside the furnace hot zone. After the desired temperature was reached, the sample was lowered to the furnace hot zone using the main lift. Benefiting from previous knowledge of slag melting time, reaction time was noted and stirring was started after the melting time. After pre-determined time, stirrer was stopped and lifted out from the sample, which took around 1-2 seconds. The whole crucible system was then quenched by lifting them to the cooling chamber using the main lift.

Yet another different technique which utilizes pressurized gas to feed the matte to the slag through a silica tube were used by Fagerlund (2000), and similarly Tahmasebi (2013), in their studies of copper matte formation and settling process in the slag. These techniques have already been described in a previous chapter of this work.

There are many different techniques in multiphase system modelling experiments. Different approaches are used by different investigators to control reaction time, as well as to obtain accurate data by reliable sampling techniques. Summary of these different techniques is given in Table 2.

Table 2. Summary of Different Techniques in Multiphase System Modelling Experiments

No.	Investigators	Reaction Time Control Mechanism	Data/Sample Collection Mechanism	Note
1.	Fagerlund (2000) Tahmasebi (2013)	Controlled by sample addition mechanism to the reaction chamber after desired temperature is reached	Quenching at different time intervals Analysis of image sequences using X-ray image transmission system CVPI technique	Solid sample (matte/chalcopyrite) is suspended in a fused quartz tube with small hole in a bottom, and introduced to the slag by charging the tube with pressurized gas (or just waited until it melts)
2.	Shin *et al* (2016)	Controlled by slag addition mechanism to the reaction chamber after desired temperature is reached	Dipping of steel rod to the samples and quenching it	Slag is introduced in form of melt through a guiding tube
	Park *et al* (2014)		Sampling using quartz tube (unclear)	Slag is introduced in form of pellet through a guiding tube
3.	Deng *et al* (2010) (a)	Controlled by determining slag melting time, in which initial reaction time is noted after this.	Several runs in different length of time	Slag and samples were introduced together to the furnace as solid particles
	Deng *et al* (2012)	Controlled by determining slag melting time, in which	Several runs for different length of time	Include stirring mechanism, initiated

		initial reaction time is noted after this.		after samples are completely molten
4.	Deng *et al* (2010) (b)	Controlled by immersion of briquetted / pelletized sample to the reaction chamber after desired temperature is reached	Several runs for different length of time	Dimension of briquetted samples are measured after each run
	Vardar and Eric (2008)		Sucking of samples through a silica tube	

In the present work, a multiphase reaction consisting of copper slag and matte is analyzed, and formation of SO_2 gas is also expected during the experiment, which make this system a gas-melt-melt system. Therefore, an optimum combination of these aforementioned experimental apparatus is essential in order to achieve accurate and reliable results.

PART II: EXPERIMENTAL PROCEDURE

Experimental arrangements and analysis used in this work are elaborated in this chapter, as well as the raw materials used.

7. Raw Material

Two primary raw materials were used in the experiments: synthetic slag and copper concentrate.

7.1. Slag

The slag used in this experiment was synthesized from a mixture of hematite powder (Alfa Aesar, 99.99% purity) and silica powder (Umicore, 99.99% purity), with the mass ratio of 65% Fe_2O_3 and 35% SiO_2. After mixing, the slag was synthesized by heating it in a furnace at the temperature of 1300^{o}C in air atmosphere. The slag samples were heated for a minimum of 8 hours, so that it could be given enough time to reach equilibrium. The resulting slag samples were then analysed with LEO 1450 (Carl Zeiss Microscope GmbH, Germany) Scanning Electron Microscope (SEM) equipped with Oxford Instrument X-Max 50 + INCA energy dispersive X-ray spectroscopy (EDS) analyser (Oxford Instruments plc, UK). The micrograph of the slag is shown in Figure 26.

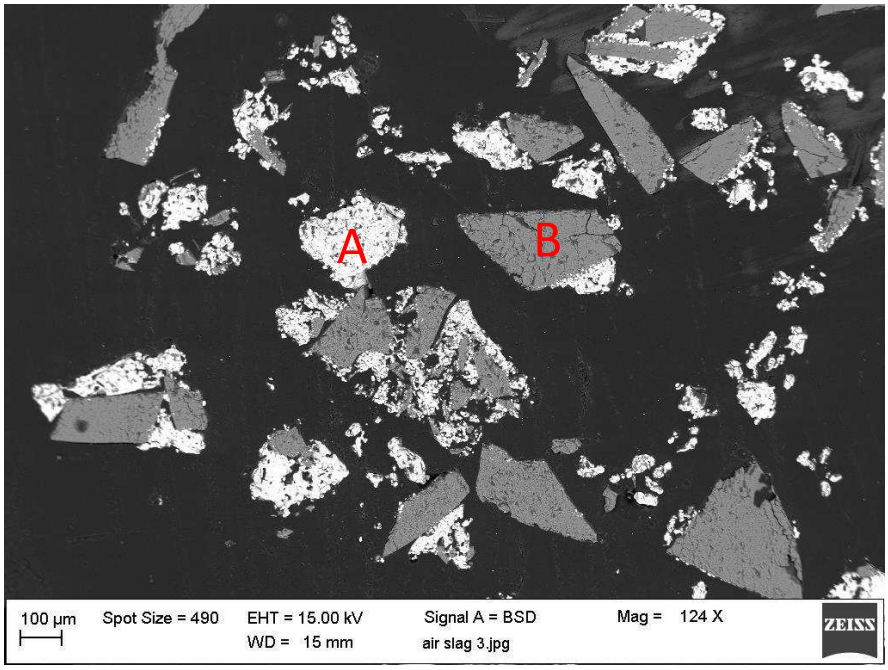

Figure 26. Slag Analysis with SEM, showing Iron Oxide (A) and Silica (B)

The slag remained in the solid form after heating in 1300°C for minimum 8 hours. Two distinctive phases were detected, the silica phase and the iron oxide phase. This result corresponds well with phase equilibria calculation for Fe_2O_3-SiO_2 system that have been studied by Laughlin *et al* (2014) shown in Figure 27.

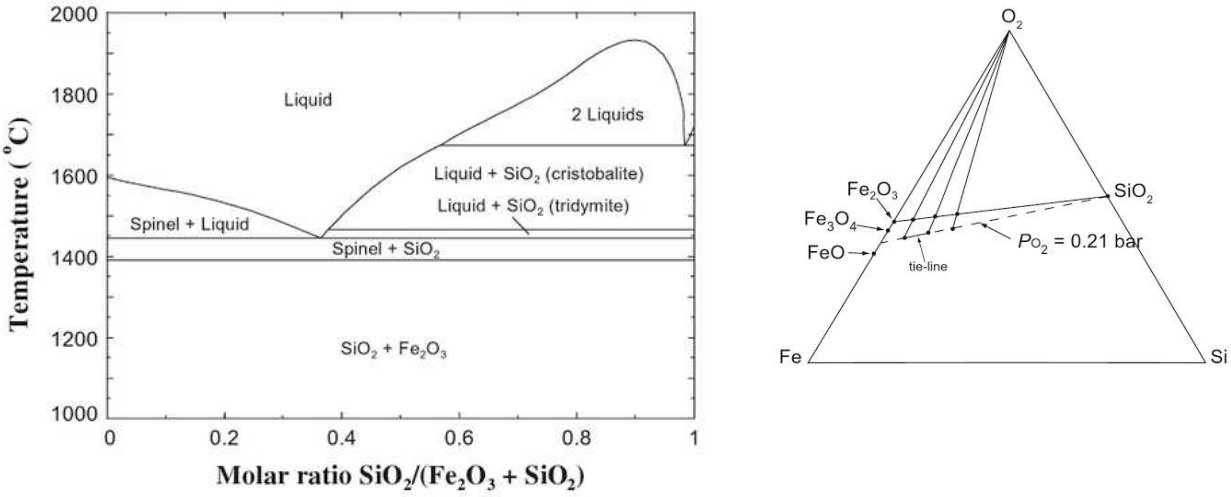

Figure 27. Phase Equilibria of Fe_2O_3-SiO_2 System in Air (left) and Ternary Phase Diagram of Fe Si O (right) (Laughlin and Hono, 2014)

It is important to note that Figure 27 (left) is not a binary phase diagram; it is actually a ternary section along constant P_{O_2} from the ternary phase in the Figure 27 (right). This means that while the molar ratio of SiO_2 / (Fe_2O_3 + SiO_2) is given, the total composition of these phases (SiO_2 and Fe_2O_3) in the whole Fe-Si-O system is not given. This is due to the fact that some of the Fe may also be present in the phase as FeO or Fe_3O_4, as shown in Figure 27 (right). This was confirmed in the EDS analysis (shown in Appendix A.1. EDS Results), where the iron oxide phase does not resemble Fe_2O_3, FeO nor Fe_3O_4, as it is rather a mixture of these three iron oxide phases.

7.2. Concentrate

The concentrate powder was obtained from Outotec Research Centre in Pori, Finland. The chemical analysis of this concentrate powder is given in Table 3, while the mineralogy of the concentrate is given in Table 4.

Table 3. Chemical Composition of the Concentrate Powder

Chemical composition		
Cu	**%**	27
Fe	**%**	27.2
Zn	**%**	0.18
Mo	**%**	0.27
Mn	**%**	0.008
Co	**%**	0.014
Ni	**%**	<0.005
As	**%**	<0.005
Cd	**%**	<0.005
Sb	**%**	<0.005
Pb	**%**	<0.05
Bi	**%**	<0.005
Na	**%**	0.15
Mg	**%**	0.17
Al	**%**	0.78
K	**%**	0.29
Ca	**%**	0.4
Cr	**%**	0.01
S	**%**	29.8
SO4	**%**	0.64
C	**%**	0.18
Au	**ppm**	2.24
Ag	**ppm**	71.1

Table 4. Mineralogy of the Concentrate Powder

Mineral composition		
Chalcopyrite	**%**	78.0
Pyrite	**%**	4.3
Sphalerite	**%**	0.3
Molybdenite	**%**	0.5
Quartz	**%**	7.9
Feldspar	**%**	3.5
Muscovite	**%**	1.2
Hematite	**%**	1.6
Butlerite	**%**	1.4
Dolomite	**%**	1.4
Hessite	**ppm**	113.2
Gold	**ppm**	2.2
Total		100

Although the chemical and mineralogical analysis of the concentrate have already been done, SEM-EDS of this concentrate was done again for reference. The SEM image of the concentrate is given in Figure 28.

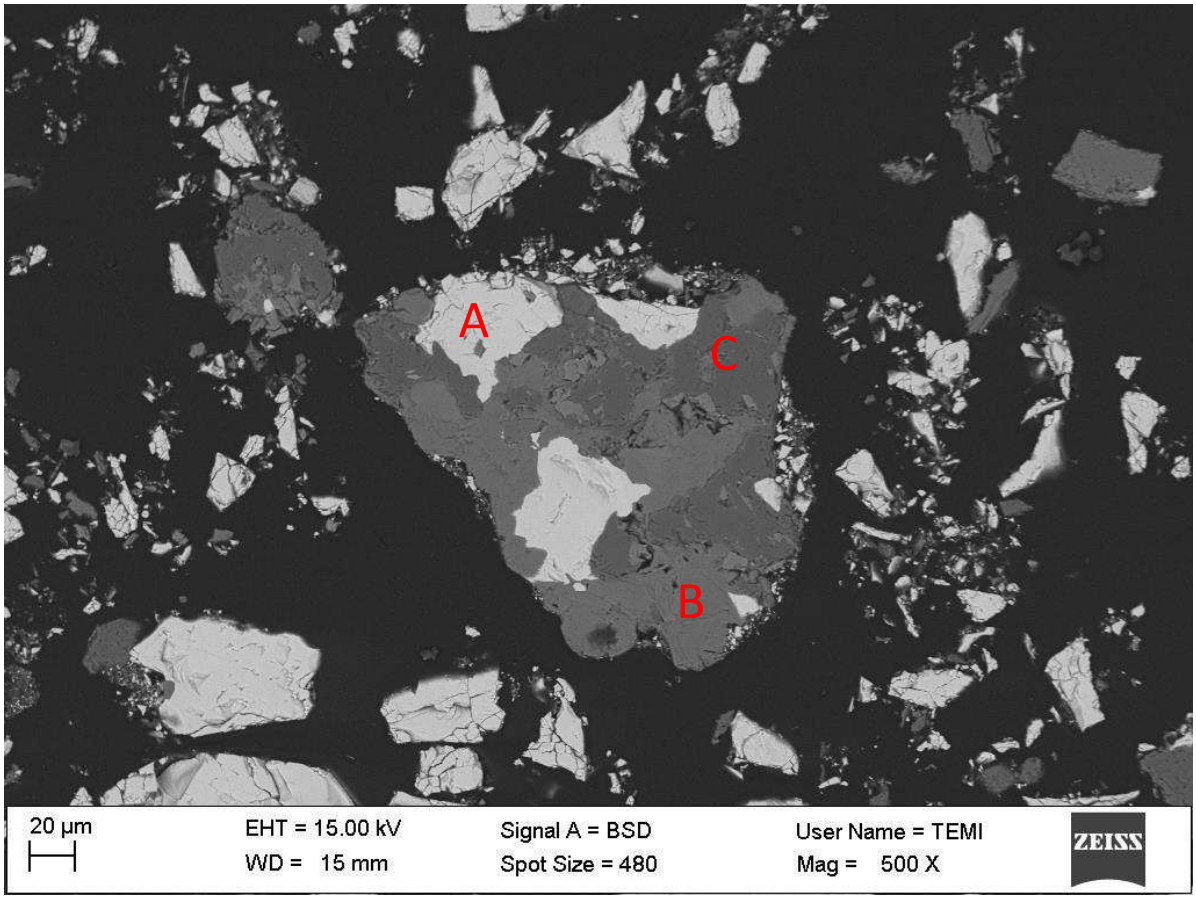

Figure 28. Micrograph of the Concentrate Specimen, showing Chalcopyrite (A), Gangue (B), and Silica (C)

Three major phases of minerals were detected, which are chalcopyrite, silica (quartz), as well as gangue minerals. Most of the concentrate were liberated into their respective minerals, although some remain unliberated, as it can be seen in Figure 28 where the three minerals chalcopyrite, gangue minerals, and silica are within one solid particle (More of this micro-image can be found in Appendix A.2. SEM Images). The gangue minerals mostly contain Ca, Al, Si, and Fe. It is expected that these elements would end up in the slag phase after contacting experiments.

7.3. Slag-Concentrate Sample Preparation

The slag-concentrate mixture was prepared to contain 22 wt% silica, which will bring the system to be above the silica saturation point. As it can be seen in Figure 10, for 57 wt% FeS (which corresponds the concentrate used in this experiment), the system will be silica-saturated if it contains minimum around 12 wt% silica. Nevertheless, the use of silica crucible would also mean that there would be more than enough silica for the system to saturate it, as it could also react with the mixture during contacting process.

The oversaturation with silica was needed to ensure the matte and slag in the mixtures could effectively be separated during contacting at high temperature. In industrial smelting process, overfeeding of silica is unwanted, since silica tends to polymerize when it is melted, therefore increasing the difficulties in slag handling (Schlesinger *et al*, 2011). However, since only small amount of sample was used during laboratory experiments, slag handling would not pose a major problem.

The fluxing ratio (SiO_2/Fe) of the mixture is calculated to be 0.89. This value corresponds well to the typical fluxing ratio used in flash smelting, whereas according to Schlesinger, *et al.* (2011), the SiO_2/Fe ratio in a typical Outotec flash smelting furnace falls between the range of 0.7 – 1.0.

8. Main Experimental Procedure

The schematic of the furnace used in the present work is shown in Figures 29 and 30.

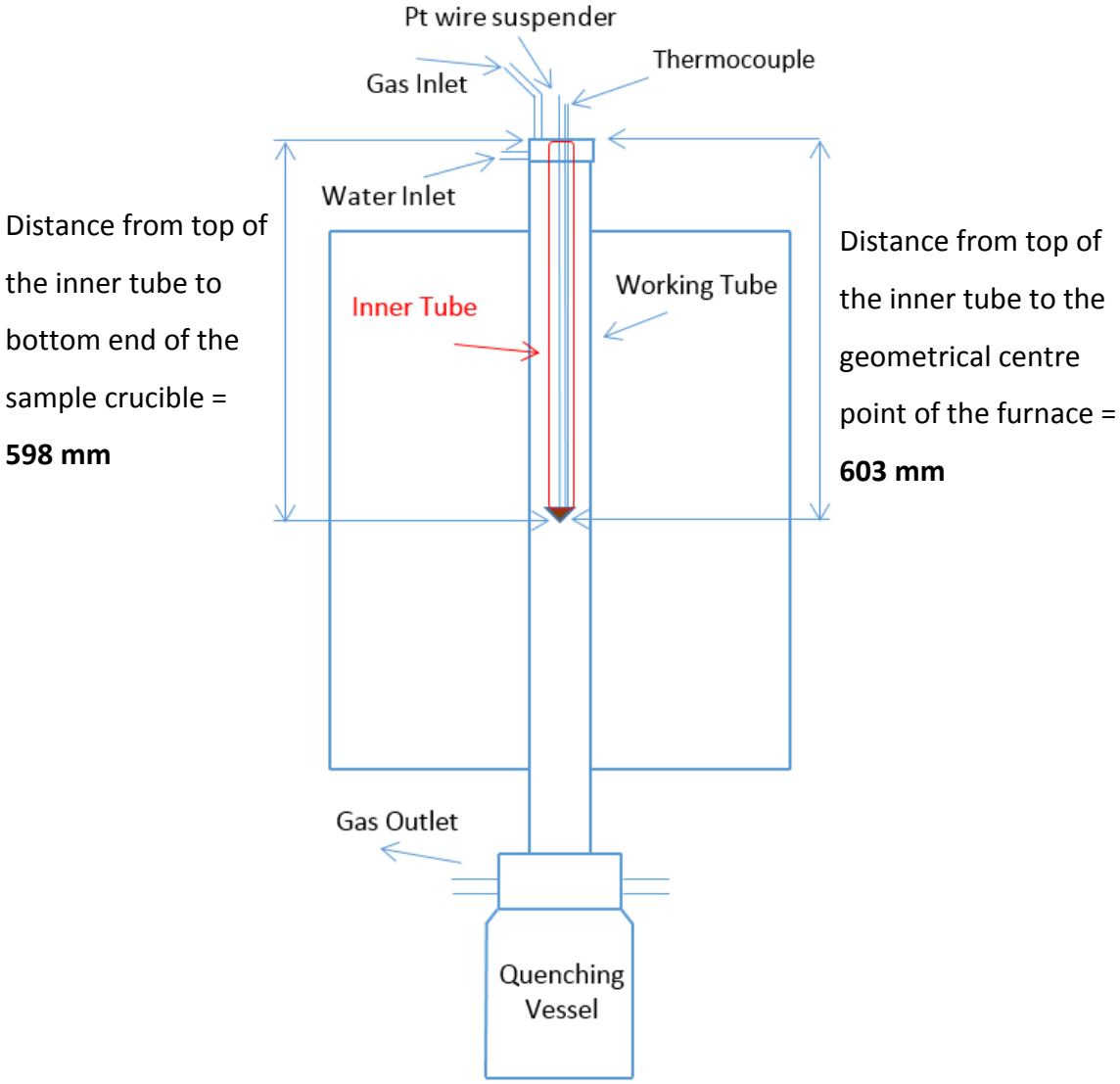

Figure 29. Experimental Furnace Scheme

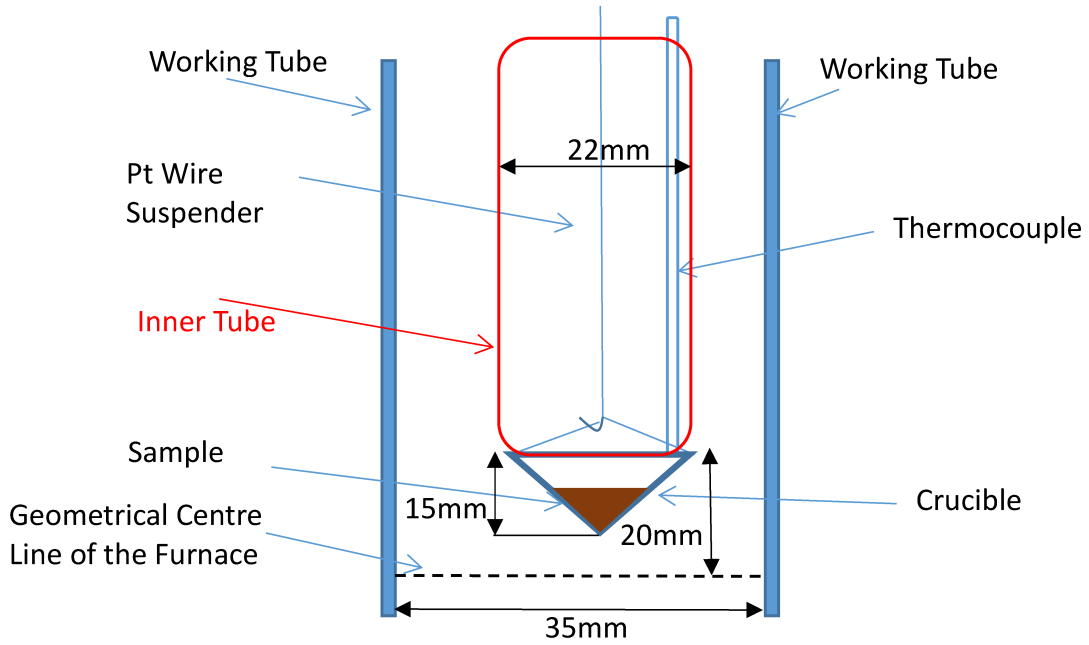

Figure 30. Close up of the Crucible inside the Furnace

The vertical tube furnace (Lenton LTF 16/450) is equipped with four silicon carbide (SiC) heating elements. An alumina working tube with 35 mm inner diameter (Friedrichs feld AL23, Germany) was placed inside the furnace. Then, a smaller alumina tube (22 mm inner diameter) was inserted inside the working tube, which for the sake of simplicity will be referred to as the inner tube in the present work. Both tubes were connected to a metal lid equipped with two small holes, enabling the insertion of thermocouple protective alumina tube (Friatec Keramik, Germany) and Pt suspension wire. The thermocouple tube placement relative to the sample crucible is shown in Figure 30. The furnace lid was also equipped with water cooling system. Temperature of the furnace is controlled using a Eurotherm PID controller. In addition, temperature in the hot-zone of the furnace is constantly monitored using S-type Pt/Pt-10Rh thermocouple (Johnson-Matthey Noble Metals, UK). The voltage measurement output of the thermocouple was monitored with a Keithley 2000 DMM multimeter (Keithley, USA). A PT100 resistance thermometer (SKS-Group, Finland) was connected to a Keithley 2010 DMM multimeter as a cold junction compensation. Temperature data was logged with LabVIEW software. The sample crucible is made from quartz (Finnish Special Glass, Finland), and the cone shape is chosen so that materials would accumulate in the bottom of the cone, so contact between materials could be enhanced. The cone crucible dimensions are shown in Figure 30, with its diameter being the same as the inner tube, so that it could not be lifted further upward

after it reached the bottom mouth of the inner tube. Since the position of the inner tube is fixed against the furnace, the sample would be located roughly 5 mm above the geometrical centre point of the furnace. Quenching vessel was filled with ice water.

8.1. Furnace Temperature Profile Measurements

Prior to the experiments, temperature profile of the furnace was measured to fully understand the furnace behaviour. The furnace temperature was profiled at 1300°C around the geometrical centre point of the furnace. It is expected that the furnace hot zone would be located close to this geometrical centre point. The temperature profile of the furnace is shown in Figure 31.

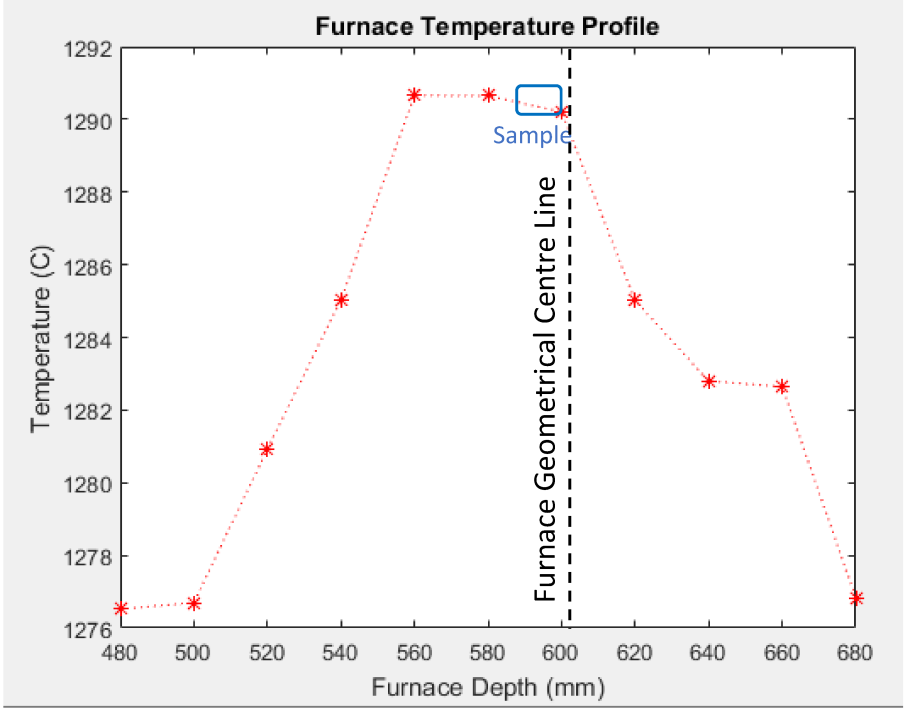

Figure 31. Furnace Temperature Profile

Figure 31 shows that the hot zone of the furnace, where the temperature is at highest and relatively constant, is between 560 – 600 mm from the top of the inner tube. The profile indicates that the furnace hot zone extends roughly 40 mm above the geometrical centre line. Regarding the sample placement, as the current set-up makes the sample located between 583 – 598 mm, or roughly 20 mm above the geometrical centre point which is still within the furnace hot zone. Therefore, it was concluded that the set-up is correct and the whole body of sample should be located within this hot zone.

8.2. Air Atmosphere Experiments

In the first experiments, natural draft air atmosphere was used. The furnace was heated so that the thermocouple reading could reach the desired temperature, which is 1300^{o}C. 0.5 grams of sample was then introduced to the crucible, followed by hooking the crucible to a Pt-wire used to suspend it. After the desired temperature was reached, the crucible was lifted until it touched the bottom mouth of the inner tube, which is located 20 mm above the furnace geometrical center point. The samples were melted for several different time intervals, in order to observe the matte formation and separation progression. In each experiment, after the desired time interval had passed, the sample was immediately quenched, by pulling the suspending wire to break the connecting hook, so that the sample dropped downward to the quenching vessel filled with ice water. The quenched samples were then cross sectioned and mounted in epoxy resin for subsequent SEM-EDS analysis.

8.3. Inert Atmosphere Experiments

Using the same experimental arrangements and same temperature setting of 1300 ^{o}C, another set of experiments were conducted using protective Ar gas (purity ≥99.999%) atmosphere. The Ar gas flow was controlled with a rotameter (Aalborg 052-01-SA, USA). The crucible containing the sample was hooked to the suspended Pt wire, and lifted up slightly so that it rested at the lower side of the furnace, far below the hot zone. The bottom opening of the furnace working tube was closed with a plug, so the furnace was gas tight, except for the gas outlet. Knowing the furnace working tube dimensions (Diameter 35 mm, Length 1206 mm), the required argon gas flow rate and time to purge away the remaining air inside the furnace could be calculated. Gas flow was set to 200 mL/min, so with known furnace volume, a minimum of 6 minutes argon gas purging is required.

A bubbler tube filled with tap water was connected to the gas exit stream, in which bubbles would be formed if the furnace was over-pressured. After sufficient purging for several times, the gas flow was reduced to around 50 mL/min, so that the superficial velocity of the gas flow would not flush away the concentrate samples from the crucible. The sample-containing crucible was lifted up to the hot zone, and as soon as it reached

the hot-zone, reaction time was noted. The quenching was done in such a way that the bottom part of the furnace was completely immersed in the ice water. When the sample was about to be quenched, the bottom plug of the furnace was opened carefully while keeping it immersed in the ice water. The ice water would function as a barrier minimizing air diffusion into the furnace through the bottom opening of the furnace, so that the inert atmosphere inside the furnace could be maintained. The quenched samples were cross sectioned and mounted in an epoxy resin for subsequent SEM-EDS analysis.

8.4. Key Aspects in the Experimental Procedure

Some of the key aspects of the experimental procedure in the present work are as follows:

- The starting time of the reaction was taken as the time crucible reached the hot zone, and the ending time when the crucible was quenched. To some extent, this could be affected by mechanical issues such as how quickly the crucible was lifted, the suspending wire getting stuck or jammed, etc. However, in the case of everything going smoothly, the accuracy of this procedure should be within 1-2 seconds.

- The starting mixture used is a homogenous mixture of chalcopyrite and synthetic slag. Although it was discussed earlier in subsection 6.2 that sample addition/contacting mechanism is desired, it was proven that it is difficult to do so in the present work. Therefore, it was assumed that due to small amount of mass used (0.5 gram) reactions would start right away, as melting of this amount of sample would take milliseconds.

- Due to the additional complication of the quenching process in inert atmosphere experiments, experiments less than 5 minutes were difficult to conduct. Carefully removing the furnace plug while maintaining it to be immersed in ice water was quite challenging and time consuming. This preparation for quenching already took 1-2 minutes. Therefore, 5 minutes were taken as the minimum contacting time in the experiments in inert atmosphere.

- It is also worth noting that in the present work, different experiments are done in different time intervals to produce an overall time-dependent behaviour of the sample. This will create a condition in which the samples are statistically independent from each other. It is critical to maintain the reproducibility of the experiments, so that the correlation between each samples could be deduced accurately.
- Cross sections of the samples are mostly made vertically, so all layers of the matte and slag can be examined. In the case of crucible breakage, samples from different parts of the crucible are taken for analysis to ensure representative samples.

9. Results and Discussion

In this chapter, the results of the experiments are elaborated, including the experiments in air and inert atmosphere. The initial results of PCB addition to the mixture are also elaborated. Most of the micro-images presented in this chapter are those which best represents the sample, while all of the other micro-images are presented in the Appendix A.2. SEM Images. Finally, the reaction sequences and limiting factors involved are also discussed in this chapter.

9.1. Contacting in Air Atmosphere

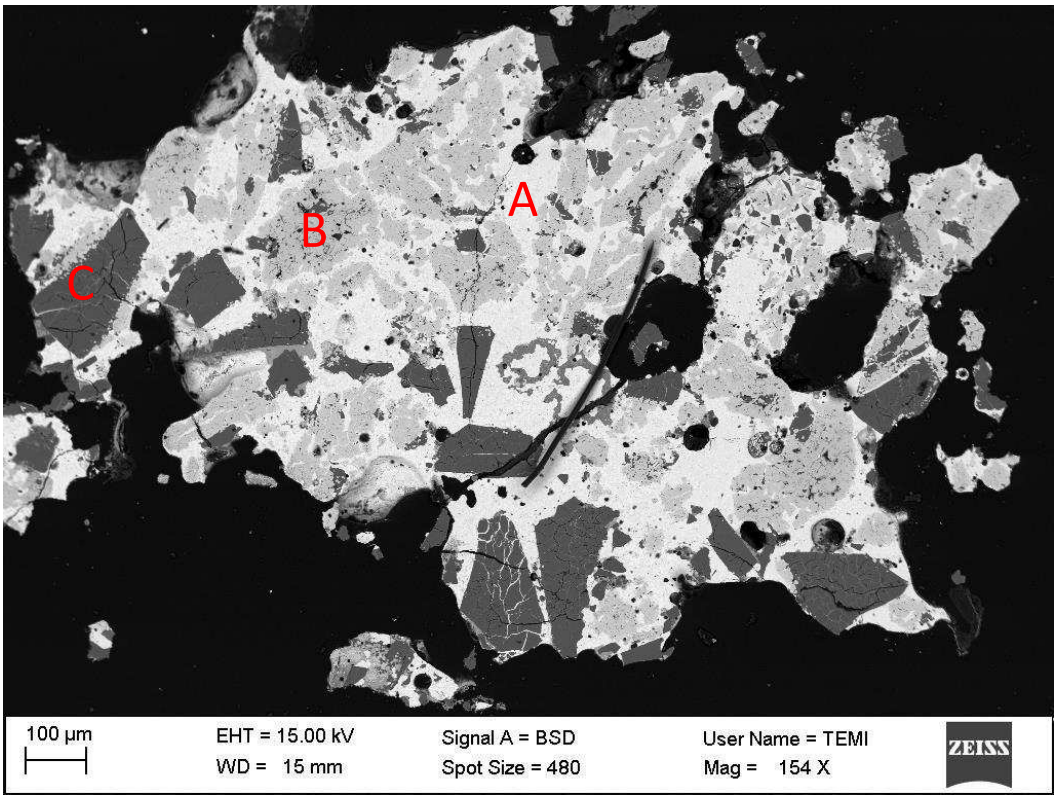

Figure 32. Micrograph of the Specimen after 10 Seconds Contacting Time, showing Matte (A), Magnetite (B), and Silica (C)

After just 10 seconds of contacting time, matte was already observed in the sample. This is mainly due to the rapid oxidation kinetics of the sulfidic concentrates through reaction (6) and (7).

$$5CuFeS_2 \rightarrow Cu_5FeS_4 + 4Fe_{1-x}S + 4\,x\,Fe + 2S \quad (6)$$

$$2Cu_5FeS_4 + O_2 \rightarrow 5Cu_2S + 2FeS + SO_2 \quad (7)$$

Magnetite was also already observed in the sample, suggesting the progression of magnetite forming reactions (reaction 8 and 9).

$$3Fe + 2O_2 \rightarrow Fe_3O_4 \quad (8)$$

$$3FeS + 5O_2 \rightarrow Fe_3O_4 + 3SO_2 \quad (9)$$

Fayalite slag was also observed to some extent at some part of the sample, while at some other part of the sample, like in Figure 32, no slag was observed, just magnetite. Nevertheless, the results support the idea of slag formation through magnetite formation, in which the iron would be oxidized first into magnetite through reactions (8) and (9), then, due to the present of silica, it would subsequently form fayalite slag (Fe_2SiO_4) through reactions (10), and/or through 2 stages of Reaction (11) and (5)

$$3Fe_3O_{4(s)} + FeS_{(matte)} + 5SiO_{2(s)} \rightarrow 5(Fe_2SiO_4)_{slag} + SO_{2(g)} \quad (10)$$

$$3Fe_3O_{4(s)} + FeS_{(matte)} \rightarrow 10FeO_{(s)} + SO_{2(g)} \quad (11)$$

$$FeO_{(s)} + SiO_{2\,(s)} \rightarrow FeO - SiO_{2(slag)} \quad (5)$$

Reaction (10) is basically the combination of both Reactions (11) and (5), in which magnetite oxidizes FeS in matte into FeO solid, followed by reaction between FeO and SiO_2 to produce fayalite slag.

The observation of holes in Figure 32 indicates the progression of SO_2 gas formations. The matte formed after this contacting time also contained a considerable amount of iron. This indicates that the iron components in matte have not been fully oxidized into magnetite and slag phase, and at longer contacting time it was expected that the iron content in the matte would decrease. Silica solids were also present, confirming the oversaturation of the sample with silica.

One last thing to note is that the matte and slag were still rather randomly distributed throughout the sample. This suggests that the separation and settling process of matte through the slag layer had not taken place yet.

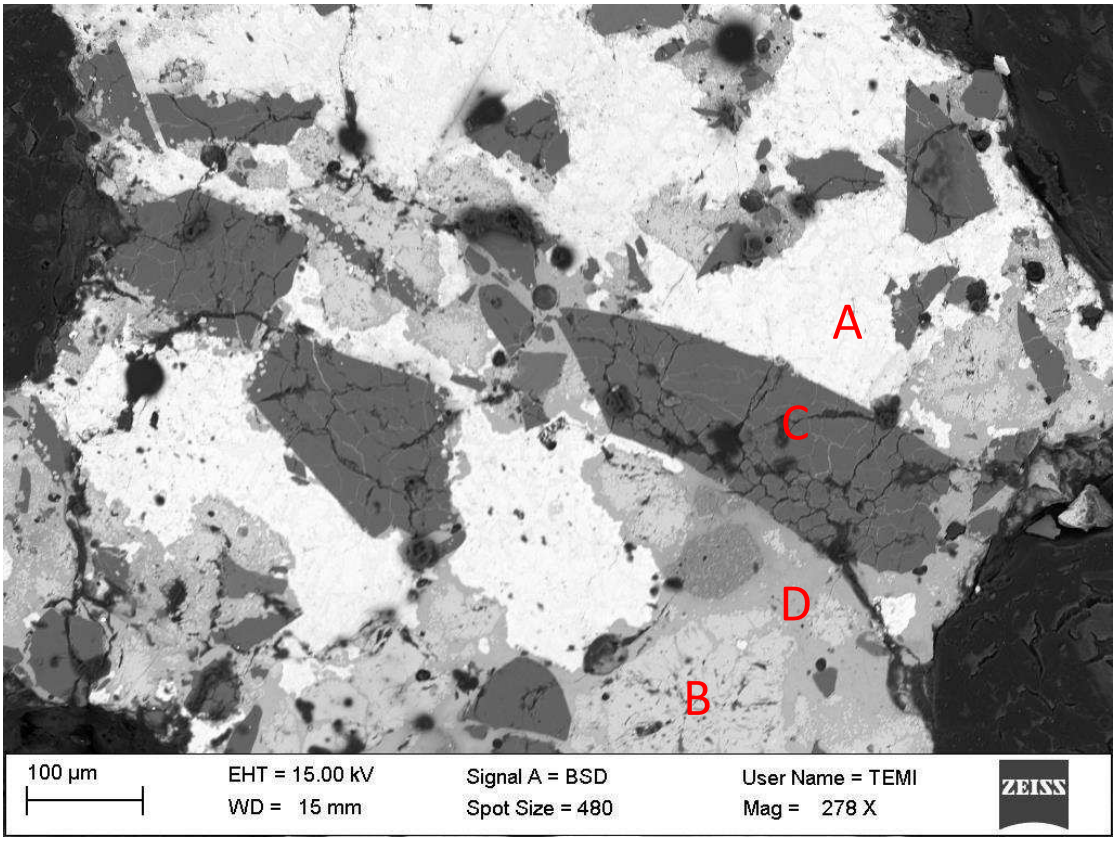

Figure 33. Micrograph of the Specimen after 20 Seconds Contacting Time, showing Matte (A), Magnetite (B), Silica (C), and Fayalite Slag (D)

Compared to the sample from 10 seconds of contacting time, no significant difference was observed after 20 seconds of contacting time, as shown in Figure 33. Magnetite is still prevalent, while fayalite slag is still limited in the sample. Matte was again rather randomly distributed in the sample, suggesting that the separation and settling process of the matte had not started yet.

The prevalence of magnetite in Figures 32 and 33 shows that the slag formation reactions (reactions 10 and 12) were still limited. While oxidation reactions and magnetite forming reactions (reactions 8 and 9) were taking place rapidly, the subsequent slag forming reactions were relatively slower. The most possible explanation is that there exists a mass transport limitation, as slag forming reactions are primarily reactions between solid magnetite, iron components in liquid matte (Fe and FeS), and solid silica particles (no gas involved). Since Fe_3O_4 is formed from oxidation of FeS in reaction 9, the contact between FeS and Fe_3O_4 should also happen instantly. Therefore, it is thought that the silica mass transport is the one that limits the slag forming reactions.

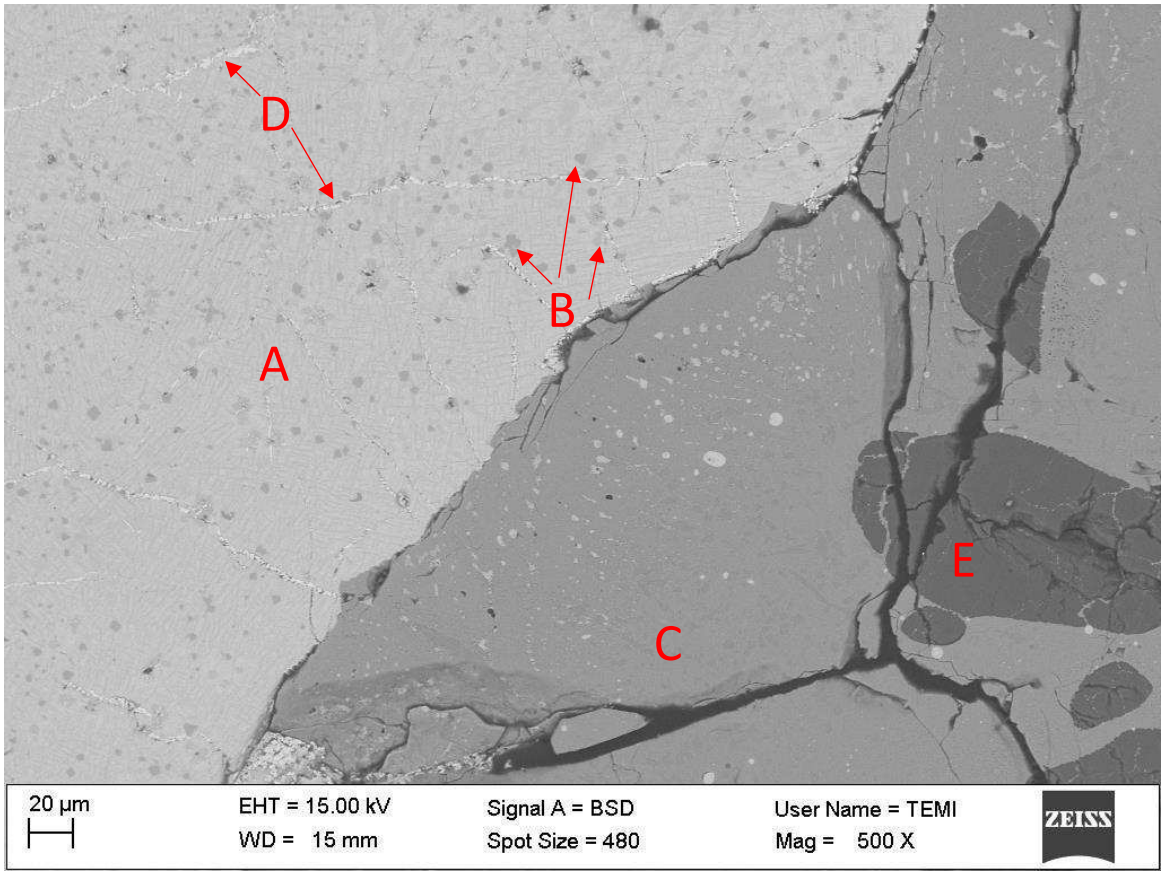

Figure 34. Micrograph of the Specimen after 30 Seconds Contacting Time, showing Matte (A), Magnetite Precipitates (B), and Fayalite Slag (C), Cu-rich veins (D), Silica (E)

Figure 34 shows that after 30 seconds of contacting time, fayalite slag becomes more prevalent, suggesting the progression of slagging through reactions (10) and (12). This is further confirmed by the lack of magnetite in the sample, in which would react with silica to produce fayalite slag.

Taking a closer look at the matte, it can be seen that there are some magnetite precipitates in the matte phase. The magnetite precipitates are thought to be formed through reaction (9), in which FeS in the matte is oxidized into magnetite.

The needle-like structure observed in the matte is associated with the cooling of the samples, because rapid cooling (such as in quenching) would often result in such structure, as it has been experimentally found by Fan *et al* (2014). The observation of copper veins in the sample is also associated with the cracks formed during quenching (Hidayat *et al,* 2016).

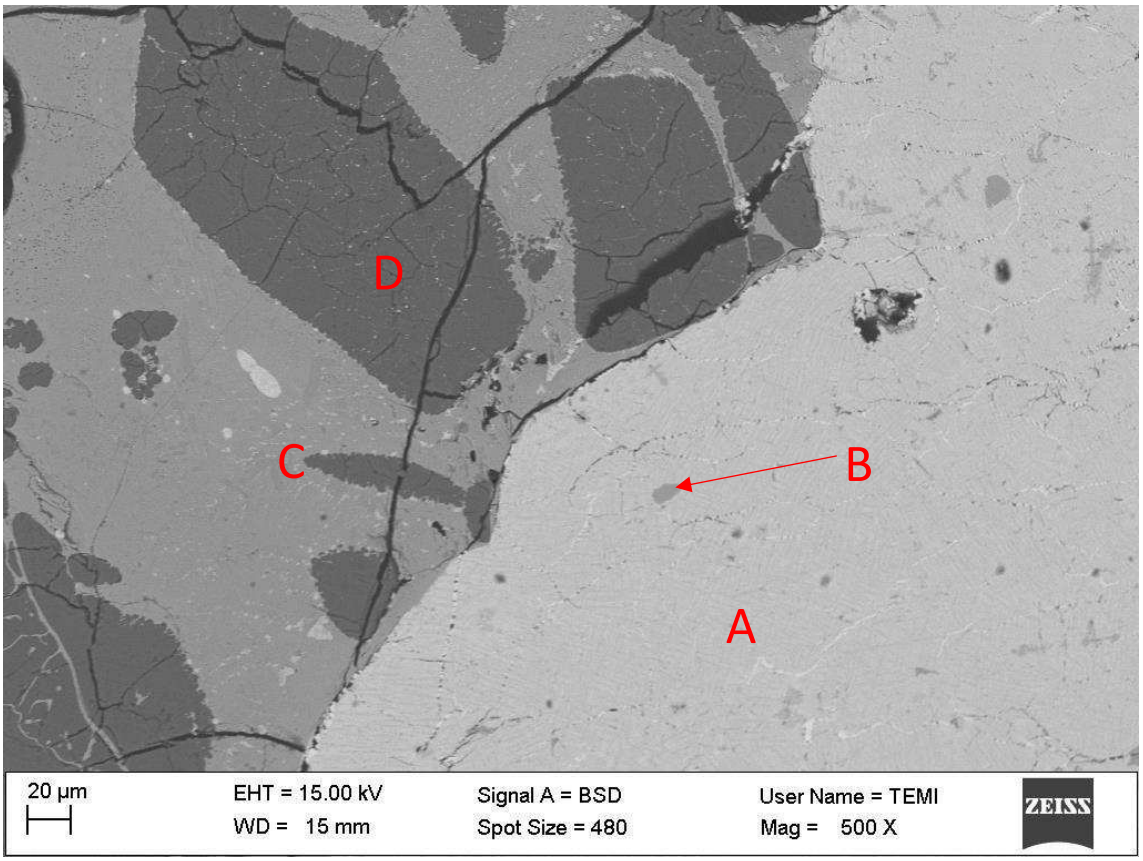

Figure 35. Micrograph of the Specimen after 60 Seconds Contacting Time, showing Matte (A), Magnetite Precipitates (B), Fayalite Slag (C) , and Silica (D)

Compared to the sample after 30 seconds of contacting, only minor difference was observed in the sample after 1 minute of contacting time, as shown in Figure 35. The microstructure of the matte was still similar to the previous sample, which suggested that the microstructure was developed during the quenching process (it has nothing to do with the settling and separation process of matte and slag). Magnetite precipitates in the matte began to disappear, as it would ultimately react with silica to form fayalite slag.

Moreover, as seen from Figures 34 and 35, it should be noted that after 30-60 seconds, the matte was more or less isolated from the slag phase. This suggested that during this time, separation between matte and slag had progressed.

Upon closer observation of Figure 35, some small amount of impure metallic copper, often termed as white metal in the industry (Schlesinger, 2011), is observed, as shown in Figure 36. These white metal areas have different morphology compared to the Cu-rich veins that was formed during quenching (shown as D in Figure 34). These white metal

areas are characterized by having a relatively low Fe content (around 5%) and low S content (less than 5%). Although the term white metal in the industry often associated with impure Cu_2S with especially low Fe content (less than 1%), it still can be viewed that the composition of these impure Cu_2S found in the samples still resemble that of white metal. The white metal areas in the sample was thought to be formed from further oxidation of FeS in the matte through reaction (9), as well as partial desulfurization through reaction (20) (Peretti, 1948). The complete elemental composition of this sample is given in Appendix A.1. EDS Results.

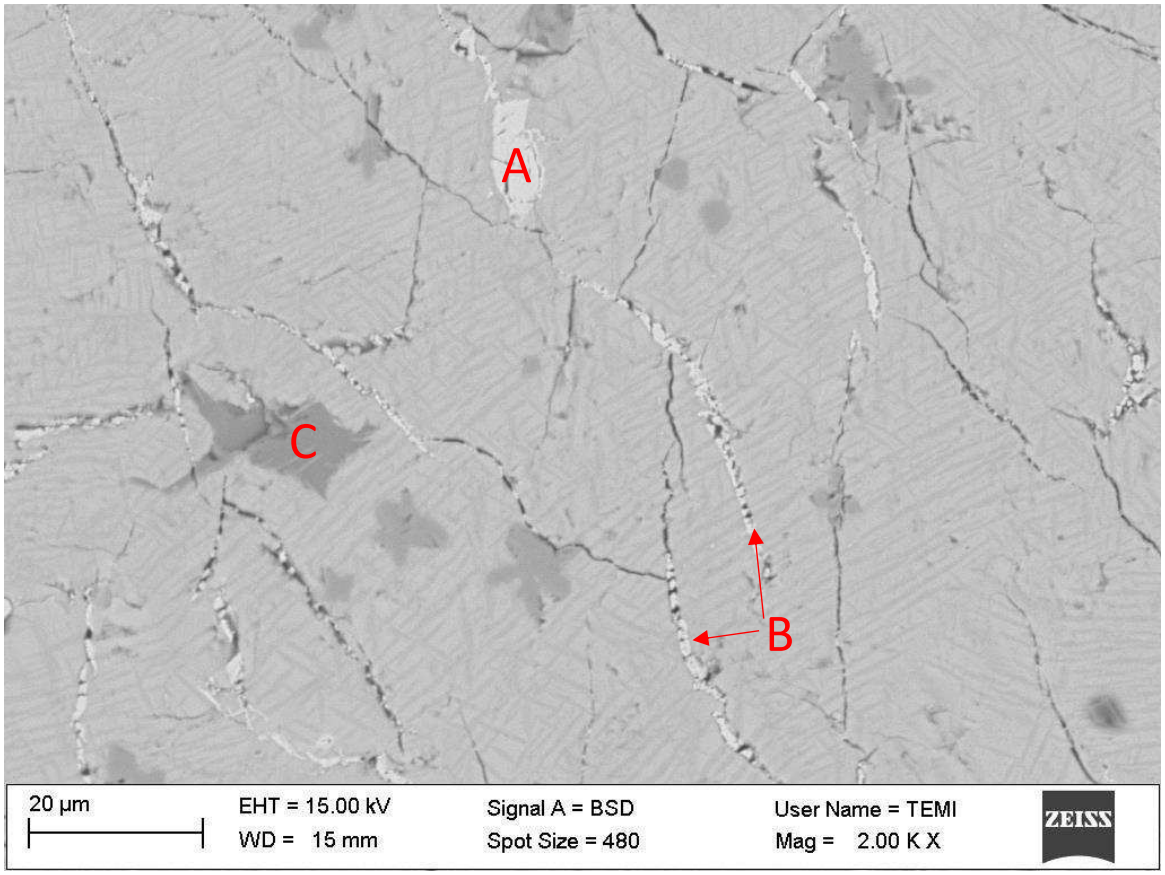

Figure 36. Closer Observation of Figure 35, showing Impure White Metal (A), Cu-rich Veins (B), and Magnetite (C)

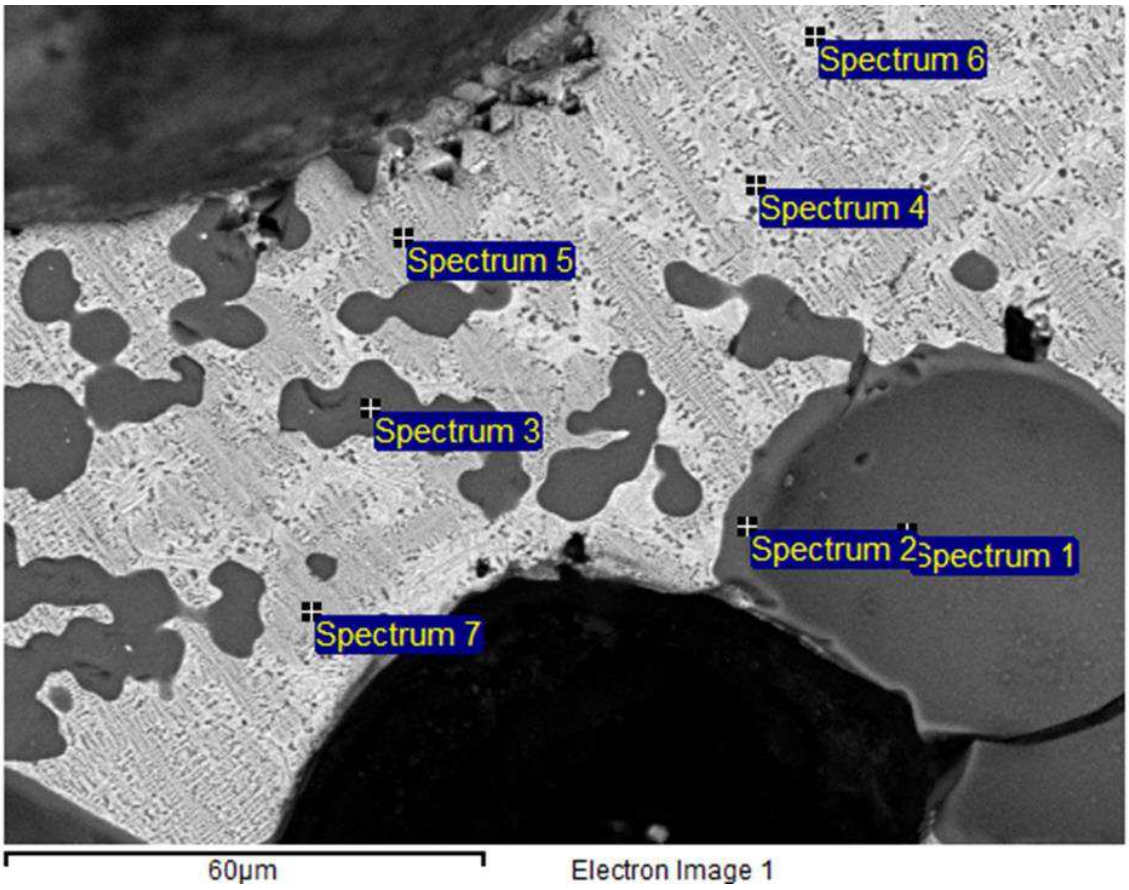

Figure 37. Micrograph of the Specimen after 5 minutes Contacting Time, showing Cu-rich oxide phase (spectrum 4 and 6), Fe-rich oxide phase (5 and 7), and Silica (1,2,3)

After 300 seconds or 5 minutes of contacting time, no sulphides were observed in the sample in Figure 37. Initially, FeS will be preferentially oxidized. Cu_2S will start to oxidize only when the Fe content in the matte is lower than 1%, while substantial oxidation of copper only starts when Cu_2S is almost devoid of sulphur, somewhere in the level of 0.001 – 0.03% S (Schlesinger, 2011). This phenomena is the principle in copper converting process, which is governed by reactions (2), (15) and (30).

$$Cu_2S_{(l)} + 1.5O_2 \rightarrow Cu_2O_{(slag)} + SO_2 \quad (2)$$

$$Cu_2S_{(l)} + 2Cu_2O_{(slag)} \leftrightarrow 6Cu_{(l)} + SO_{2(g)} \quad (15)$$

$$Cu_2S_{(l)} + O_2 \leftrightarrow 2Cu_{(l)} + SO_2 \quad (30)$$

In industrial practice, oxygen/air blow during copper converting is controlled, so that Cu_2S is not over-oxidized into Cu_2O, especially in the later stage where not much sulphide (Cu_2S)

is left. This explains why in the experiments no metallic copper was observed, as air was blown continuously into the system, allowing over-oxidation of copper into Cu_2O.

Since all the sulphur in the system had been oxidized into SO_2 (and subsequently removed from the system), the system now could be treated as Cu-Fe-Si-O system. Phase equilibria of this system is shown in Figure 15. It can be seen from Figure 37 that after 5 minutes, none of the equilibrium phases (cuprite, tridymite, delafossite, cuprous ferrite and spinel), were found in the sample. Copper and iron oxides were still in the form of solid solution within the slag, and silica is not yet in the tridymite phase. Tridymite would resemble an elongated structure, as shown in Figure 38, whilst in Figure 37, silica seems to still be in a liquid phase. The absence of these stable phases means that after 5 minutes, the system was not yet in equilibrium.

It can be seen from Figure 37 that the oxide products exhibit crystallized needle-like structures. Fan et al., (2014), have already studied this crystallization behaviour and phase equilibria of copper smelter slag. These structures are thought to be formed due to the rapid cooling of the samples, as it also has been found earlier in the matte phase from shorter time samples.

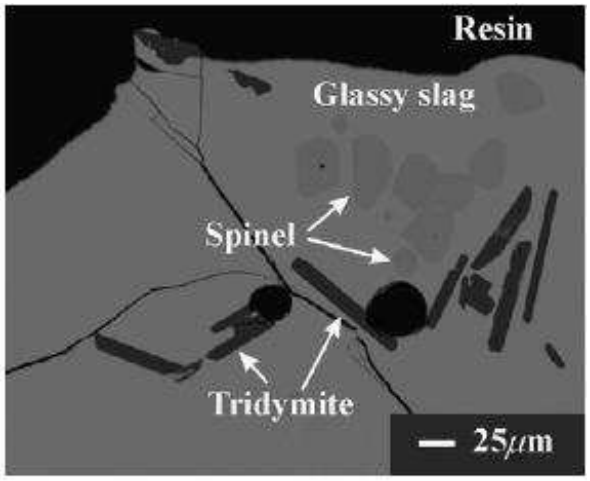

Figure 38. SEM Micrograph of Quenched Slag in Cu-Fe-Si-O System in Equilibrium with Air (Hidayat et al, 2012)

9.2. Inert Atmosphere Experiments

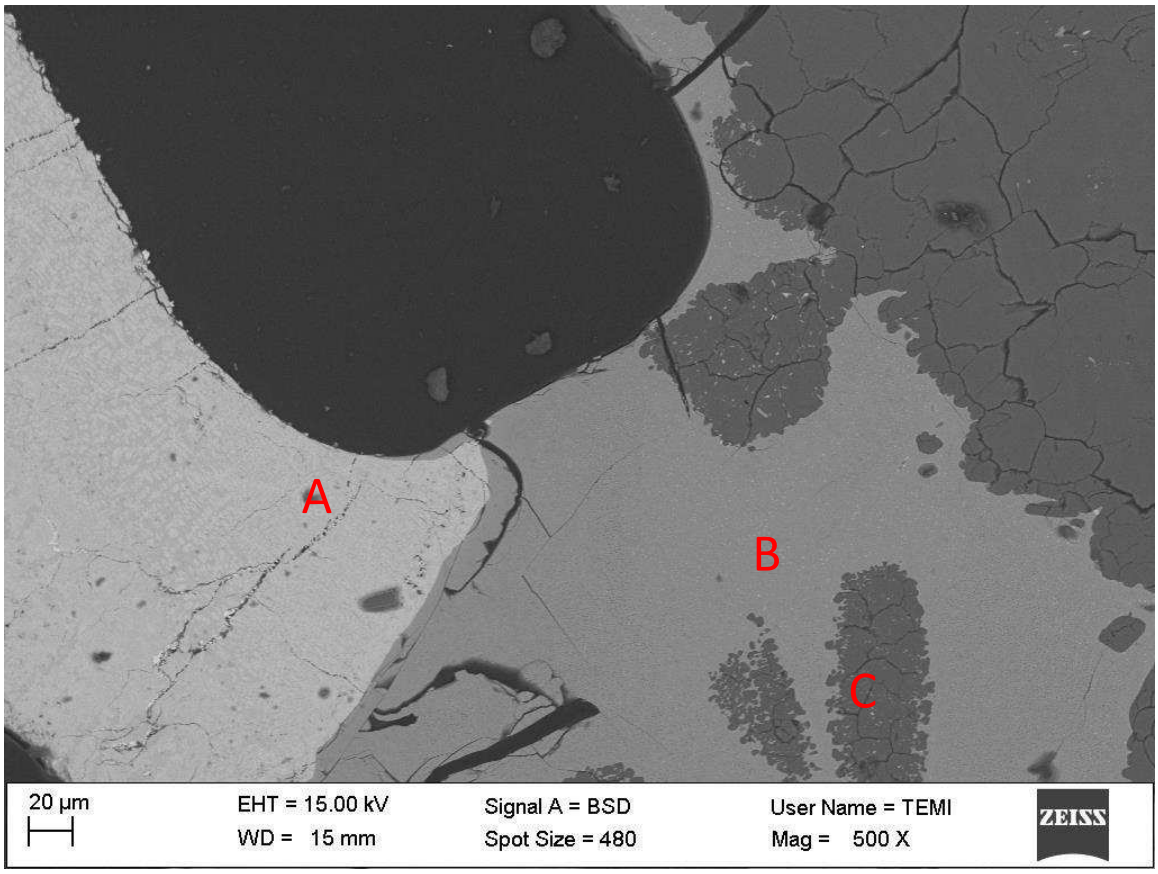

Figure 39. Micrograph of the Specimen after 5 Minutes Contacting Time in Inert Atmosphere, showing Matte (A), Fayalite Slag (B), and Silica (C).

After 5 minutes, most part of the matte was isolated and separated from the slag phase, as shown in Figure 39. The overall observation of this sample is that the matte is not as randomly distributed as in the 10-20 seconds contacting time samples in air (Figure 32 and Figure 33). This means that some separation and settling of the matte had been initiated. As it has been explained in Chapter 8.4, due to some additional complications involved in inert atmosphere experiments, the 5 minutes contacting time was chosen as the minimum contacting time.

No magnetite was supposed to be found in the sample. This is because of the absence of oxygen in the atmosphere makes further oxidation reactions of iron into magnetite (Reactions 8 and 9) to proceed slowly. The observation of fayalite slag in the sample indicates that the slag forming reactions (Reaction 10) proceed comparably faster than the magnetite forming reactions. The formed magnetite would be consumed immediately through the slagging reactions, leaving no magnetite in the sample. Such theory could be

proven by having samples with shorter contacting time (under 60 seconds), or using pressure transducer and gas analyser, or using TGA analysis at constant temperature. The former, as it has been discussed earlier, was not technically feasible due to the experimental arrangements used.

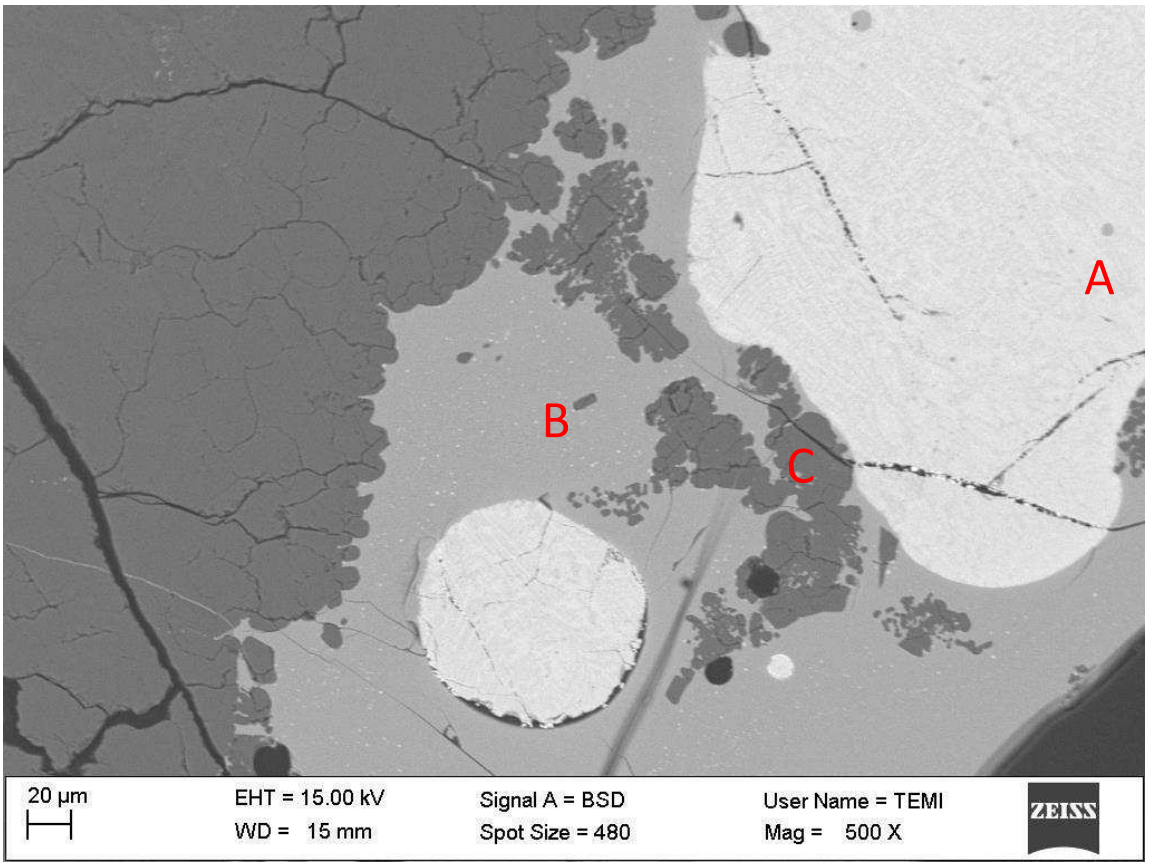

Figure 40. Micrograph of the Specimen after 10 Minutes Contacting Time in Inert Atmosphere, showing Matte (A), Fayalite Slag (B), and Silica (C)

Compared to the previous samples after 5 minutes of contacting time, no significant differences were observed after 10 minutes of contacting time, as it can be seen in Figure 40. Slag, and matte, as well as silica solids were observed. Compared to the samples contacted in air, the oxidation reactions in inert atmosphere are severely limited, due to the absence of oxygen in the atmosphere. It is expected that no copper oxide would form in this experiment.

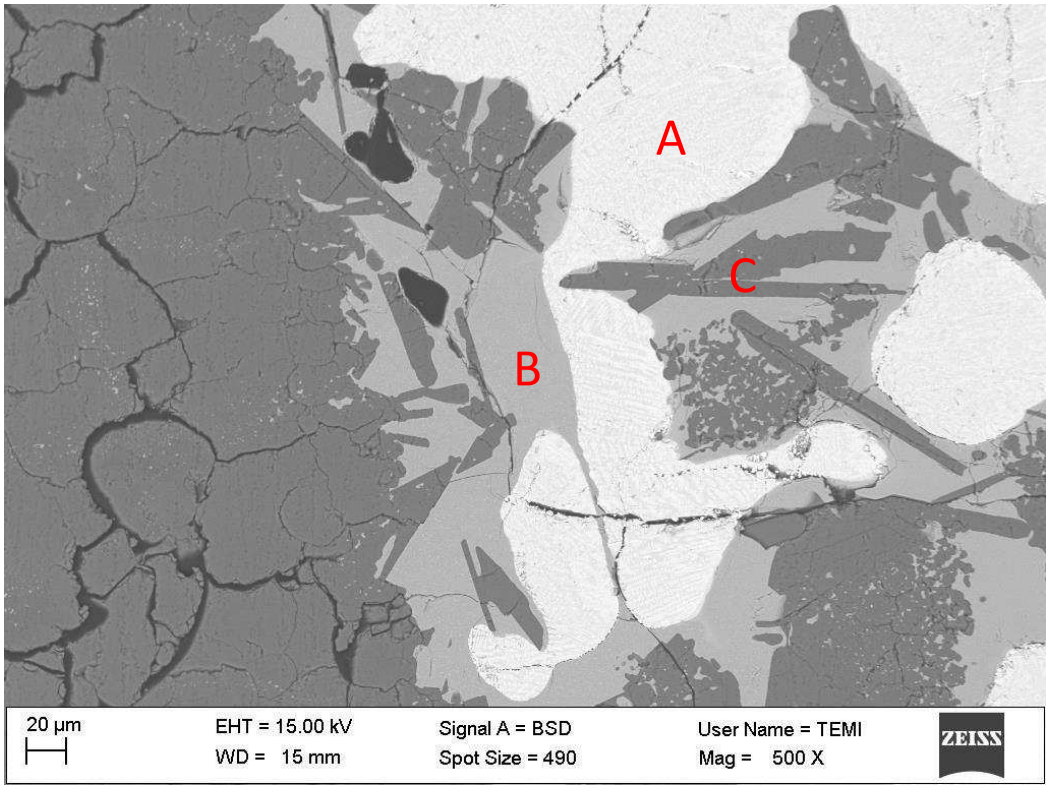

Figure 41. Micrograph of the Specimen after 60 Minutes Contacting Time in Inert Atmosphere, showing Matte (A), Fayalite Slag (B), and Silica (C)

Similar to previous samples, after 60 minutes three phases were observed: matte, fayalite slag, and silica, as it can be seen in Figure 41. The significant difference is that after 60 minutes the silica solid were now transforming into elongated shapes close to the shape of tridymite, similar to that shown in Figure 38. Tridymite is a thermodynamically stable phase of silica at high temperature (1100-1400^{o}C) in the Cu-Fe-Si-O system (Hidayat *et al,* 2012).

9.3. EDS Analysis

The EDS analysis was done to analyse the Cu, Fe and S content in the matte. The progression of the smelting reactions can be seen through the behaviour of matte content through time. The result summary for both experiments are shown in Figure 42 and 43, while complete EDS results can be found in Appendix A.1. EDS Results.

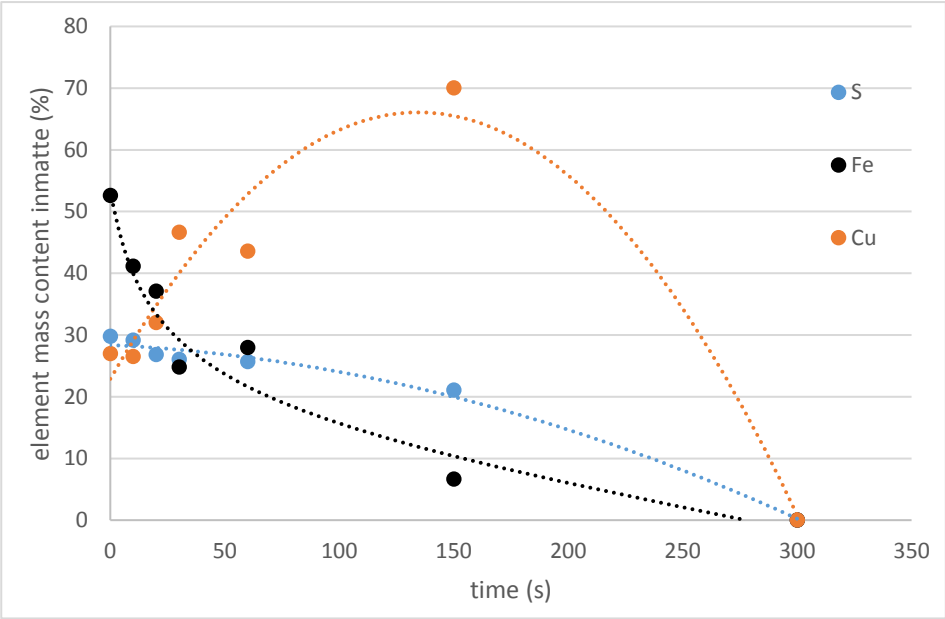

Figure 42. Chemical Content of Matte as a Function of Time in Air Atmosphere Experiments, with Dotted Lines as Estimation

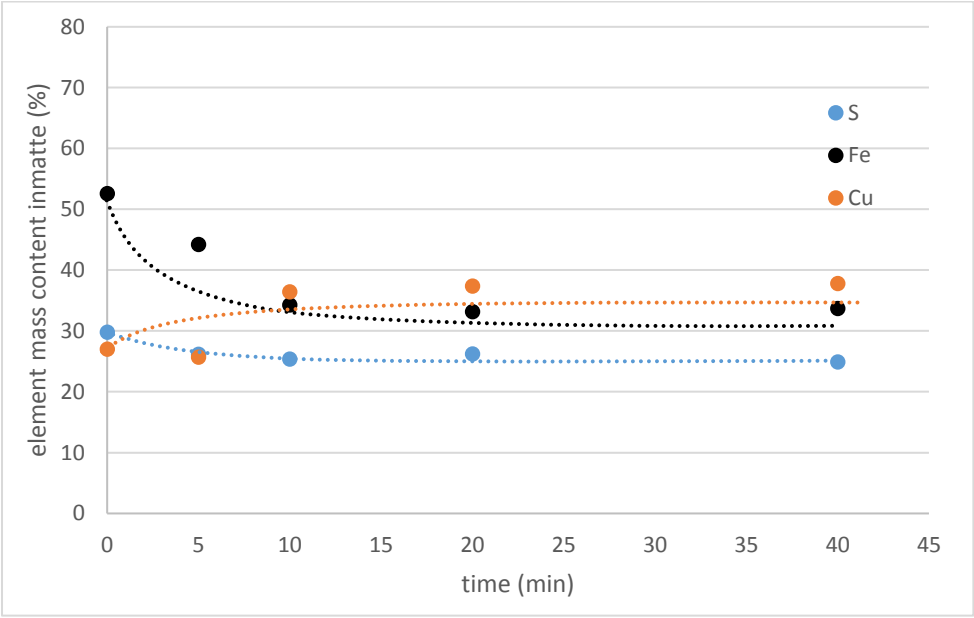

Figure 43. Chemical Content of Matte as a Function of Time in Inert Atmosphere Experiments, with Dotted Lines as Estimation

In air atmosphere, due to the constant availability of oxygen, the oxidation reaction would proceed until all the major elements are in their most stable oxidation state. This is confirmed by the EDS result in Figure 42, where the Cu content in matte is increasing due to preferred oxidation of Fe and S from matte to its oxide phase in slag (therefore the decreasing of Fe and S content in the matte). After 150 seconds, the Cu content in matte was quite high, and it was expected that after this point, oxidation of Cu would start, as

there were not much Fe and S left in the matte phase. The SEM results for 300 seconds (5 minutes) contacting time revealed that there were no matte found in the sample; it had all been oxidized into copper and iron oxides. This finding also suggested that oxygen gas diffusion into reaction interface would not be the limiting step, as oxidation proceeded with ease even without any forced draft of air.

The absence of oxygen in the atmosphere would limit the oxidation reactions in the sample during contacting in an inert atmosphere. Theoretically, the only oxidising agent is the slag, and as the slag runs out, there would be no oxidation reactions taking place anymore. However, the diffusivity of oxygen in the slag would also play important role in oxidising the matte.

As it can be seen from Figure 43, in inert atmosphere, after 5 minutes, the Cu content in matte is still similar to the Cu content after 10 seconds contacting in air atmosphere. This suggested that the deironization and desulfurization of the matte was severely limited because of the absence of oxygen in the atmosphere. Note, however, that in Figure 399, most of the matte and slag had been isolated from each other, in contrast to that seen in earlier samples in air (Figure 32 and Figure 33). This result suggested that the settling process had actually proceeded far, and the chemical content in the matte should already be near the equilibrium value, even though it was relatively low compared to the experiments in air atmosphere. This was confirmed in longer contacting times, since the content of the matte was pretty much stabilized after 10 minutes, similar to the 15 minutes found by Fagerlund (2000). This means that after this period, the oxidation reactions and separation process had ceased and the final elemental contents in matte could be concluded.

9.4. Discussion – Reaction Steps and Limiting Factors

Using the SEM micrographs and EDS analysis, the reaction sequence in a copper flash smelting process could be concluded. Some ideas regarding limiting factors in the process are also suggested in this chapter. Summary of the compounds found in the experiments is shown in Table 5.

Table 5. Components Found in the Samples and Some Important Notes

Time	Air Atmosphere	Inert Atmosphere
10-20 seconds	Cu_2S-FeS (matte), Fe_3O_4, Fe_2SiO_4 (slag), SiO_2 notes: matte is still randomly distributed, while not much fayalite slag is observed	
30-60 seconds	Cu_2S-FeS (matte), Fe_3O_4, Fe_2SiO_4 (slag), SiO_2, Cu_2S (impure white metal) notes: matte is isolated from slag, magnetite exists only in small amount, and white metal is only observed in some parts of the matte	
5 minutes	copper-iron oxides, SiO_2 notes: no sulphide compounds are observed	Cu_2S-FeS (matte), Fe_2SiO_4 (slag), SiO_2 notes: matte is already isolated from slag
10 -20 minutes		Cu_2S-FeS (matte), Fe_2SiO_4 (slag), SiO_2
40 - 60 minutes		Cu_2S-FeS (matte), Fe_2SiO_4 (slag), SiO_2 notes : SiO_2 resembles the tridymite shape

In the very beginning of the flash smelting process, as the concentrate is introduced to the burner, most of the particles would be immediately combusted and oxidized into matte in the reaction shaft. Ahokainen and Jokilaakso (1998) have studied the steps taking place in the combustion of a single chalcopyrite particle. However, some larger particles may not fully oxidize in the reaction shaft, therefore they come to contact with slag as partly reacted concentrate particles. The result of the present work offers a plausible explanation regarding this phenomena.

1. The first step, which is the oxidation of chalcopyrite into matte and SO_2 gas, proceeds very rapidly in air atmosphere. Ahokainen and Jokilaakso (1998), have proposed the mechanism through reactions (6) and (7)

$$5CuFeS_2 \rightarrow Cu_5FeS_4 + 4Fe_{1-x}S + 4\,x\,Fe + 2S \quad (6)$$

$$2Cu_5FeS_4 + O_2 \rightarrow 5Cu_2S + 2FeS + SO_2 \quad (7)$$

As neither bornite solution nor chalcopyrite concentrate were observed in the sample, both reaction (6) and (7) could be regarded as one stage rapid reaction, given in reaction 38.

$$2CuFeS_2 + O_2 \rightarrow Cu_2S + 2FeS + SO_2 \quad (38)$$

Based on the results in the present work, it is most probable that gas diffusion does not play an important role in this step, as reactions proceeded rapidly in air atmosphere. Meanwhile, in inert atmosphere oxygen would be sourced from the slag, so that oxygen mass transport holds a critical role. However, the role of oxygen diffusion / mass transport in the bulk slag phase in this step could not be confirmed, as it was technically difficult to produce samples with short contacting time (10-20 seconds) in inert atmosphere. By comparing the samples in inert and air atmosphere, especially in shorter contacting time, the difference between reaction with oxygen from air and oxygen from slag can be inferred, such comparison is illustrated in Figure 44.

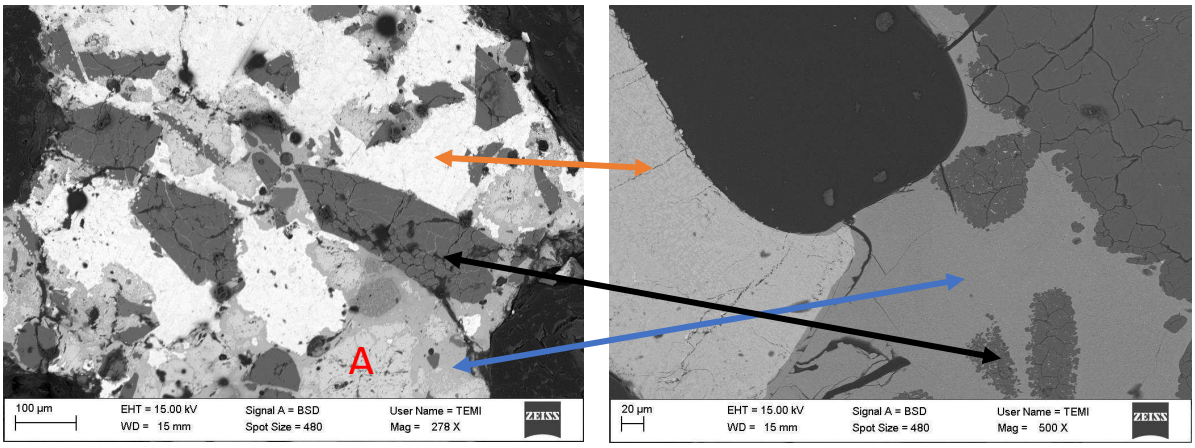

Figure 44. Comparison of Air Atmosphere after 20 seconds (Left) and Inert Atmosphere after 5 minutes (Right), showing matte (red), silica (yellow), fayalite slag (blue), and magnetite (A)

2. The products from the first step could be oxidized further, with the preference of iron and sulphur being oxidized first rather than copper. In air atmosphere, magnetite was also immediately formed during the first step of matte forming reactions. The magnetite forming reactions are shown in reactions (8) and (9)

$$3Fe + 2O_2 \rightarrow Fe_3O_4 \quad (8)$$

$$3FeS + 5O_2 \rightarrow Fe_3O_4 + 3SO_2 \quad (9)$$

After 10-20 seconds of contacting in air, a large amount of magnetite was observed, while a little amount of slag was also observed. This further confirms the slagging reaction of iron oxide through the magnetite formation. The iron and iron sulphide will be oxidized first into magnetite, and then with the presence of silica, it will form fayalite slag through reaction (10)

$$3Fe_3O_{4(s)} + FeS_{(matte)} + 5SiO_{2(s)} \rightarrow 5(Fe_2SiO_4)_{slag} + SO_{2(g)} \quad (10)$$

Reaction (10) could also proceed through two stages, in which magnetite would oxidize FeS in matte to produce FeO solid, which would subsequently react with silica to produce iron silicate slag.

$$3Fe_3O_{4(s)} + FeS_{(matte)} \rightarrow 10FeO_{(s)} + SO_{2(g)} \quad (11)$$

$$FeO_{(s)} + SiO_{2(s)} \rightarrow FeO - SiO_{2(slag)} \quad (5)$$

The formation of magnetite happens very rapidly in air atmosphere, comparable to the chalcopyrite combustion and oxidation reactions. However, the subsequent reaction between magnetite and silica through Reaction 10 proceeds relatively slower than the magnetite forming reactions, leaving many unreacted magnetite solids behind (hence the low amount of slag observed in the shorter contacting time samples). Further studies are needed to analyze the limiting stage in Reaction (10), as it may also proceed in two stages through Reaction (11) and (5).

Meanwhile, as illustrated in Figure 44, in contrast to the samples from contacting in air atmosphere, no magnetite was observed during contacting in inert atmosphere, whereas fayalite slag was indeed observed. In inert atmosphere, oxidation reactions take place with the available oxygen in the synthetic slag. Since

that, the slag forming reactions proceed through magnetite formation, this observation in inert atmosphere concludes that the oxygen mass transport in slag greatly limits the magnetite formation reactions, therefore limiting the overall slag formation sequences. This could be explained as follows: Reactions (8) and (9) proceed slowly, so that any produced magnetite would be consumed immediately through reaction (10).

3. After the slag is formed, matte begins to coagulate and separate from the slag. Due to its higher density, matte would settle to the bottom through the slag layer. In the air atmosphere experiment, this process could be seen clearly as the randomly distributed matte from the initial samples began to be isolated from the slag, together forming larger matte phase, illustrated in Figure 45. In Figure 45, the consumption of magnetite for the slagging reactions could also be inferred, because at the later stage magnetite is not prevalent anymore as it was in the early stage.

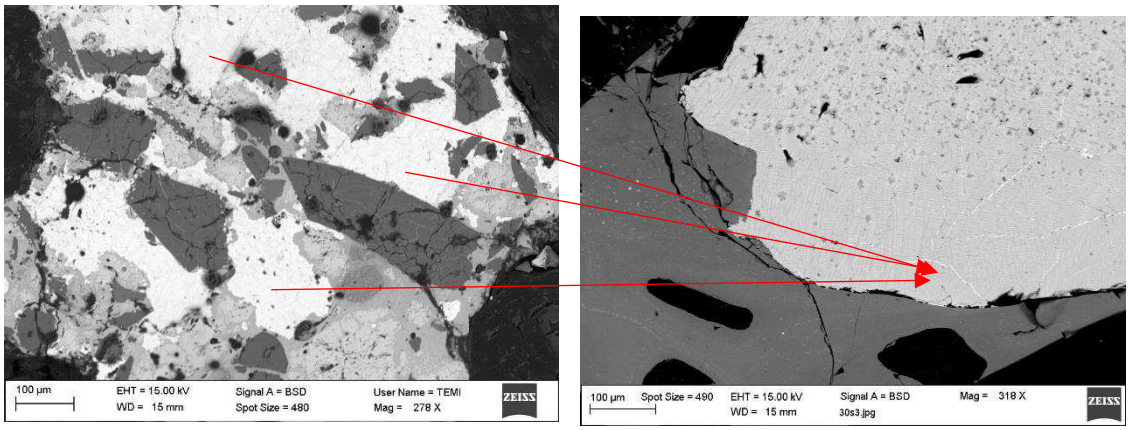

Figure 45. Separation of Matte and Slag

In inert atmosphere, the matte and slag were already isolated after 5 minutes, so the separation could not be inferred from the SEM micrographs. However, it could be concluded from the EDS analysis, that the separation could be regarded as complete when the content of matte more or less stabilizes, meaning reactions between slag and matte had ceased. In inert atmosphere, this process ceased just after 10 minutes. Without any mixing, further matte-slag reactions would be virtually impossible, as the oxygen mass transport in slag phase greatly limits these reactions. This could suggest that in industrial smelting process, prolonging the settling time (or increasing the settler dimension) would not have the best effect

to the separation process; other variables such as silica charge or mixing would bear more significances.

4. In the case of air atmosphere, the constant availability of oxygen makes further oxidation possible. The iron and sulphur content in the matte further decreased, as more of these elements are oxidized into the slag phase. Then, Cu_2S will start to oxidize only when the Fe content in the matte is lower than 1% (Schlesinger, 2011). Oxidation of Cu_2S is the principle in copper converting process, governed by equations (2), (15), and (30).

$$Cu_2S_{(l)} + 1.5O_2 \rightarrow Cu_2O_{(slag)} + SO_2 \quad (2)$$

$$Cu_2S_{(l)} + 2Cu_2O_{(slag)} \leftrightarrow 6Cu_{(l)} + SO_{2(g)} \quad (15)$$

$$Cu_2S_{(l)} + O_2 \leftrightarrow 2Cu_{(l)} + SO_2 \quad (30)$$

In industry, oxygen/air blowing is controlled so that copper is not over-oxidized into Cu_2O, especially when the sulphur level in the system is low, as Cu_2S would be no longer available to reduce Cu_2O back to metallic copper through reaction (15). Other reactions, such as reactions (13) and (14) are also important in copper converting, as the remaining FeS can attract the oxygen from Cu_2O to produce Cu or Cu_2S, the latter can be oxidized again through reaction (30) to produce copper. These reactions are possible due to iron having higher affinity for oxygen compared to copper.

$$FeS_{(matte)} + Cu_2O_{(slag)} + 0.5SiO_{2(s)} \leftrightarrow CuS_{(matte)} + 0.5(Fe_2SiO_4)_{slag} \quad (13)$$

$$FeS_{(matte)} + 3Cu_2O_{(slag)} + 0.5SiO_{2(s)} \leftrightarrow 6Cu_{(l)} + 0.5(Fe_2SiO_4)_{slag} + SO_{2(g)} \quad (14)$$

Since in the air experiments there was no control regarding air feeding to the furnace, no metallic copper was observed, as all of the Cu_2S was over-oxidized into Cu_2O. The compounds found in the final stage of these experiments were copper-iron oxides and silica.

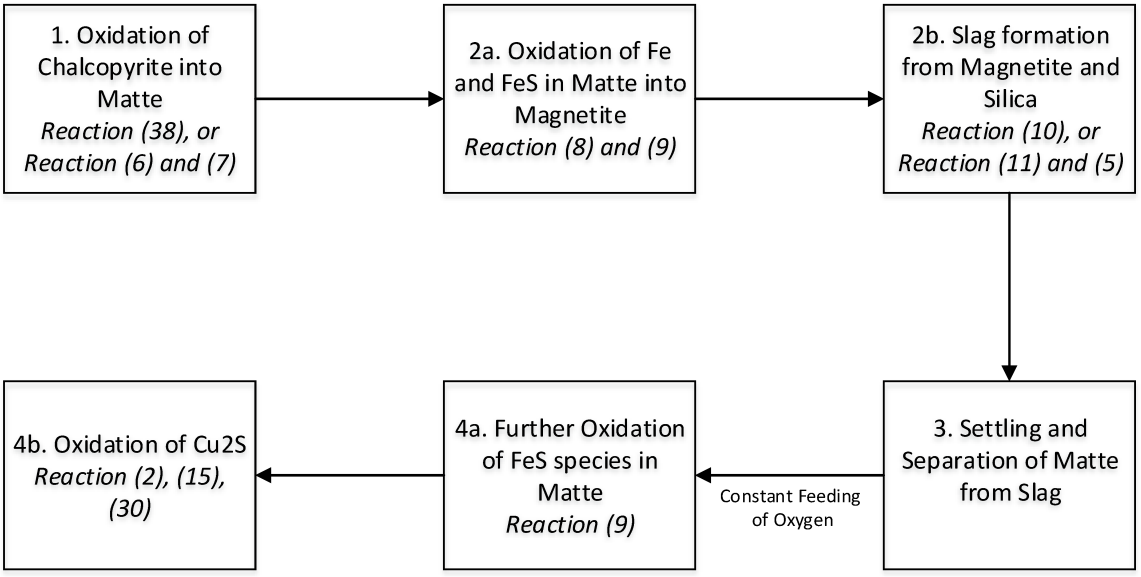

Figure 46. Sequences of Matte-Slag Reactions in Copper Flash Smelting

Based on the experimental observation in the present work, a reaction sequence has been constructed to describe matte-slag formation in flash smelting settler condition. This is shown in Figure 46. Step 2a is the limiting factor in inert atmosphere with the oxygen mass transport in slag limiting Reactions (8) and (9). Step 2b is limiting the overall process in air atmosphere, especially the silica mass transport in slag, which limits the contact between magnetite and silica to form fayalite slag through Reaction (10). In both cases, the overall sequences are limited in step 2, which is largely affected by the physical phenomena of mass transport in slag. This suggests the critical importance of physical properties (viscosity and density) of the slag in copper smelting.

Steps 4a and 4b are possible due to constant availability of oxygen in air atmosphere, in which step 4b was observed to be fully completed after just 5 minutes. When the oxygen is absent in the atmosphere, the process in Figure 46 ceased at step 3, which in the present work was completed after 10 minutes of contacting time, as shown in Figure 43.

These four steps in the reaction sequences in Figure 46 found in the present work are more or less similar with the previous works of Ahokainen and Jokilaakso (1998), Fagerlund (2000) as well as Tahmasebi (2013). It can be concluded that the experimental and analytical procedures employed in present work were good enough to draw meaningful conclusions regarding reaction sequence and limiting steps in matte-slag interaction system.

9.5. Addition of Crushed Printed Circuit Board Pieces to the Samples

Some amount of PCBs (Printed Circuit Boards) was added to the concentrate-slag mixtures. The amount of PCB was adjusted to comprise 40% of the total mixture mass, so that if the mixture used is 0.5 gram, then 0.2 gram of PCB were added to it. The slag-concentrate mixtures used were the same as in the previous experiments. These additional experiments were conducted to get an initial idea of how the PCB behaves in a slag-matte interaction system. The PCB were loosely crushed to bits sized around 5x5 mm and 1 mm thick, shown in Figure 47.

In the present work, the PCB was crushed and had its top components removed (shown as A in left Figure 47), so that only the board of the PCB was left. This could make the sample more homogenous, at the cost of losing some elements contained in the components. The approach is suitable for time-dependent experiments, as repetitive samples can be obtained.

Figure 47. PCB (left), Crushed PCB Pieces (right)

The PCBs are added so that the idea regarding distribution of the precious metals in the PCBs during copper flash smelting can be identified. Beforehand, cross sectional micrographs of the PCB were taken, so that the major components in the PCB could be inferred. The cross sectional micrograph of the PCB is shown in Figure 48.

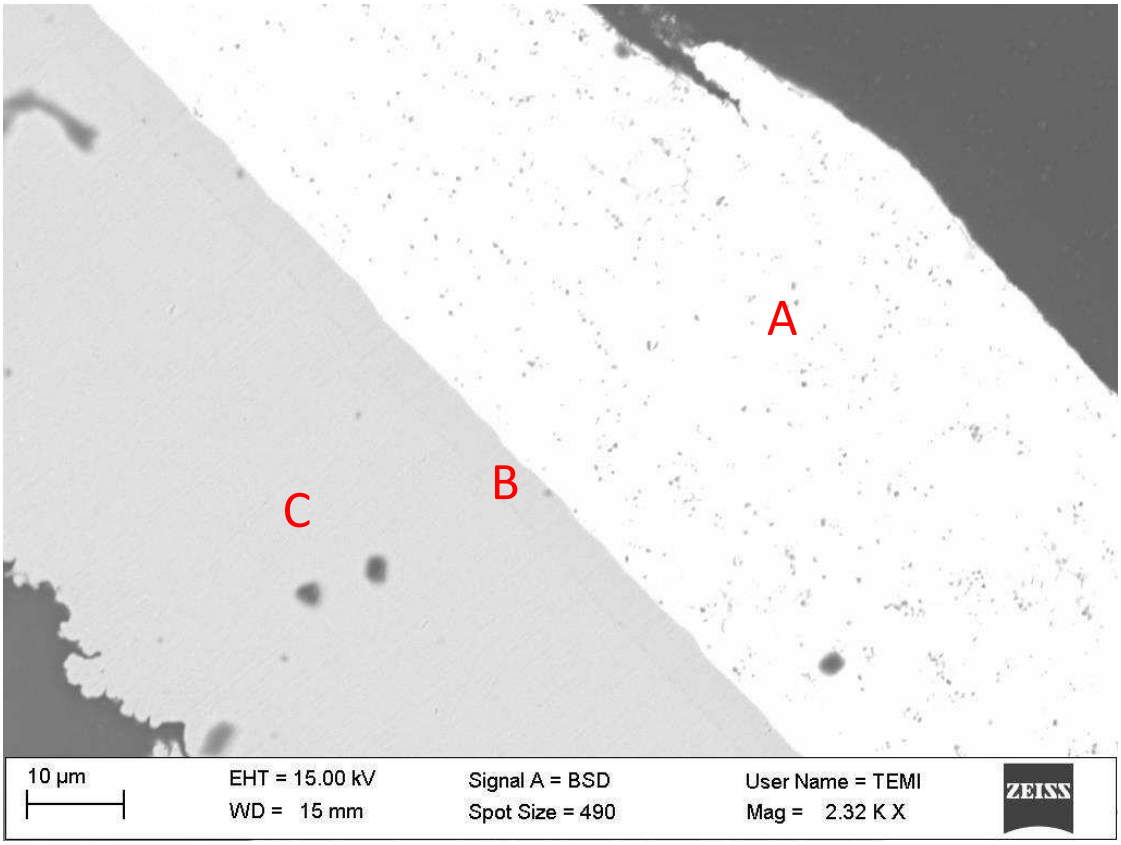

Figure 48. PCB Cross Sectional Micrographs, Showing Tin-Lead Solder (A), Nickel Coating (B), and Copper (C)

From the cross-section in Figure 48, three basic components of the PCB were identified, namely Tin-Lead, Nickel, and Copper. Both Tin-Lead and Nickel are found on the outer surface of the PCB, while copper forms most of the inside body part of the PCB. There were no precious metals to be found in the cross sections of the PCBs. However, as it is quite well known, most of the precious metals are located on top of the PCB surface, so another analysis was taken from the top surface of the PCB. The elements found on the PCB according to EDS analysis are shown in Table 6. The minor elements were found in certain parts of the PCB, and in general only make up a small part of the whole PCB.

Table 6. Elements in the PCB

Major				**Minor**	
Copper	Tin	Lead	Nickel	Gold	Silver

To analyse further, these PCBs were then melted in an inert atmosphere furnace. This melting was conducted to see how the metals distributed in the melt, and whether the

concentration of the minor elements is detectable by EDS. The resulting melt was quenched, yielding solidified metal droplets and some ash from the non-metal part of the PCB. The solidified metals were then analysed by SEM-EDS. Figure 48 shows a micrograph of the quenched sample.

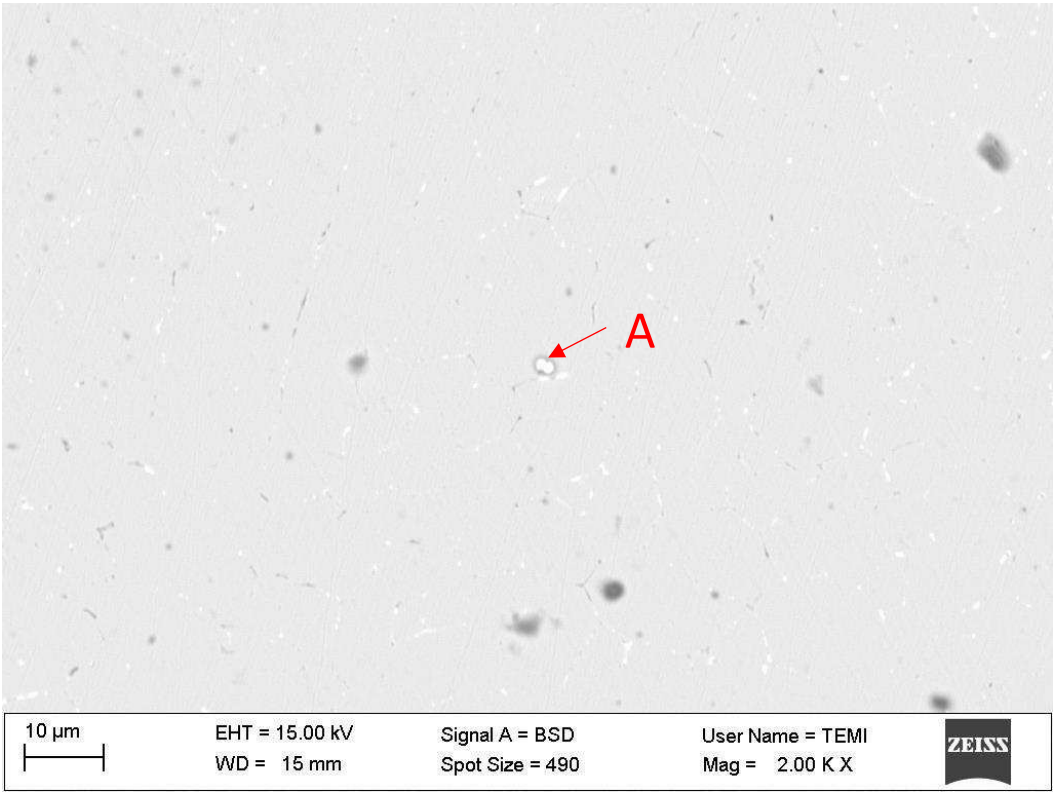

Figure 49. Molten PCB Cross Sectional Micrographs

Figure 49 shows that the minor heavy metals (shown as the bright spots) are dispersed throughout the major metal. The major metal was revealed by EDS as copper. The elements found in the molten PCB are shown in Table 7.

Table 7. Elements found in the molten PCB

Major	**Minor**		
Copper	Tin	Nickel	Lead

The bright spots mainly composed of copper with some minor amounts of tin, nickel, and lead. Moreover, there was a relatively large bright spot on the sample (shown as A in Figure 49), and EDS analysis revealed that asides from copper, it also contains some amount of silver, technetium, antimony, arsenic, and tellurium. Nevertheless, the fact that these metals are dispersed as small spots will surely increase the difficulties in

analysis, as more precise and accurate analysis technique will be required to quantify these spots.

To get an indication where these metals are distributed in a matte-slag system, these PCBs were melted with slag-concentrate mixtures. The micrograph of a quenched sample is shown in Figure 50, while the elements found are shown in Table 8

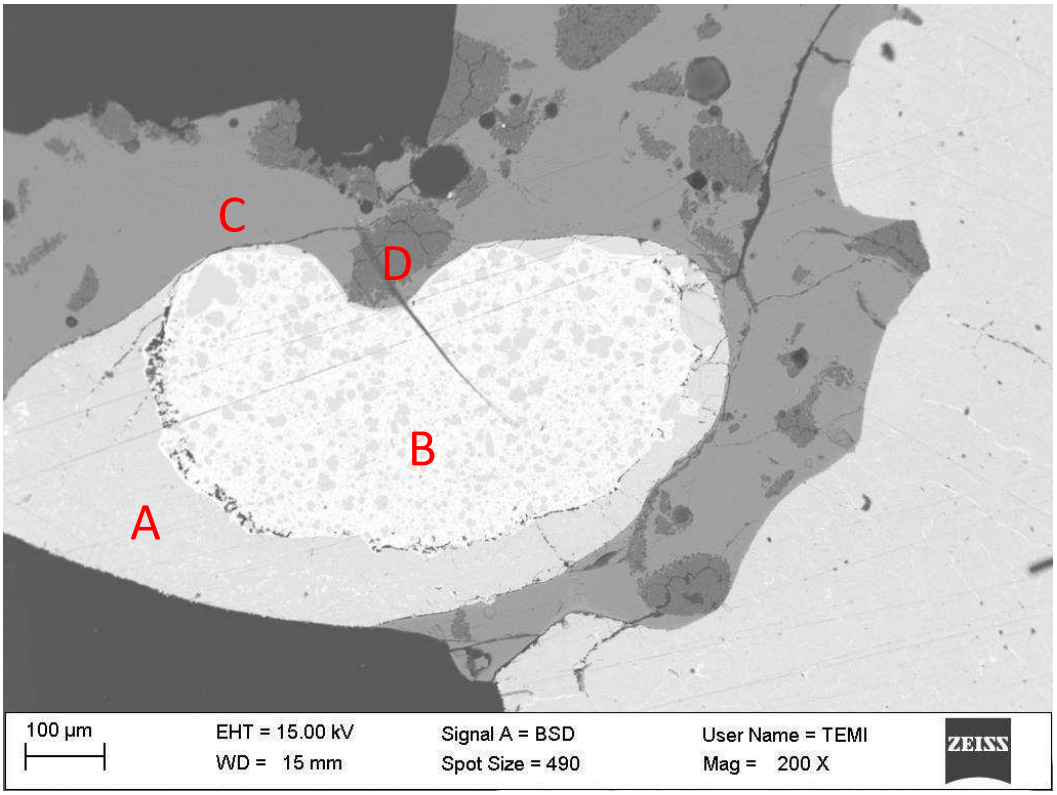

Figure 50. Matte-Slag-PCB Mixture, Melted after 5 minutes in Inert Atmosphere, Showing Matte (A), Cu-Fe Alloy (B), Fayalite Slag (C), Silica (D)

Table 8. Elements Found the Matte-Slag Mixture

	MATTE	**SLAG**	**ALLOY**
MAJOR	Copper	Iron	Copper
	Iron	Silica	Iron
	Sulfur	Oxygen	
MINOR		Aluminum	Tin
		Calcium	Nickel
			Antimony

Due to the additional copper from the PCB, the matte shown in Figure 50 has an elevated Cu content, around 56 wt%, even though the melting experiments were only conducted

for 5 minutes. Moreover, a Cu-Fe alloy phase was found within the matte, which contains most of the minor elements found in the PCB. Repetitions of this experiment was done, and the Cu-Fe alloy phase was found to be dispersed throughout the matte phase. The result in Figure 50 was an occasional finding, where the alloy clustered into one large phase within the matte, as normally this Cu-Fe alloy would be randomly dispersed throughout the matte, as shown in Figure 51.

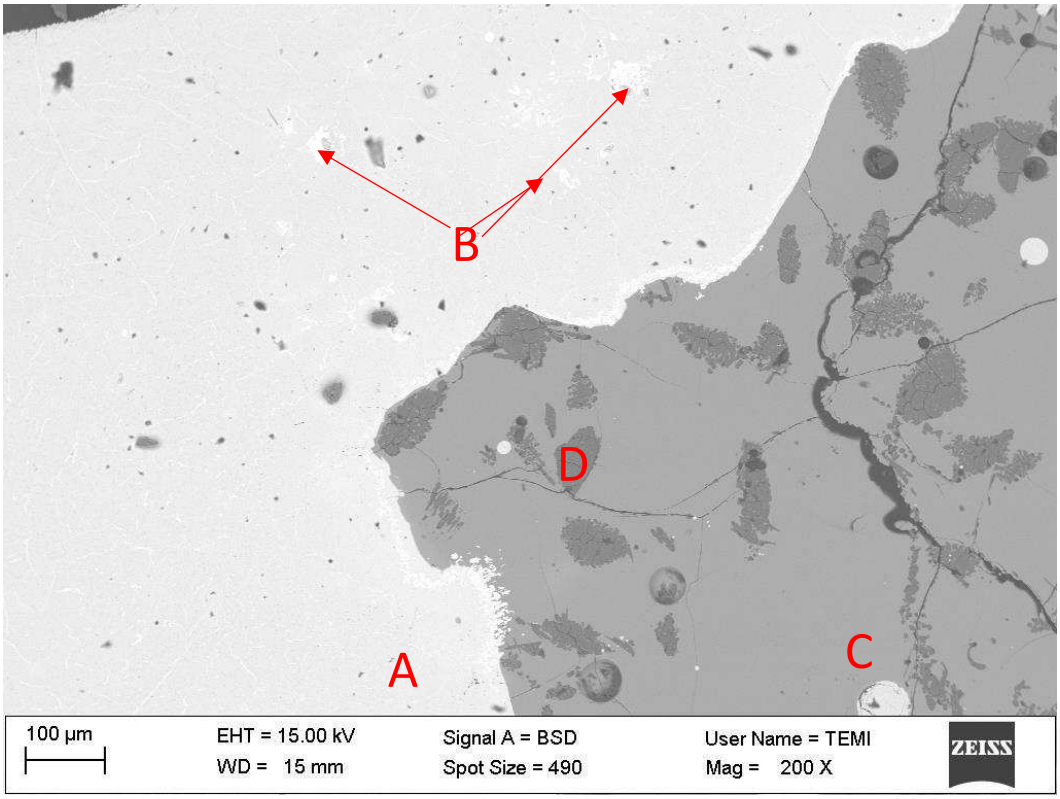

Figure 51. Matte-Slag-PCB Mixture, Melted after 5 minutes in Inert Atmosphere, Showing Matte (A), Cu-Fe Alloy (B), Fayalite Slag (C), Silica (D)

Nevertheless, no precious metals such as gold or silver were found in the mixture. Lead, one of the main components in the PCB, was also not found after the experiment. This is due to the fact that elements make up only a small amount in the whole PCB, so the presence of these elements in the matte-slag system could be overlooked, especially using EDS analysis.

Djordjevic *et al.* (2011) made an extensive study regarding distribution coefficient of minor elements (Pb, Sb, As, Ni, Ag, Au, Zn) between copper matte and slag from industrial furnaces, and their results indicated that most of these elements existed in very small concentrations, like 0.1 wt%. Most of these elements have distribution coefficients ($L_{me}^{S/M}$)

lower than 1, with the exception of Zn. This means that most part of these elements would be found in the matte phase. Experiments conducted by adding a small amount (1 wt% of the matte weight) of pure precious metals such as Ag, Au, Pd, Pt, and Rh to the copper matte and fayalite slag have been conducted by Avarmaa *et al.* (2016). Similarly, it was found that these elements have distribution coefficients less than 10^{-2}, meaning it will practically be found mostly in matte. While the EPMA was sufficient to detect these elements in the matte, Avarmaa *et al.* stated that the Electron Probe Micro Analyzer (EPMA) was not sufficient to reliably detect most of these elements in slag, due to their concentrations being below the detection limit of EPMA. They suggested using Laser Ablation Inductively Coupled Mass Spectroscopy (LA-ICP-MS) analysis for more accurate and precise result. In the present experiment, such elements were not detected in the matte phase, let alone slag. This concludes that EDS would not be suitable in this case, EPMA or LA-ICP-MS would be better.

10. Conclusions and Future Recommendations

Concluding remarks, as well as recommendations for continuation work are presented in this chapter.

10.1. Conclusions

- The experimental and analytical procedures employed in this work are generally sufficient to draw qualitative conclusions regarding reaction sequences and limiting steps in copper flash smelting settler conditions. However, the procedure lacks the ability to quantitatively evaluate the copper matte smelting and settling process, which is critical for rate equation formulation.
- A plausible reaction sequences and limiting steps in copper flash smelting settler conditions have been described in the present work, from concentrate oxidation, matte and slag formation, matte settling through the slag layer, and further matte oxidation into their oxides.
- The results in the present work suggested that mass transport limits the overall process of matte-slag interactions in copper smelting. In air atmosphere mass transport limits the slag forming reactions, while in inert atmosphere oxygen mass transport in slag limits the magnetite forming reactions.
- Based on the results in the present work, copper content in matte would reach peak only after 2-3 minutes in air atmosphere, while afterwards it will start to drop due to oxidation of copper in matte. In inert atmosphere, matte content is stabilized after 10 minutes contacting time, indicating that the separation of matte and slag had ceased within this time.
- Most of the minor and precious metals from the PCB tend to disperse throughout the matte phase as Cu-Fe alloy spots, making analysis difficult. Moreover, the heterogeneity of the crushed PCBs also pose difficulties in obtaining a representative and reproducible samples for the experiments.

10.2. Suggestions and Recommendations for Future Work

- Physical phenomena and mechanisms are sometimes difficult to catch with SEM-EDS; a continuous x-ray imaging system would be a good complimentary analysis in this case. Using this as well, quenching of the sample could be done according to the imaging observation, i.e. when a certain physical phenomena is observed in imaging system, sample can be quenched at that exact moment, so micro-images of the sample during the physical phenomena can be obtained.

- The EDS analysis is not sufficient for formulating kinetic rate equation, as it only quantifies spots and parts of the sample. A continuous time-dependent data is required for this task. This can include continuous gravimetric analysis using microbalance, or gas outlet analysis (pressure and/or composition). Initial estimation of time-dependent behaviour of matte-slag during smelting could also be analysed using Thermogravimetric Analysis (TGA).

- An alternative to this is having gravimetric data as discrete and independent samples through several experiments (similar to the present work) instead of continuous data collection in one experiment. However, care must be taken in shorter time samples (10-20 seconds), as the accuracy become critical, especially with the rapid nature of melt-melt reactions in copper smelting.

- As the precious and minor metals from the PCB are found in small amounts in the matte, a more accurate and precise analysis other than EDS is needed. Such analysis could be EPMA and LA-ICP-MS. Similarly, by producing samples through several experiments, time dependent distribution of these elements could be concluded.

REFERENCES

Ahokainen, T. Jokilaakso, A. (1998) 'Numerical Simulation of The Outokumpu Flash Smelting Furnace Reaction Shaft', *Canadian Metallurgical Quarterly*. 37(3-4). pp. 275-283.

Ajersch, F. Toguri, J.M. (1972) 'Oxidation Rates of Liquid Copper and Liquid Copper Sulfide', *Journal of Metallurgical Transactions.* 3. pp. 2187-2193.

Alyaser A.H. Brimacombe, J.K. (1995) 'Oxidation Kinetics of Molten Copper Sulfide', *Journal of Metallurgical and Materials Transactions B*. 26B. pp. 25-40.

Aracena, A. Jerez, O. Ortiz, R. Morales, J. (2016) 'Pyrite Oxidation Kinetics in an Oxygen-Nitrogen Atmosphere at Temperatures from 400 to 500^{o}C', *Canadian Metallurgical Quarterly.* 55:2. pp. 195-201.

Asaki, Z. Ando, S. Kondo, Y. (1988) 'Oxidation of Molten Copper Matte', *Journal of Metallurgical Transactions B.* 19B. pp. 47-52.

Avarmaa, Katri. Johto, Hannu. Taskinen, Pekka. (2016) 'Distribution of Precious Metals (Ag, Au, Pd, Pt, and Rh) Between Copper Matte and Iron Silicate Slag', *Journal of Metallurgical and Materials Transactions B*. 47B. pp. 244-255.

Beychok, Milton. (2009) *Schematic Diagram of an Outukumpu Flash Smelter and Its Waste Heat Boiler.* Available at: http://en.citizendium.org/wiki/File:Flash_Smelter_Waste_Heat_Boiler.png. (Accessed 22.11.2016).

Chakrabarti, D.J. Laughlin, D.E. (1983) 'The Cu-S (Copper-Sulfur) System' *Bulletin of Alloy Phase Diagrams,* 4(3). pp. 254-269.

Cook Jr., William R. (1972) *Phase Changes in Cu_2S as a Function of Temperature,* Paper Presented in The 5th Materials Research Symposium.

Davenport, W.G., King, M., Schelsinger, M. Biswas, A.K. (2002) *Extractive Metallurgy of Copper.* Fourth Edition. Elsevier: England.

Deng, T. Gran, J. Sichen D. (2010) 'Dissolution of Lime in Synthetic 'FeO'-SiO_2 and CaO-'FeO'-SiO_2 Slags' *Steel Research International 81*, *No. 5.*

Deng, Tengfei. Glaser, Björn. Sichen, Du. (2012) 'Experimental Design for the Mechanism Study of Lime Dissolution in Liquid Slag' *Steel Research International 83 No. 3.*

Devia, M.I. Sanchez, M.A. (2011) 'Comparative Analysis of Slag Systems Cu-Fe-O-SiO_2 and Cu-Fe-O-CaO between 1100 and 1300^{o}C' *Mineral Processing and Extractive Metallurgy,* 120:3, pp. 177-190.

Djordjevic, P. Mitevska, N. Mihajlovic, I. Nikolic, Dj. Manasijevic, D. Zivkovic, Z. (2011) 'The Effect of Copper Content in the Matte on the Distribution Coefficients Between the Slag and The Matte for Certain Element in the Sulphide Copper Concentrate Smelting Process', *Journal of Mining and Metallurgy.* 28(1). pp. 143-151.

Fagerlund, Kim O. Jalkanen, Heikki. (2000) 'Microscale Simulation of Settler Processes in Copper Matte Smelting', *Journal of Metallurgical and Materials Transactions B.* 31B. pp. 439-451.

Fagerlund, Kim. (1998) *Formations and Separation of Molten Phases in Copper Smelting*. PhD. Diss. Helsinki University of Technology.

Fan, Yong. Shibata, Etsuro. Lizuka, Atsushi. Nakamura, Takashi. (2014) 'Crystallization Behaviors of Copper Smelter Slag Studied Using Time-Temperature-Transformation Diagram', *Journal of Materials Transaction,* 55 No.6, pp. 958-963.

Firdu, Fiseha Tesfaye. (2009) *Kinetics of Copper Reduction from Molten Slags.* MSc. Thesis. Helsinki University of Technology.

Gupta. (2014) *Lecture 12: Reverberatory and Induction Furnace.* Available at: http://nptel.ac.in/courses/112107144/metalcasting/lecture12.htm (Accessed 22.11.2016)

Henao, Hector M. Nexhip, Colin. George-Kennedy, David P. Hayes, P.C. Jak, E. 'Investigation of Liquidus Temperature and Phase Equilibria of Copper Smelting Slags in the FeO-Si_2O-CaO-MgO-Al_2O_3 System at PO_2 10^{-8} atm' *Journal of Metallurgical and Materials Transactions B,* 41, pp. 757-779.

Hidayat, Taufiq. Fallah-Mehrjardi, Ata. Chen, Jeff. Hayes, Peter. Jak, Evgueni. (2016) *Experimental Study of Metal-Slag and Matte-Slag Equilibria in Controlled Gas*

Atmospheres. Unpublished paper presented at the 9th International Copper Conferences. Kobe, Japan

Hidayat, Taufiq. Henao, Hector M. Hayes, Peter C. Jak, Evgueni. (2012) 'Phase Equilibria Studies of the Cu-Fe-O-Si System in Equilbrium with Air and with Metallic Copper', *Journal of Metallurgical and Materials Transactions B.*

Ip, S.W. and Toguri, J.M. (1992) 'Entrainment Behavior of Copper and Copper Matte in Copper Smelting Operations', *Journal of Metallurgical Transactions B,* 23B, pp. 305-311.

Jalkanen, H. (1981) ' Phenomenology of the Oxidation Kinetics of Molten Cuprous Sulphide and Copper', *Scandinavian Journal of Metallurgy,* 10, pp. 257-262.

Jokilaakso, A. Suominen, R. Taskinen, P. Lilius, K. (1991) 'Oxidation of Chalcopyrite in Simulated Suspension Smelting' *IMM Transactions*, Sect. C 100. C79-90.

Kim, Hang Goo. Sohn, H.Y. (1998). 'Effects of CaO, Al_2O_3, and MgO Additions on The Copper Solubility, Ferric/Ferrous Ratio, and Minor Element Behavior of Iron Silicate Slags' *Journal of Metallurgical and Materials Transactions B,* 29, pp. 583-590.

Laughlin, David E. Hono, Kazuhiro. (2014) *Physical Metallurgy Volume 1.* Fifth Edition. Elsevier: Netherlands.

Matousek, J.W. (1994) 'Equilbrium Oxygen Pressures of Iron Silicate Slag', *Journal of Metallurgical and Material Transcations B,* 25(3), pp. 463-465.

Mulenshi, Jane. (2015) *Mapping of Settling Process at Boliden Rönnskär and Harjavalta Smelters.* MSc. Thesis. Luleå University of Technology.

Nagamori M. Mackey P.J. Tarassoff, P. (1975) 'Copper Solubility in FeO-Fe_2O_3-SiO_2-Al_2O_3 Slag and Distribution Equilibria of Pb, Bi, Sb, and As between Slag and Metallic Copper' *Journal of Metallurgical Transactions B,* 6, pp.295-301.

Park, Jiwon. Sridhar, Seetharaman. Fruehan, Richard J. (2014) 'Kinetics of Reduction of SiO_2 in SiO_2-Al_2O_3-CaO Slags by Al in Fe-Al(-Si) Melts' *Journal of Metallurgical and Material Transactions B,* 45B, pp. 1380-1388.

Peretti, E. A. (1948) 'An Analysis of the Converting of Copper Matte' *Discuss. Faraday. Soc.* 4, pp. 179-184.

Potysz, Anna. van Hullebusch, Eric D. Kierczak, Jakub. Grybos, Malgorzata. Lens, Piet N.L. Guibaud, Gilles. (2015) 'Copper Metallurgical Slags – Current Knowledge and Fate: A Review', *Critical Reviews in Environmental Science and Technology*, 45(22). pp. 2424-2488.

Roghani, G. Takeda, Y. Itagaki, K. (2000) 'Phase Equilbrium and Minor Element Distribution between FeO_x-SiO_2-MgO-based Slag and Cu_2S-FeS Matte at 1573 K under High Partial Pressure of SO_2' *Journal of Metallurgical and Materials Transaction B,* 31, pp. 705-712.

Rottmann, G. Wuth, W. (1975) *Copper Metallurgy: Practice and Theory,* M.J. Jones, Institution of Mining and Metallurgy, London.

Sano, H. Nishikawa, K. Hong, J.H. Sasaki, Y. (2016) *Considerations for the Influence of Slag Composition on the Copper Loss in Slag.* Unpublished paper presented at the 9th International Copper Conferences. Kobe, Japan

Schlegel, H. Schuller A. (1952) 'Das Zustansbild Kupfer-Eisen-Schwefel', *Zeitschrift fur Metallkunde*. 43. pp 421-428.

Schlesinger, Mark E. King, Matthew J. Sole, Kathryn C. Davenport, William G. (2011) *Extractive Metallurgy of Copper*. Fifth Edition.

Shin, Jae Hong. Chung, Yongsug. Park, Joo Hyun. (2016) 'Refractory-Slag-Metal-Inclusion Multiphase Reactions Modelling Using Computational Thermodynamics: Kinetic Model for Prediction of Inclusion Evolution in Molten Steel', *Journal of Metallurgical and Material Transactions B.*

Tahmasebi, Rasool. (2013) *Reaction of Copper Matte Droplets with an Oxidizing Slag*. MASc. Thesis. McMaster University.

Vaarno, Jussi. Järvi, Juha. Ahokainen, Tapio. Laurila, Toni. Taskinen, Pekka. (2003). *Development of a Mathematical Model of Flash Smelting and Converting Processes*. Unpublished paper presented at The Third International Conference on CFD in the Minerals and Process Industries. Melbourne, Australia.

Vardar, E. Eric, R. Hurman. (2008) 'Smelting of Iron Ore in Fe-Cr-C-Si Melts', *Journal of Materials and Manufacturing Processes,* 23:8. pp. 764-768.

Wang, Lu. Zhang, Guo-Hua. Chou, Kuo-Chih. (2016) 'Study on Oxidation Mechanism and Kinetics of MoO_2 to MoO_3 in Air Atmosphere', *International Journal of Refractory Metals and Hard Materials,* 57, pp. 115-124.

Yazawa, A. Kameda, A. (1953) 'Copper Smelting. I. Partial Liquidus Diagram for FeS-FeO-SiO_2 System', *Technological Republic Tohoku University,* 16, pp 50-58.

Zhao, B. Hayes, P. Jak, E. (2013) 'Effects of CaO, Al_2O_3 and MgO on Liquidus Temperature of Copper Smelting and Converting Slags under Controlled Oxygen Partial Pressures' *Journal of Mining and Metallurgy, Section B: Metallurgy,* 49(2)B, pp. 153-159.

Zhou, Jun. Chen, Zhuo. (2016) *Studies of the Metallurgical Processes in Settler of A Copper Flash Smelting Furnace.* Unpublished paper presented at the 9th International Copper Conferences. Kobe, Japan.

APPENDICES

Appendix A.1. EDS Results

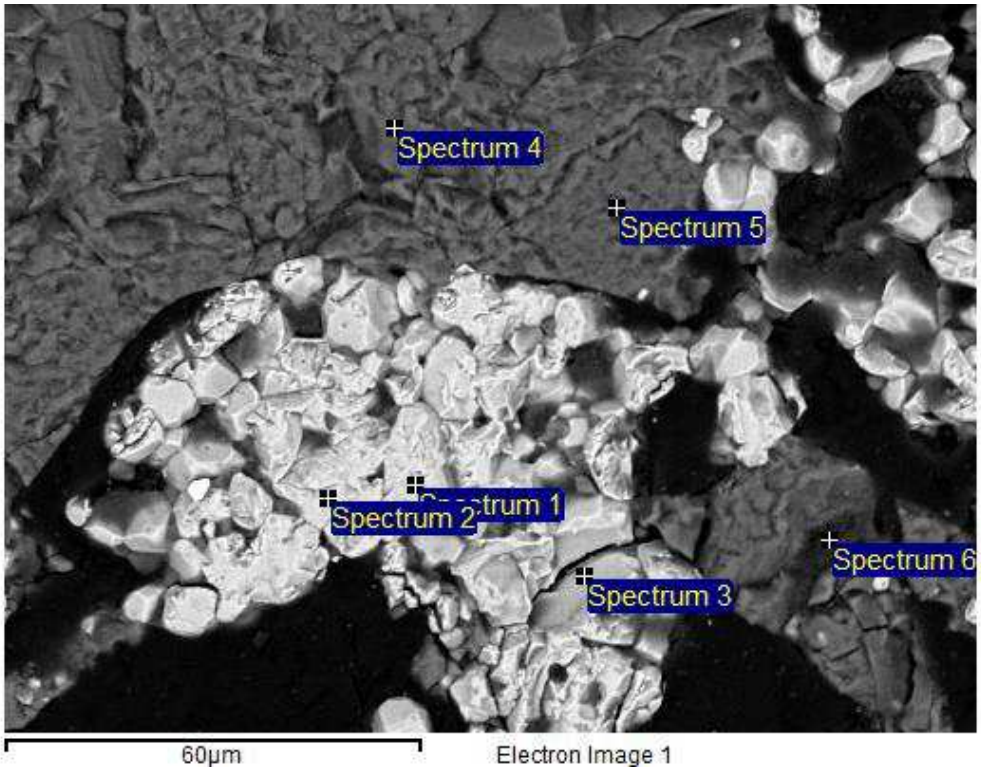

Spectrum	In stats.	O	Si	Fe	Total
Spectrum 1	Yes	33.08		66.92	100.00
Spectrum 2	Yes	36.01		63.99	100.00
Spectrum 3	Yes	30.75	0.55	68.70	100.00
Spectrum 4	Yes	55.66	43.85	0.48	100.00
Spectrum 5	Yes	52.53	46.80	0.67	100.00
Spectrum 6	Yes	40.70	57.58	1.72	100.00
Max.		55.66	57.58	68.70	
Min.		30.75	0.55	0.48	

All results in weight%

EDS Analysis Result, 10 seconds of matte-slag contacting in air atmosphere

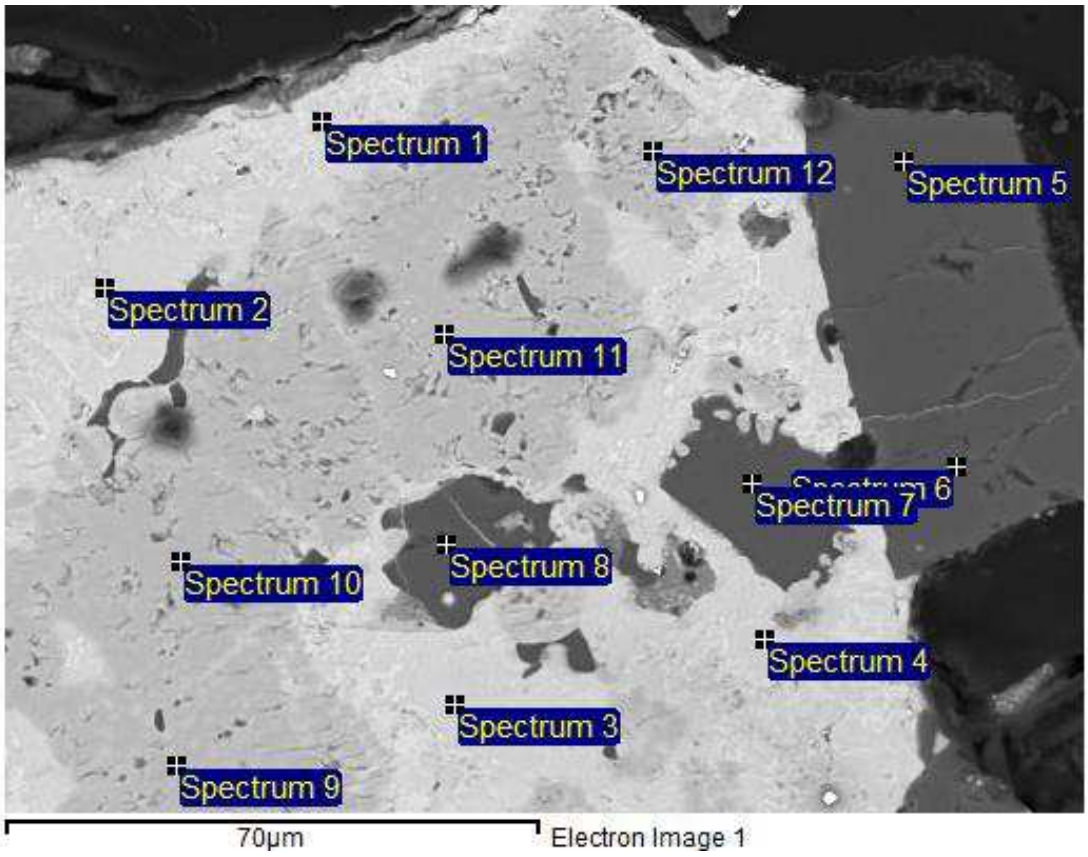

Spectrum	In stats.	O	Si	S	Fe	Cu	Total
Spectrum 1	Yes	3.00		32.16	56.34	8.50	100.00
Spectrum 2	Yes	4.05		27.44	40.03	28.49	100.00
Spectrum 3	Yes	2.79		29.96	40.51	26.73	100.00
Spectrum 4	Yes	3.90		28.41	42.20	25.49	100.00
Spectrum 5	Yes	53.95	45.70		0.36		100.00
Spectrum 6	Yes	53.20	46.39		0.41		100.00
Spectrum 7	Yes	53.52	45.69		0.79		100.00
Spectrum 8	Yes	53.70	45.16		1.14		100.00
Spectrum 9	Yes	23.61	0.19	6.85	62.15	7.20	100.00
Spectrum 10	Yes	16.72		5.38	68.96	8.94	100.00
Spectrum 11	Yes	27.55		1.93	68.91	1.60	100.00

Spectrum 12	Yes	22.42	0.25	4.18	69.06	4.09	100.00
Max.		53.95	46.39	32.16	69.06	28.49	
Min.		2.79	0.19	1.93	0.36	1.60	

All results in weight%

EDS Analysis Result, 20 seconds of matte-slag contacting in air atmosphere

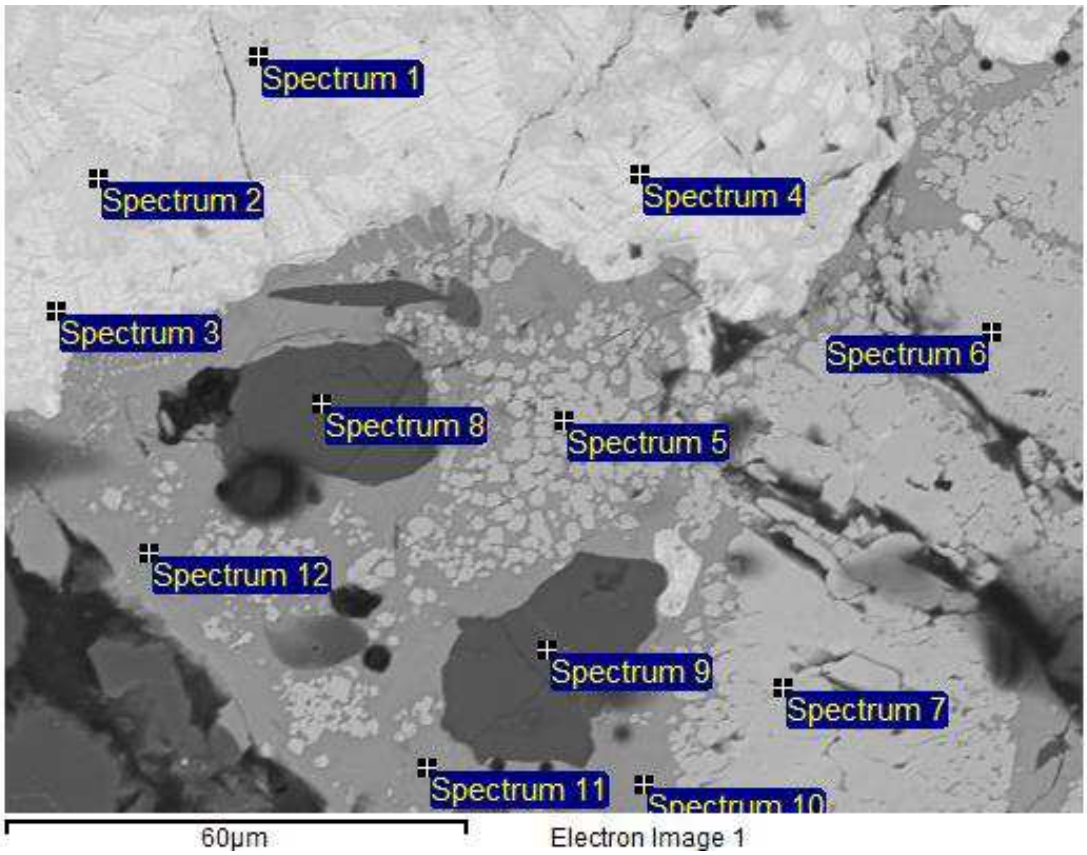

All results in weight%

Spectrum	In stats. S	O K	Na Ca	Mg Fe	Al Cu	Si Total
Spectrum 1	Yes 28.05	4.23		43.11	24.36	0.24 100.00
Spectrum 2	Yes 27.93	4.11		43.49	24.47	100.00
Spectrum 3	Yes 24.81	3.76		27.18	44.25	100.00
Spectrum 4	Yes 25.93	4.05		35.83	34.19	100.00
Spectrum 5	Yes 2.92	28.71 0.33	 0.86	0.32 51.62	0.99	14.26 100.00

Spectrum 6	Yes	32.30	0.38		1.09	14.56
	1.06	0.63	0.41	49.57		100.00
Spectrum 7	Yes	28.52		0.28	0.87	12.92
	3.66	0.24	0.70	50.66	2.15	100.00
Spectrum 8	Yes	34.70	0.37	0.28	1.24	13.84
	1.45	0.61	0.96	46.56		100.00
Spectrum 9	Yes	52.59				46.74
				0.68		100.00
Spectrum 10	Yes	53.40				46.11
				0.50		100.00
Spectrum 11	Yes	26.77				0.79
				72.44		100.00
Spectrum 12	Yes	25.96				
				74.04		100.00
Spectrum 13	Yes	28.69				0.92
				70.39		100.00
Spectrum 14	Yes	1.86				0.72
	0.11		0.43	94.76	2.11	100.00
Max.		53.40	0.38	0.32	1.24	46.74
	28.05	0.63	0.96	94.76	44.25	
Min.		1.86	0.37	0.28	0.87	0.24
	0.11	0.24	0.41	0.50	2.11	

EDS Analysis Result, 30 seconds of matte-slag contacting in air atmosphere

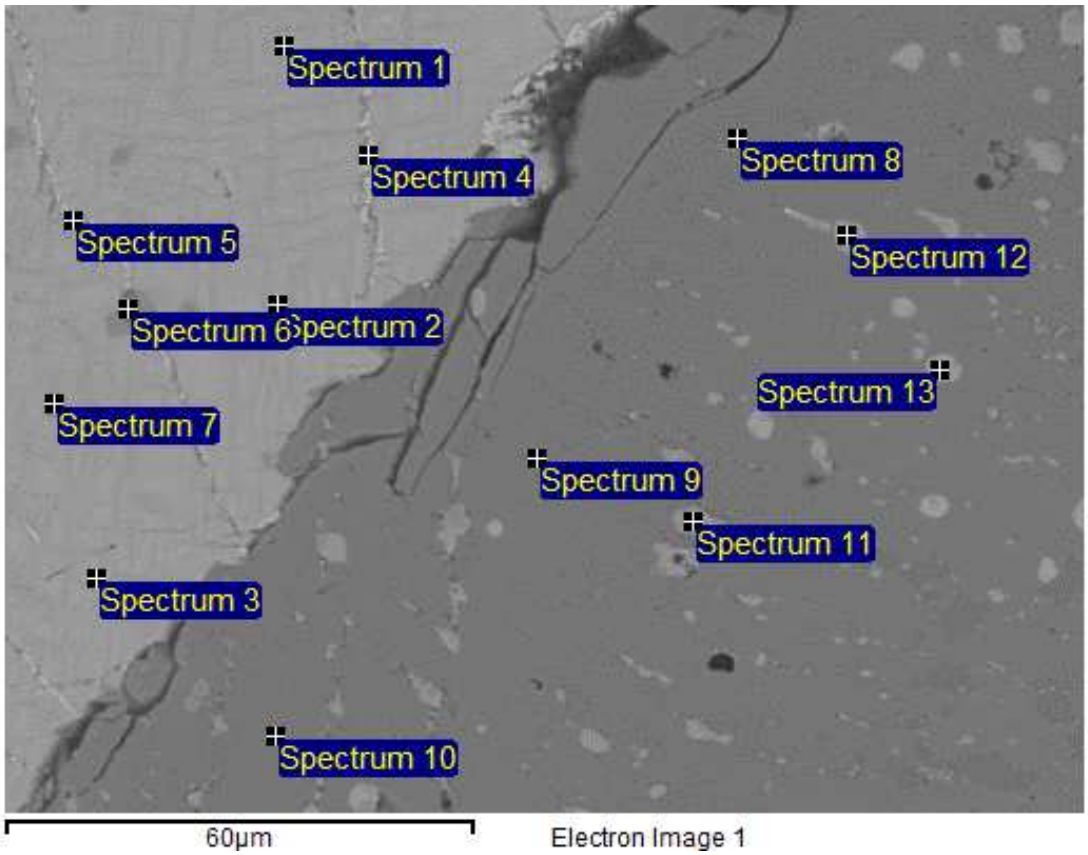

Processing option : All elements analysed (Normalised)

All results in weight%

Spectrum	In stats.	O	Mg	Al	Si	S
	K	Ca	Fe	Cu	Total	
Spectrum 1	Yes	1.88				26.63
			22.62	48.87	100.00	
Spectrum 2	Yes	1.48				25.55
			18.86	54.11	100.00	
Spectrum 3	Yes	1.39				28.18
			29.41	41.02	100.00	
Spectrum 4	Yes	4.16				13.76
			18.25	63.83	100.00	
Spectrum 5	Yes	2.24				14.63
			19.21	63.93	100.00	
Spectrum 6	Yes	12.88			3.91	1.93
		2.59	45.58	33.12	100.00	
Spectrum 7	Yes	26.32			1.57	0.36
			70.34	1.41	100.00	
Spectrum 8	Yes	31.20		0.50	15.30	
	0.38	0.23	52.40		100.00	
Spectrum 9	Yes	31.70		0.35	15.01	
	0.35		52.59		100.00	
Spectrum 10	Yes	32.08	0.24	0.44	15.07	0.33
	0.36	0.23	51.25		100.00	
Spectrum 11	Yes	1.97				30.58
			38.62	28.83	100.00	
Spectrum 12	Yes	2.22			0.28	29.86
			36.07	31.57	100.00	
Spectrum 13	Yes	2.03			0.31	29.50
			37.42	30.73	100.00	
Max.		32.08	0.24	0.50	15.30	30.58
	0.38	2.59	70.34	63.93		
Min.		1.39	0.24	0.35	0.28	0.33
	0.35	0.23	18.25	1.41		

EDS Analysis Result, 60 seconds of matte-slag contacting in air atmosphere

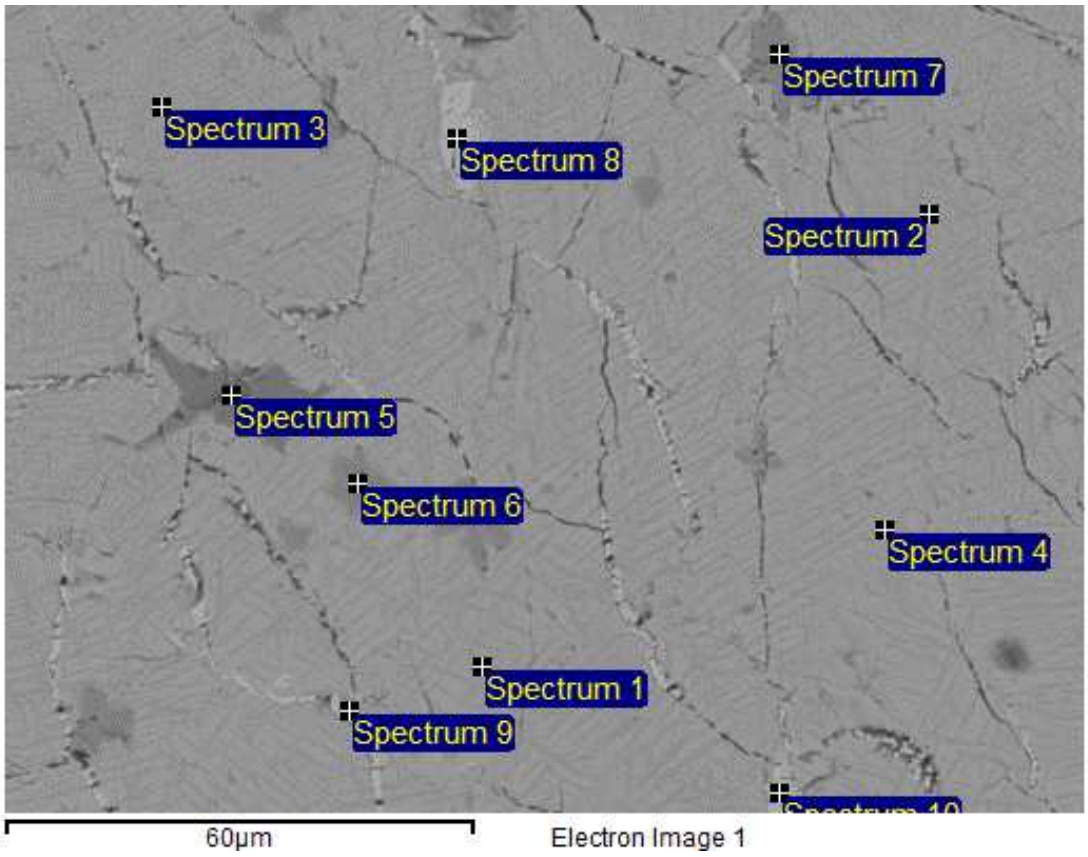

Processing option : All elements analysed (Normalised)

Spectrum	In stats.	O	Si	S	Fe	Cu	Total
Spectrum 1	Yes	2.55	0.26	24.72	26.73	45.75	100.00
Spectrum 2	Yes	1.86		28.70	38.30	31.14	100.00
Spectrum 3	Yes			28.16	24.70	47.14	100.00
Spectrum 4	Yes	1.77	0.30	25.56	19.32	53.06	100.00
Spectrum 5	Yes	17.19	9.63	2.47	66.66	4.05	100.00
Spectrum 6	Yes	25.91	0.70		72.07	1.32	100.00
Spectrum 7	Yes	27.98	0.75		69.92	1.34	100.00
Spectrum 8	Yes	0.78		0.26	2.99	95.97	100.00
Spectrum 9	Yes	2.30	0.26	5.21	10.46	81.77	100.00
Spectrum 10	Yes	1.01		17.97	16.44	64.58	100.00

EDS Analysis Result, 150 seconds of matte-slag contacting in air atmosphere

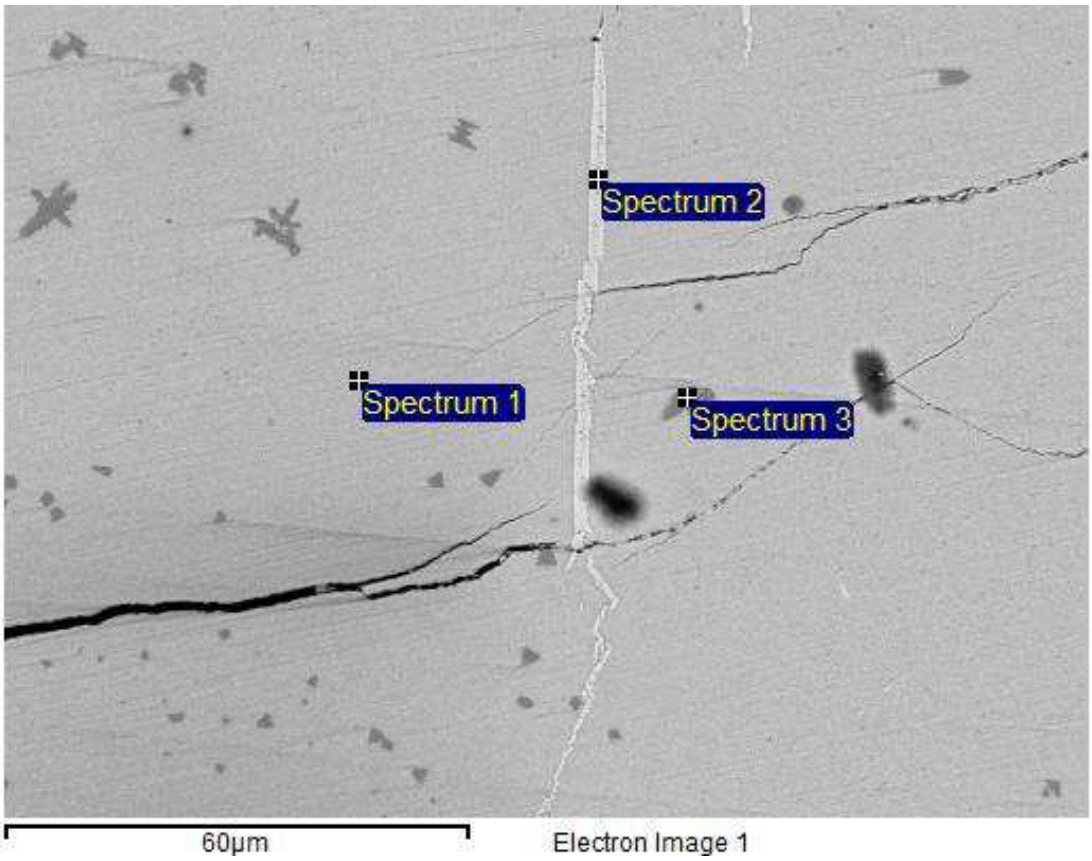

Processing option : All elements analysed

Spectrum	In stats.	O	Si	S	Fe	Cu
Spectrum 1	Yes	3.95		30.63	4.67	60.76
Spectrum 2	Yes	3.23			1.41	95.36
Spectrum 3	Yes	57.35	0.27	0.27	41.28	0.83
Max.		57.35	0.27	30.63	41.28	95.36
Min.		3.23	0.27	0.27	1.41	0.83

EDS Analysis Result, 300 seconds (5 minutes) of matte-slag contacting in air atmosphere

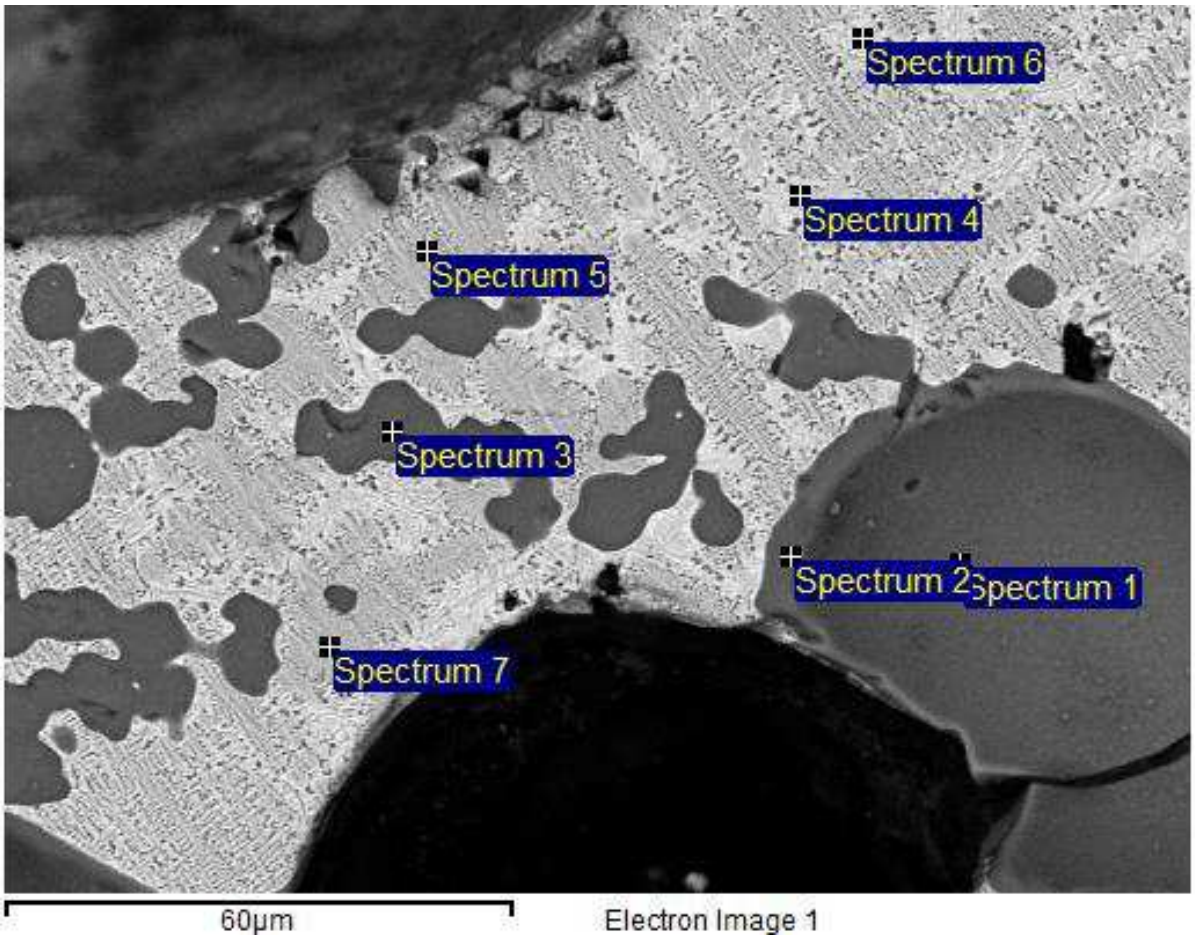

Processing option : All elements analysed (Normalised)

Spectrum	In stats.	O	Al	Si	K	Ca	Fe	Cu	Total
Spectrum 1	Yes	45.37	1.04	41.73	1.37		6.58	3.92	100.00
Spectrum 2	Yes	36.11	1.18	49.87	1.59		8.21	3.04	100.00
Spectrum 3	Yes	48.18	1.15	40.68	1.03		5.44	3.51	100.00
Spectrum 4	Yes	21.95	0.39	9.13		0.71	21.37	46.45	100.00
Spectrum 5	Yes	28.47	0.41	6.95			51.16	13.02	100.00
Spectrum 6	Yes	18.86	0.34	7.80		0.81	15.90	56.29	100.00
Spectrum 7	Yes	29.59	0.43	6.92			49.90	13.16	100.00

EDS Analysis Result, 5 minutes of matte-slag contacting in inert atmosphere

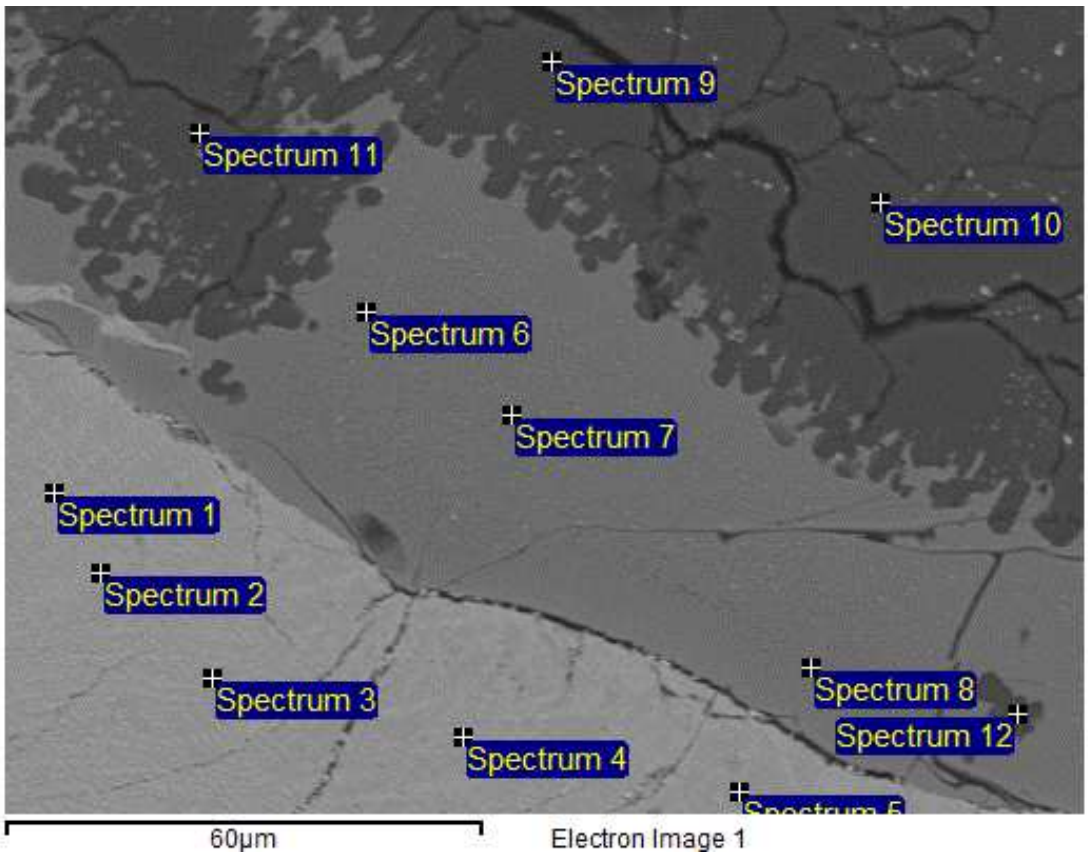

Processing option : All elements analysed (Normalised) All results in weight%

Spectrum	In stats.	O	Mg	Al	Si	S
	K	Ca	Fe	Cu	Total	
Spectrum 1	Yes	2.50				24.99
			46.22	26.30	100.00	
Spectrum 2	Yes	2.34				24.23
			38.12	35.31	100.00	
Spectrum 3	Yes	3.80				26.40
			35.52	34.28	100.00	
Spectrum 4	Yes	5.02				26.51
			47.12	21.35	100.00	
Spectrum 5	Yes	2.29				26.89
			31.26	39.56	100.00	
Spectrum 6	Yes	35.46	0.26	0.71	17.74	1.18
	0.37	0.54	43.73		100.00	

Spectrum 7	Yes	35.34	0.20	0.78	17.63	1.29
	0.34	0.56	43.85		100.00	
Spectrum 8	Yes	35.21	0.24	0.73	17.28	1.63
	0.33	0.55	43.29	0.73	100.00	
Spectrum 9	Yes	53.54			46.04	
			0.43		100.00	
Spectrum 10	Yes	54.10			45.47	
			0.43		100.00	
Spectrum 11	Yes	52.88			46.47	
			0.65		100.00	
Spectrum 12	Yes	54.71			44.46	
			0.83		100.00	
Max.		54.71	0.26	0.78	46.47	26.89
	0.37	0.56	47.12	39.56		
Min.		2.29	0.20	0.71	17.28	1.18
	0.33	0.54	0.43	0.73		

EDS Analysis Result, 10 minutes of matte-slag contacting in inert atmosphere

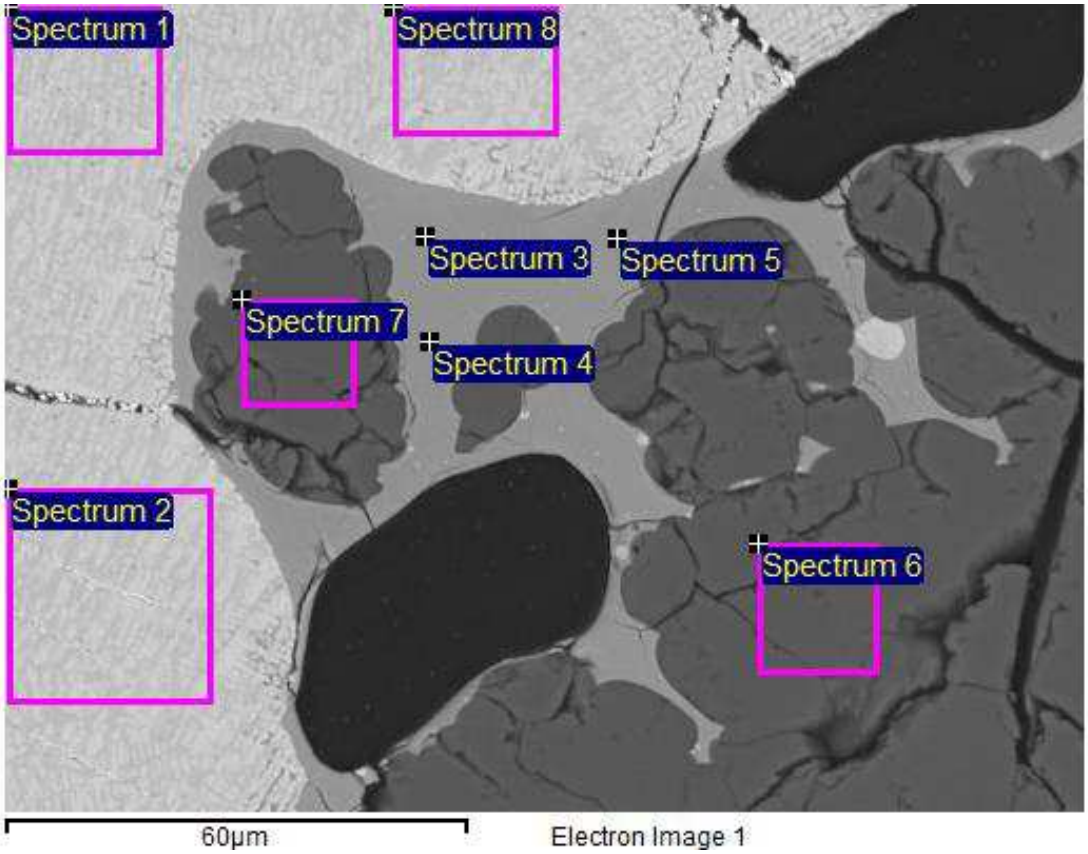

Processing option : All elements analysed (Normalised)All results in weight%

Spectrum	In stats. K	O Ca	Mg Fe	Al Cu	Si Total	S
Spectrum 1	Yes	4.95				24.73
			37.70	32.62	100.00	
Spectrum 2	Yes	4.33				25.17
			36.30	34.19	100.00	
Spectrum 3	Yes	33.11		0.59	15.88	2.25
	0.28		46.99	0.88	100.00	
Spectrum 4	Yes	33.57	0.20	0.58	15.62	2.29
	0.34	0.37	46.23	0.80	100.00	
Spectrum 5	Yes	33.21		0.57	15.22	2.28
	0.30	0.33	48.08		100.00	
Spectrum 6	Yes	54.98			45.02	
					100.00	
Spectrum 7	Yes	55.25			44.25	
			0.50		100.00	
Spectrum 8	Yes	4.00				25.09
			35.59	35.31	100.00	
Max.		55.25	0.20	0.59	45.02	25.17
	0.34	0.37	48.08	35.31		
Min.		4.00	0.20	0.57	15.22	2.25
	0.28	0.33	0.50	0.80		

EDS Analysis Result, 20 minutes of matte-slag contacting in inert atmosphere

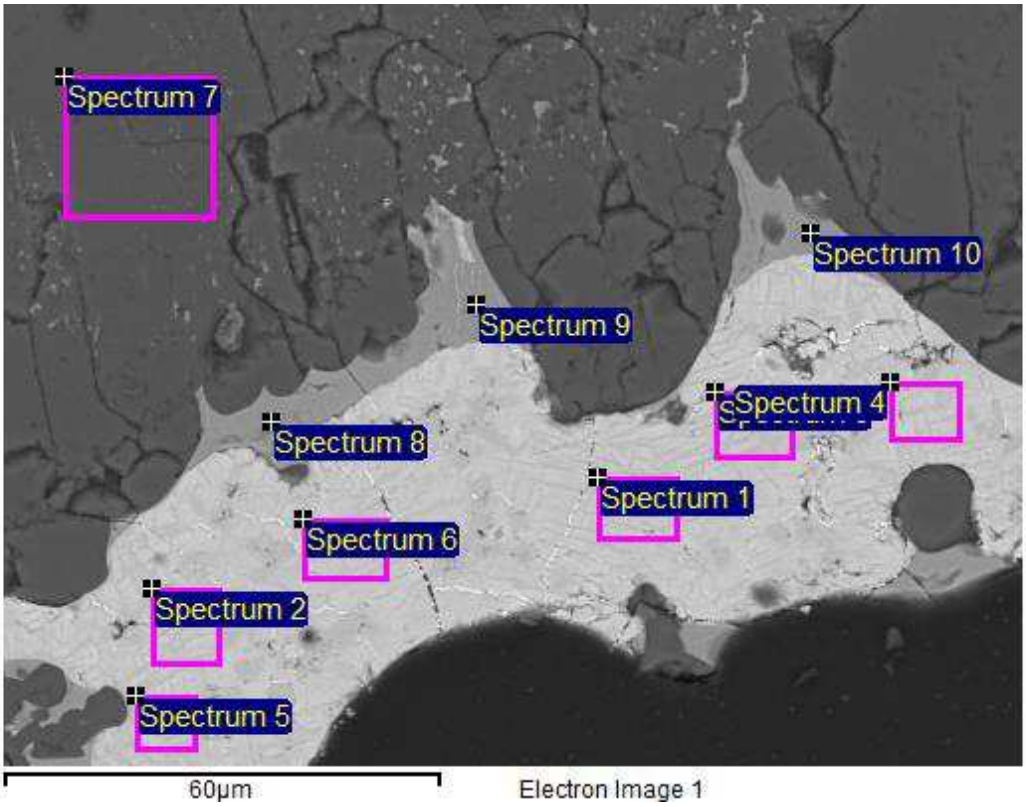

All results in weight%

Spectrum	In stats.	O	Mg	Al	Si	S
	Ca	Fe	Cu	Total		
Spectrum 1	Yes	3.55				25.42
		30.58	40.46	100.00		
Spectrum 2	Yes	3.43				25.94
		30.93	39.70	100.00		
Spectrum 3	Yes	3.52				25.86
		34.68	35.94	100.00		
Spectrum 4	Yes	2.65				26.38
		30.24	40.73	100.00		
Spectrum 5	Yes	3.46				25.92
		31.98	38.63	100.00		
Spectrum 6	Yes	3.46				25.48
		30.65	40.41	100.00		
Spectrum 7	Yes	53.91			45.35	
		0.75		100.00		
Spectrum 8	Yes	32.30		0.38	13.88	2.14
	0.18	50.48	0.64	100.00		
Spectrum 9	Yes	32.22	0.17	0.36	14.25	2.40
	0.22	48.61	1.76	100.00		

Spectrum 10	Yes	32.24		0.46	14.26	2.42
	0.31	49.72	0.58	100.00		
Max.		53.91	0.17	0.46	45.35	26.38
	0.31	50.48	40.73			
Min.		2.65	0.17	0.36	13.88	2.14
	0.18	0.75	0.58			

EDS Analysis Result, 40 minutes of matte-slag contacting in inert atmosphere

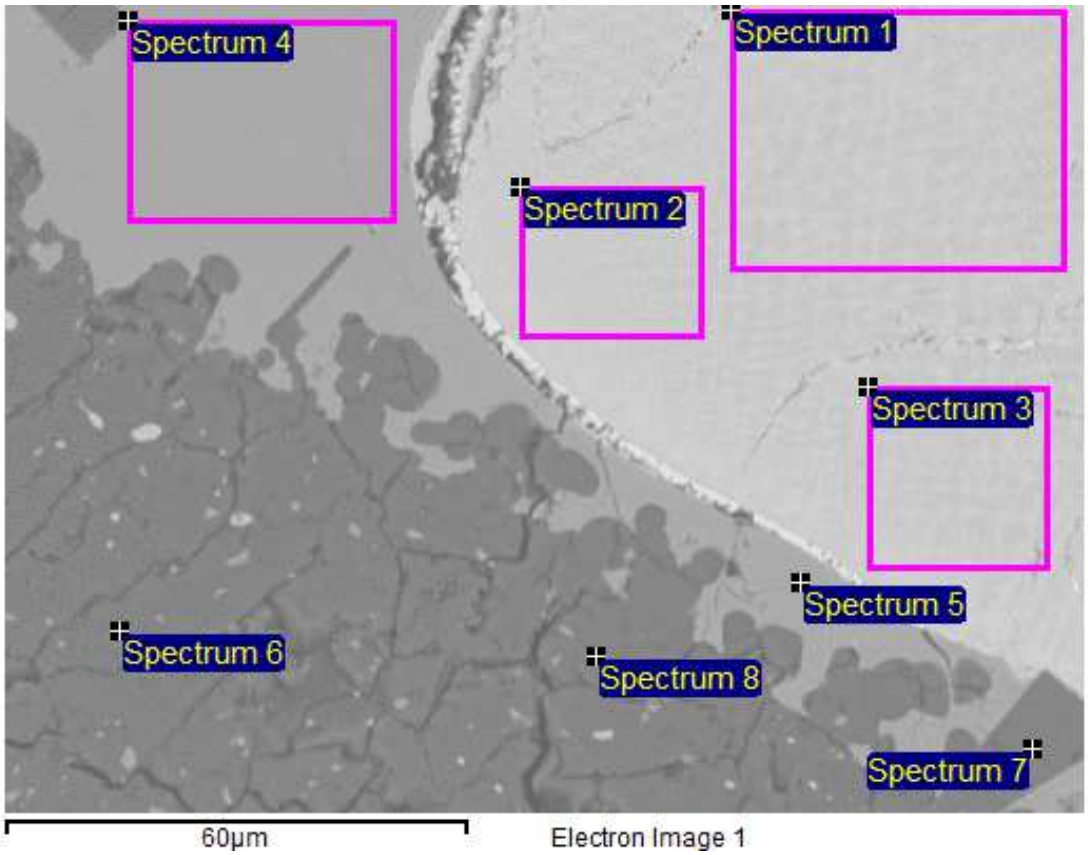

Processing option : All elements analysed (Normalised)

All results in weight%

Spectrum	In stats.	O	Al	Si	S	K
	Ca	Fe	Cu	Total		
Spectrum 1	Yes	3.69			25.10	
		34.74	36.46	100.00		
Spectrum 2	Yes	3.58			25.18	
		32.92	38.31	100.00		
Spectrum 3	Yes	3.68			25.16	
		34.05	37.10	100.00		
Spectrum 4	Yes	33.22	0.52	15.95	2.24	0.24
	0.35	46.08	1.40	100.00		
Spectrum 5	Yes	32.58	0.48	15.63	2.27	0.27
	0.31	46.47	1.98	100.00		

Spectrum 6	Yes	53.95 1.07		44.72 100.00	0.26	
Spectrum 7	Yes	54.96 0.69		44.35 100.00		
Spectrum 8	Yes	52.82 2.58	2.25	41.25 100.00	1.10	
Max.	0.35	54.96 46.47	0.52 38.31	44.72	25.18	0.27
Min.	0.31	3.58 0.69	0.48 1.40	15.63	0.26	0.24

EDS Analysis Result, 60 minutes of matte-slag contacting in inert atmosphere

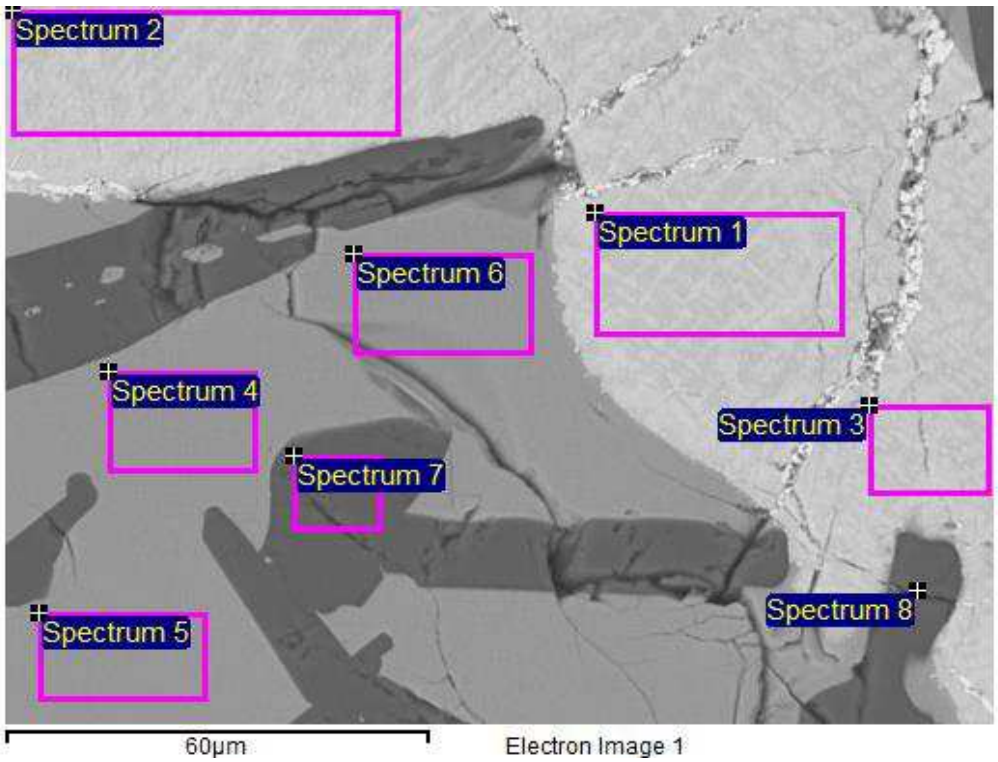

Processing option : All elements analysed (Normalised)All results in weight%

Spectrum	In stats. K	O Ca	Mg Fe	Al Cu	Si Total	S
Spectrum 1	Yes	4.02	36.57	34.25	100.00	25.16
Spectrum 2	Yes	3.82	37.14	34.88	100.00	24.16
Spectrum 3	Yes	3.90	35.49	36.06	100.00	24.55

Spectrum 4	Yes	33.47 0.38	 46.24	0.58 0.95	16.14 100.00	2.23
Spectrum 5	Yes 0.23	33.43 0.35	0.23 45.89	0.56 0.86	16.13 100.00	2.33
Spectrum 6	Yes 0.24	35.75 0.36	 43.75	0.59 1.17	15.94 100.00	2.19
Spectrum 7	Yes	54.18	 0.90		44.92 100.00	
Spectrum 8	Yes	56.44	 0.93		42.63 100.00	
Max.	 0.24	56.44 0.38	0.23 46.24	0.59 36.06	44.92	25.16
Min.	 0.23	3.82 0.35	0.23 0.90	0.56 0.86	15.94	2.19

EDS Analysis Result, Cross Section of PCB scrap

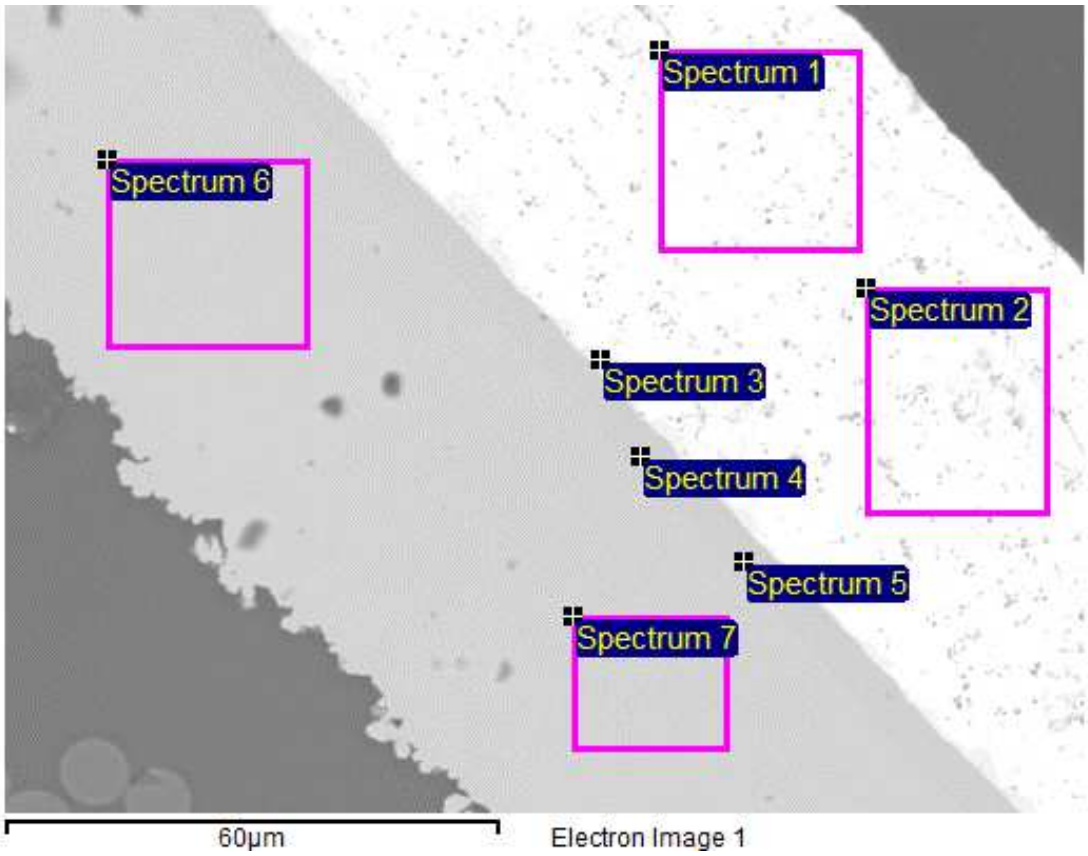

Processing option : All elements analysed (Normalised)All results in weight%

Spectrum	In stats.	O	P	Ni	Cu	Sn
	Pb	Total				
Spectrum 1	Yes	3.86				73.99
	22.15	100.00				
Spectrum 2	Yes	4.11				72.71
	23.18	100.00				
Spectrum 3	Yes			15.20	25.80	59.00
		100.00				
Spectrum 4	Yes		6.44	93.56		
		100.00				
Spectrum 5	Yes	0.40	6.37	93.23		
		100.00				
Spectrum 6	Yes				100.00	
		100.00				
Spectrum 7	Yes	0.42			99.58	
		100.00				
Max.		4.11	6.44	93.56	100.00	73.99
	23.18					
Min.		0.40	6.37	15.20	25.80	59.00
	22.15					

EDS Analysis Result, PCB scrap

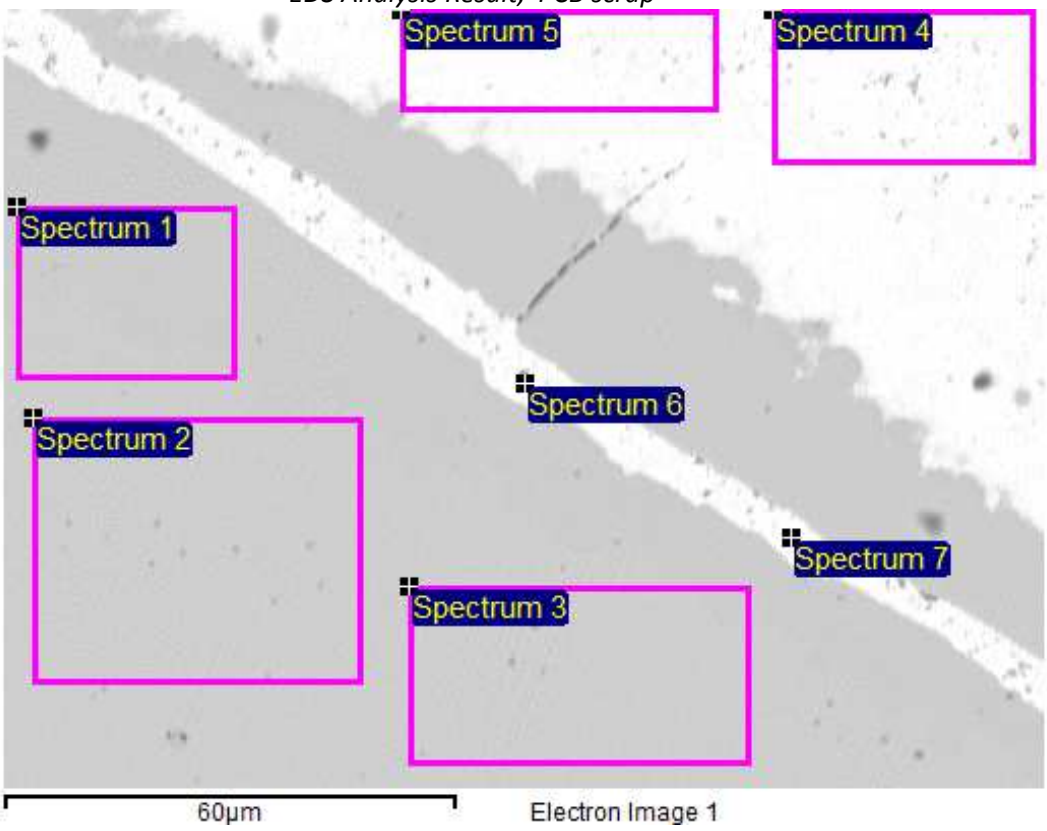

Spectrum	In stats. Sn	O Pb	P Total	Ni	Cu	Ag
Spectrum 1	Yes	0.68	4.83 100.00	55.41	39.08	
Spectrum 2	Yes	0.67	100.00		99.33	
Spectrum 3	Yes	0.67	100.00	1.18	98.15	
Spectrum 4	Yes 66.35	3.65 26.94	100.00	1.32		1.74
Spectrum 5	Yes 65.86	2.87 19.03	100.00	8.50	1.85	1.89
Spectrum 6	Yes 68.82	3.03 15.80	100.00	1.78	7.62	2.94
Spectrum 7	Yes 88.31	3.57 2.92	100.00		5.20	

EDS Analysis Result, molten PCB

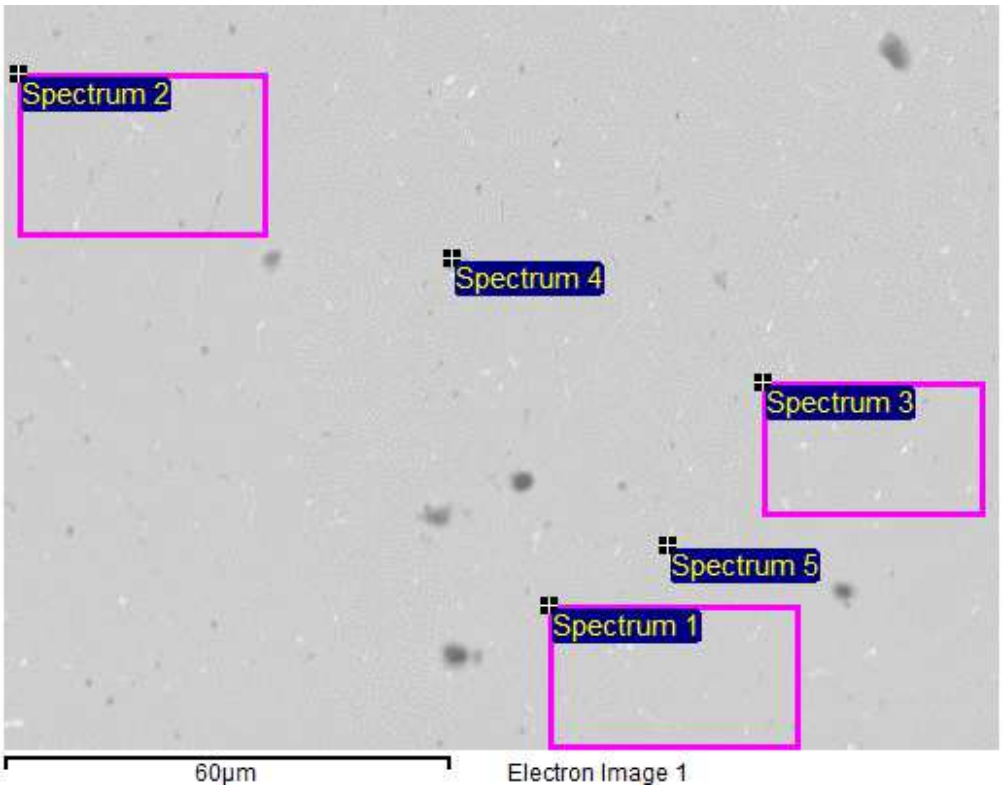

Spectrum	In stats. As Total	O Se	Si Tc	S Ag	Cl Sb	Cu Te
Spectrum 1	Yes	0.77 100.00				99.23
Spectrum 2	Yes	0.87 100.00				99.13
Spectrum 3	Yes	0.68 100.00				99.32
Spectrum 4	Yes 3.43 100.00	4.95 4.70	0.72 11.59	5.68 15.91	0.72 1.99	48.74 1.57
Spectrum 5	Yes	0.46 100.00				99.54
Max.	 3.43	4.95 4.70	0.72 11.59	5.68 15.91	0.72 1.99	99.54 1.57
Min.	 3.43	0.46 4.70	0.72 11.59	5.68 15.91	0.72 1.99	48.74 1.57

EDS Analysis Result, molten PCB

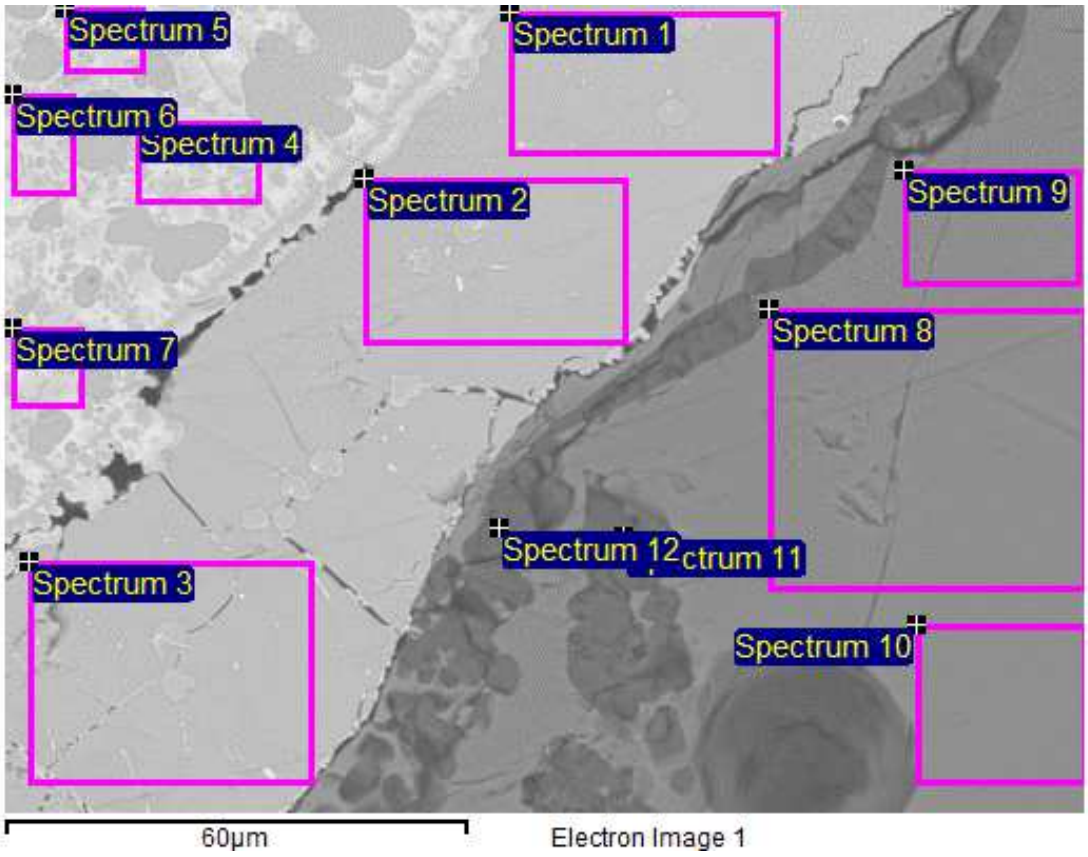

Processing option : All elements analysed (Normalised)All results in weight%

Spectrum	In stats.	O	Al	Si	S
	K	Ca	Ti	Fe	Ni
	Cu	Sn	Sb	Ba	Total
Spectrum 1	Yes	1.88			22.37
				17.64	0.79
	57.32				100.00
Spectrum 2	Yes	1.71			22.25
				17.44	0.63
	57.97				100.00
Spectrum 3	Yes	2.01			23.35
				18.22	
	56.42				100.00
Spectrum 4	Yes	0.95			0.90
				27.06	4.61
	55.94	8.32	2.22		100.00
Spectrum 5	Yes	0.91			7.09
				25.13	3.62
	57.91	5.34			100.00
Spectrum 6	Yes	0.84			1.64
				23.62	3.90
	60.56	7.86	1.57		100.00

Spectrum 7	Yes	0.84			1.34
				27.31	4.21
	55.32	8.92	2.08		100.00
Spectrum	In stats.	O	Al	Si	S
	K	Ca	Ti	Fe	Ni
	Cu	Sn	Sb	Ba	Total
Spectrum 8	Yes	40.26	2.47	21.61	0.36
	0.23	5.35	0.25	29.47	
					100.00
Spectrum 9	Yes	40.31	2.56	21.92	0.38
		5.30		29.53	
					100.00
Spectrum 10	Yes	40.26	2.48	21.57	0.39
		5.22		29.30	
	0.77				100.00
Spectrum 11	Yes	46.18		51.52	0.18
				1.50	
			0.62		
					100.00
Spectrum 12	Yes	53.16		46.38	
				0.47	
					100.00
Max.		53.16	2.56	51.52	23.35
	0.23	5.35	0.25	29.53	4.61
	60.56	8.92	2.22	0.77	
Min.		0.84	2.47	21.57	0.18
	0.23	5.22	0.25	0.47	0.63
	0.62	5.34	1.57	0.77	

Appendix A.2. SEM Images

SEM image – concentrate powder

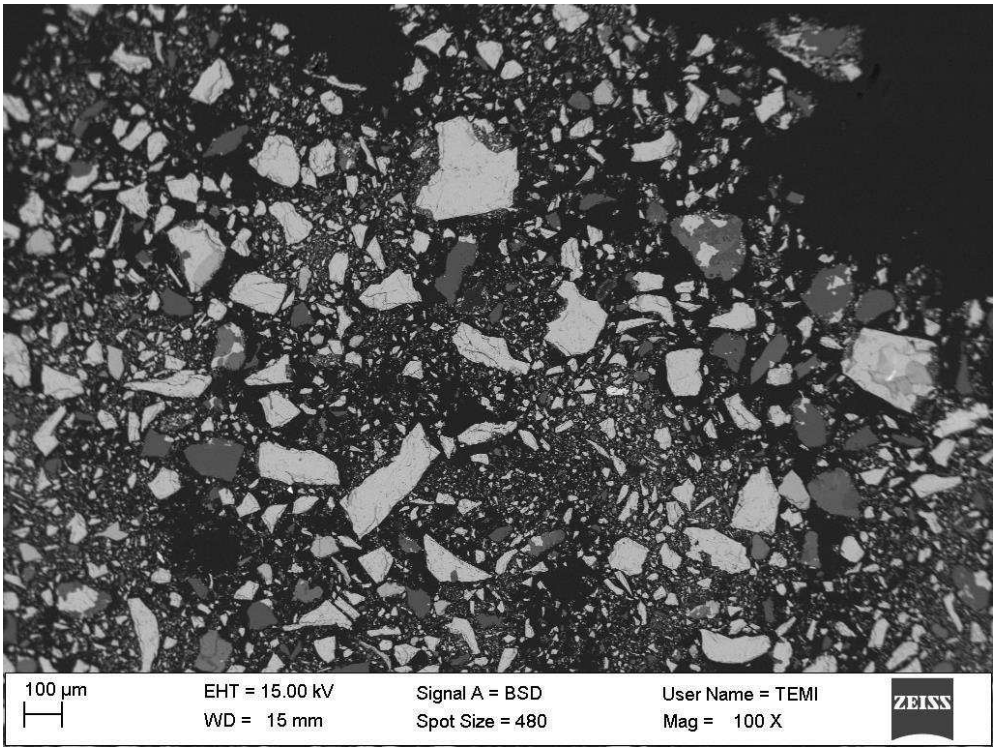

SEM image, 10 seconds of matte-slag contacting in air atmosphere

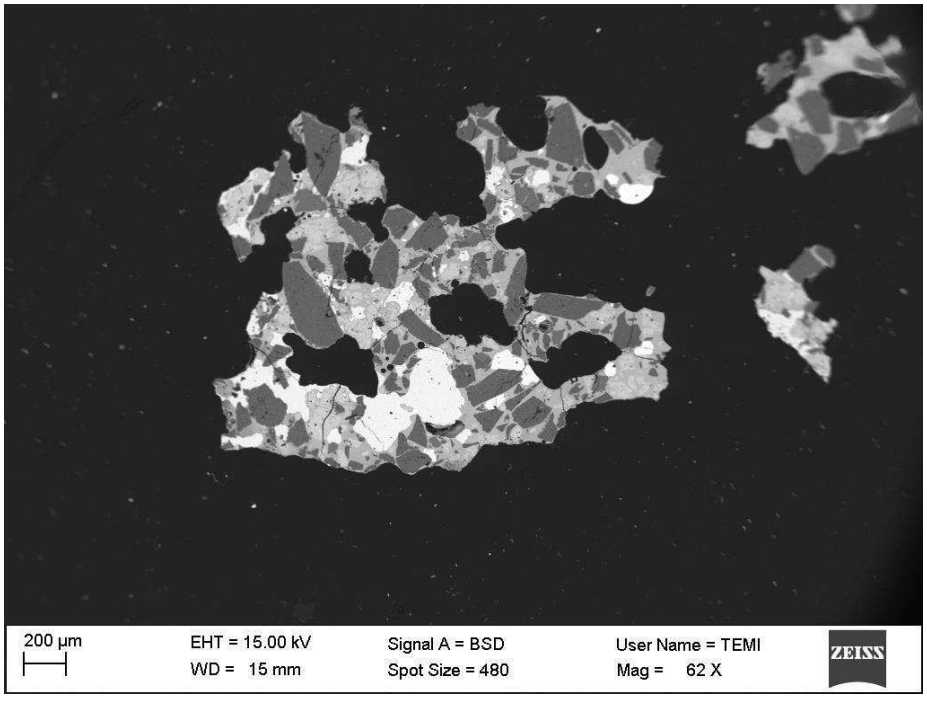

SEM image, 30 seconds of matte-slag contacting in air atmosphere

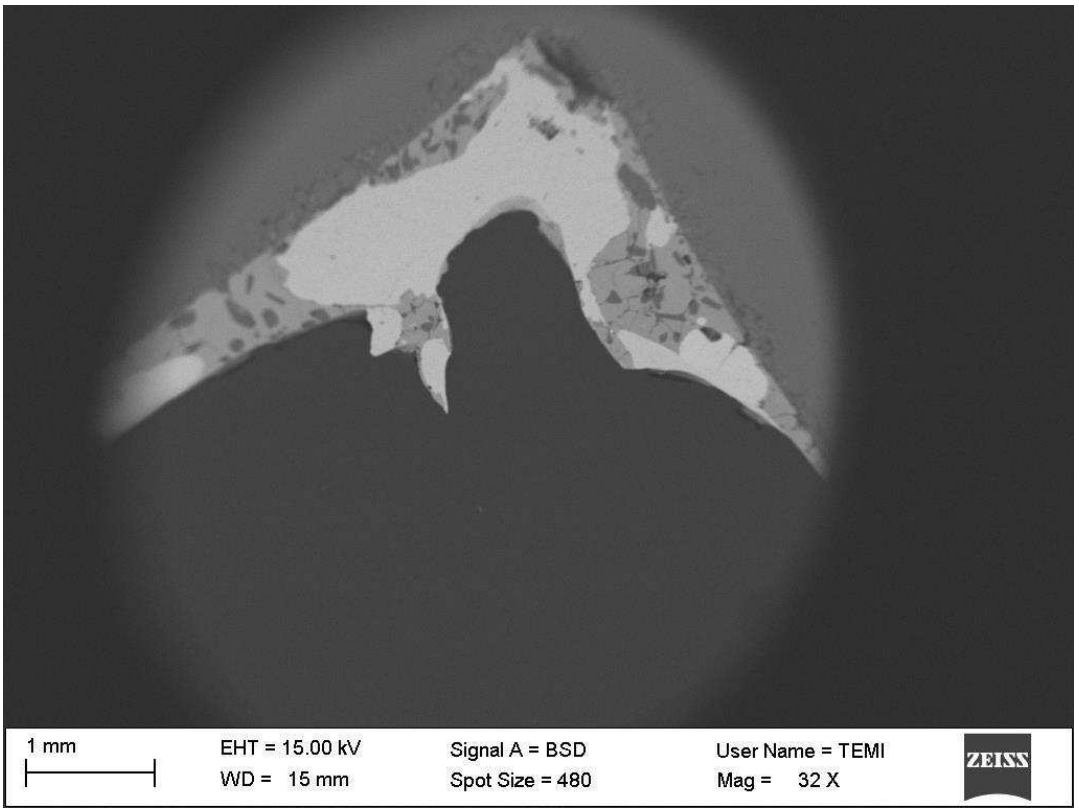

SEM image, 60 seconds of matte-slag contacting in air atmosphere

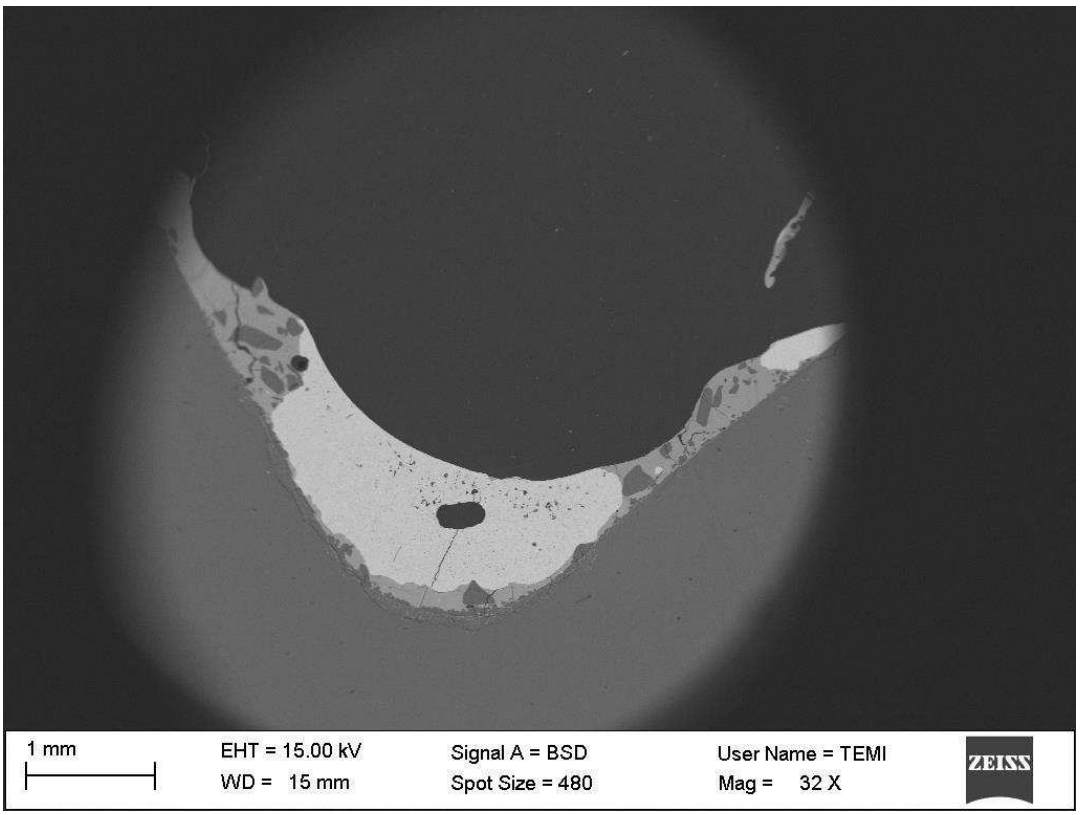

SEM image, 150 seconds of matte-slag contacting in air atmosphere

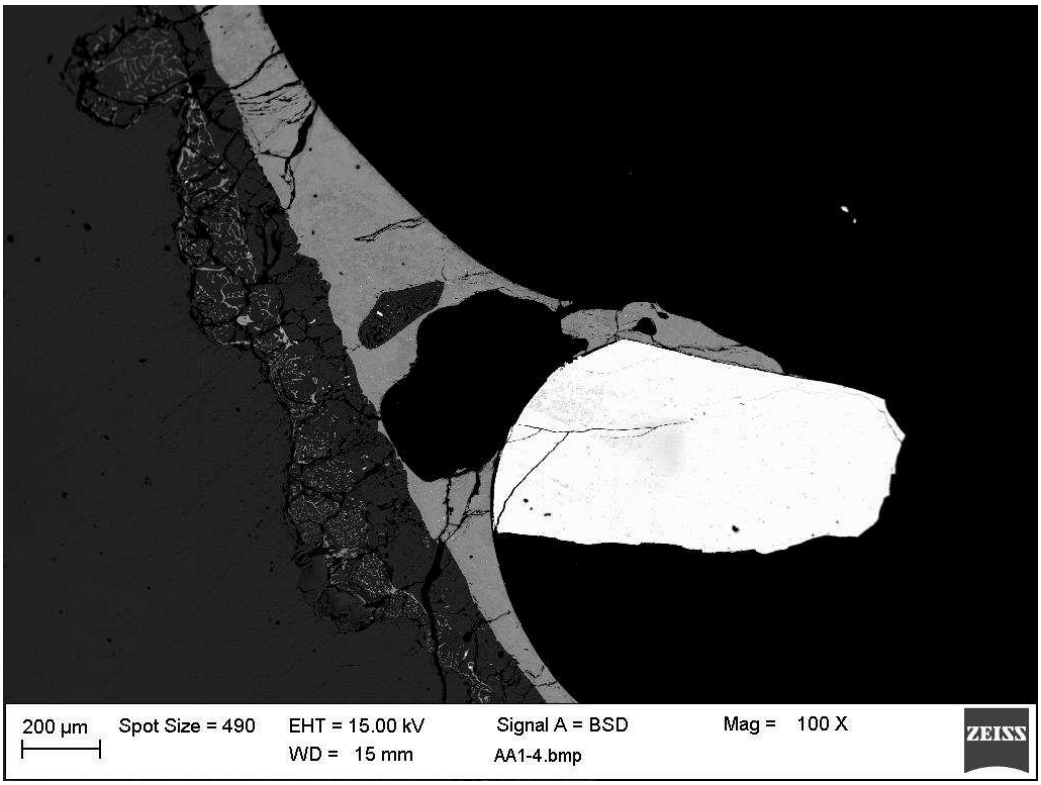

SEM image, 500 seconds of matte-slag contacting in air atmosphere

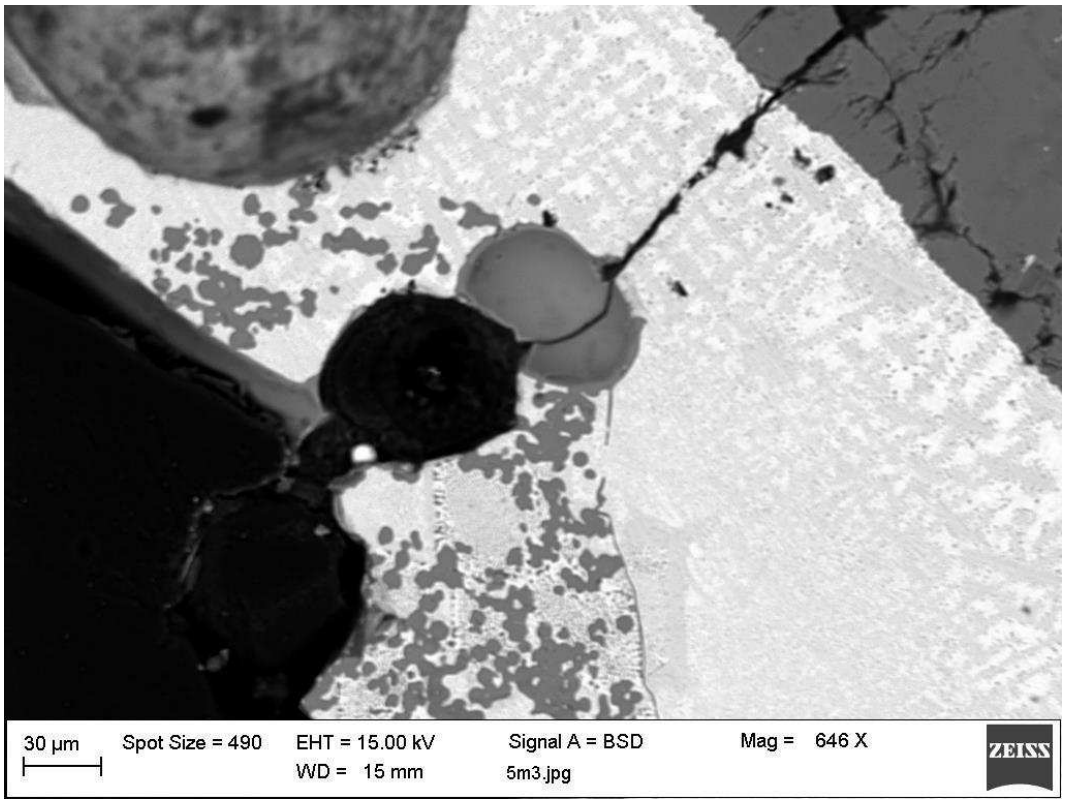

SEM image, 5 minutes of matte-slag contacting in inert atmosphere

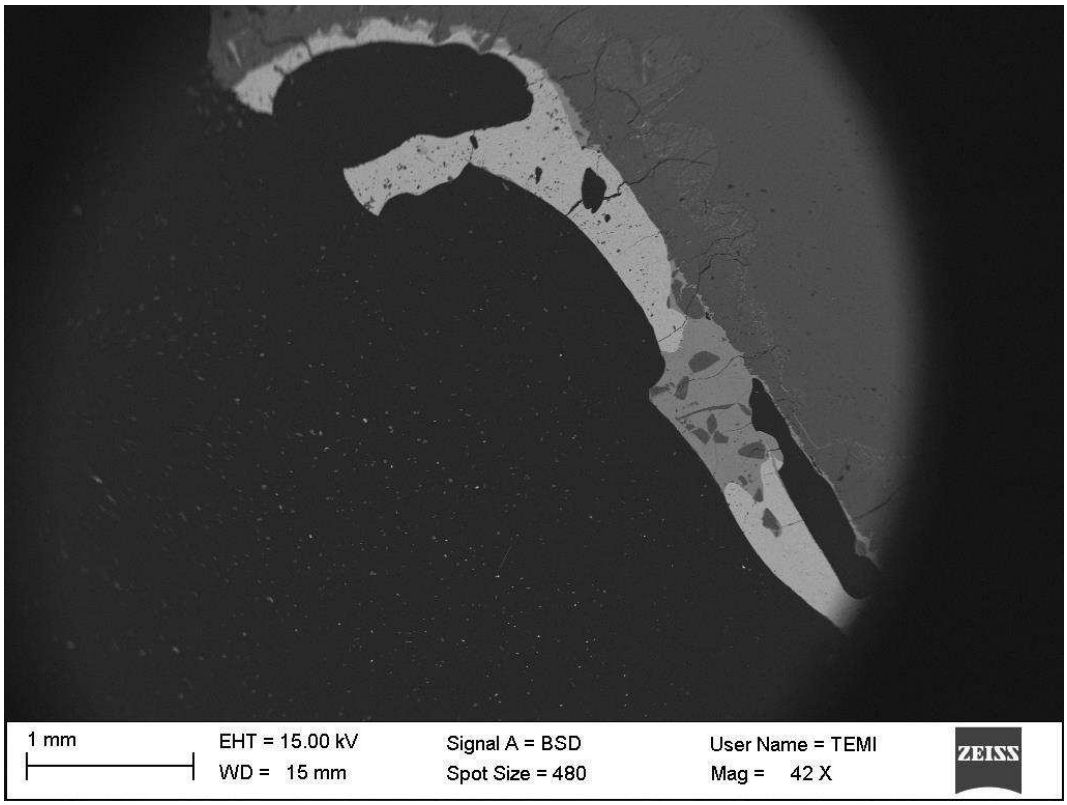

SEM image, 10 minutes of matte-slag contacting in inert atmosphere

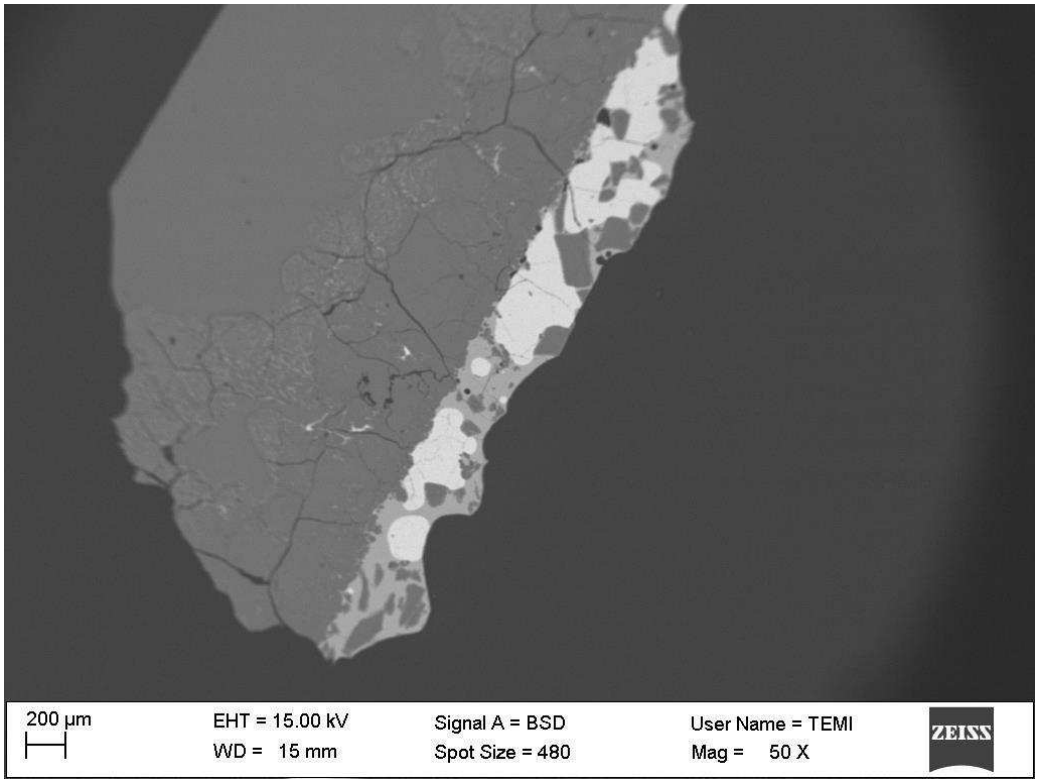

SEM image, 40 minutes of matte-slag contacting in inert atmosphere

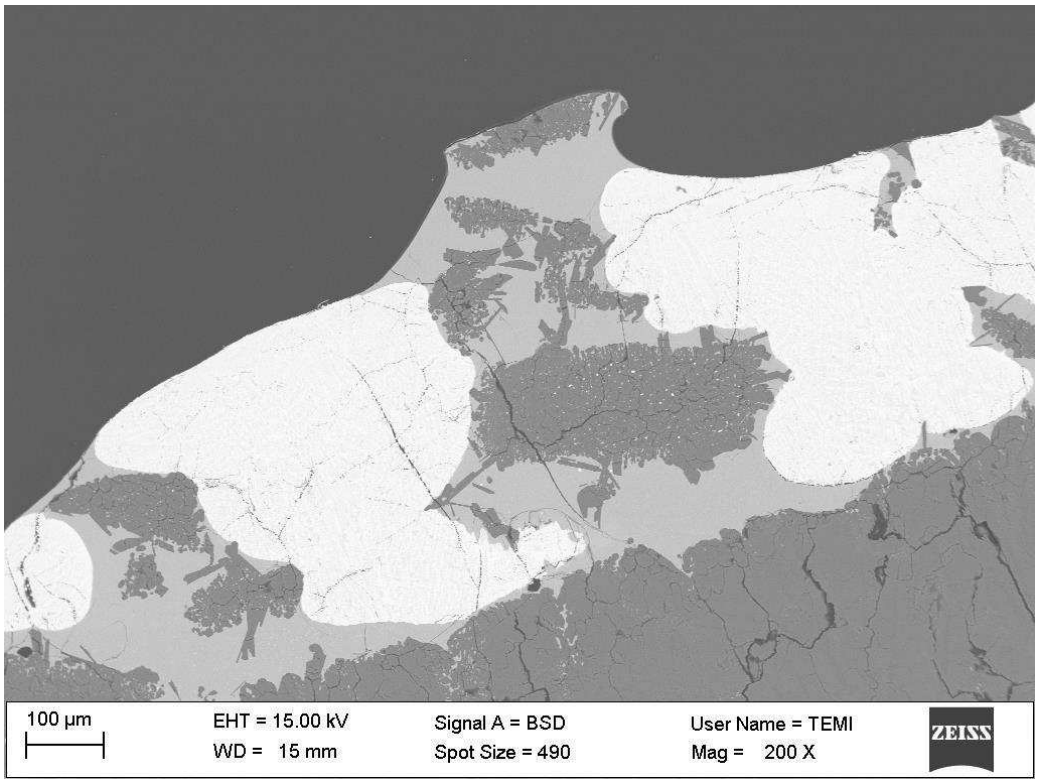

SEM image, 60 minutes of matte-slag contacting in inert atmosphere

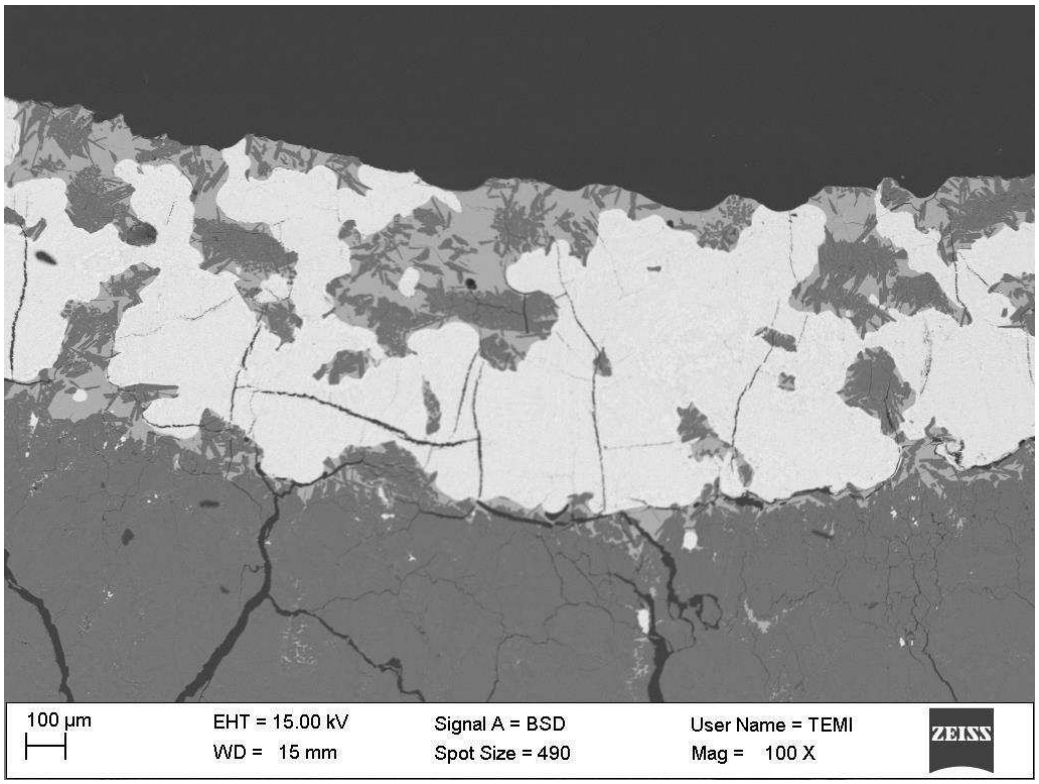

SEM Image, Cross Section of PCB scrap

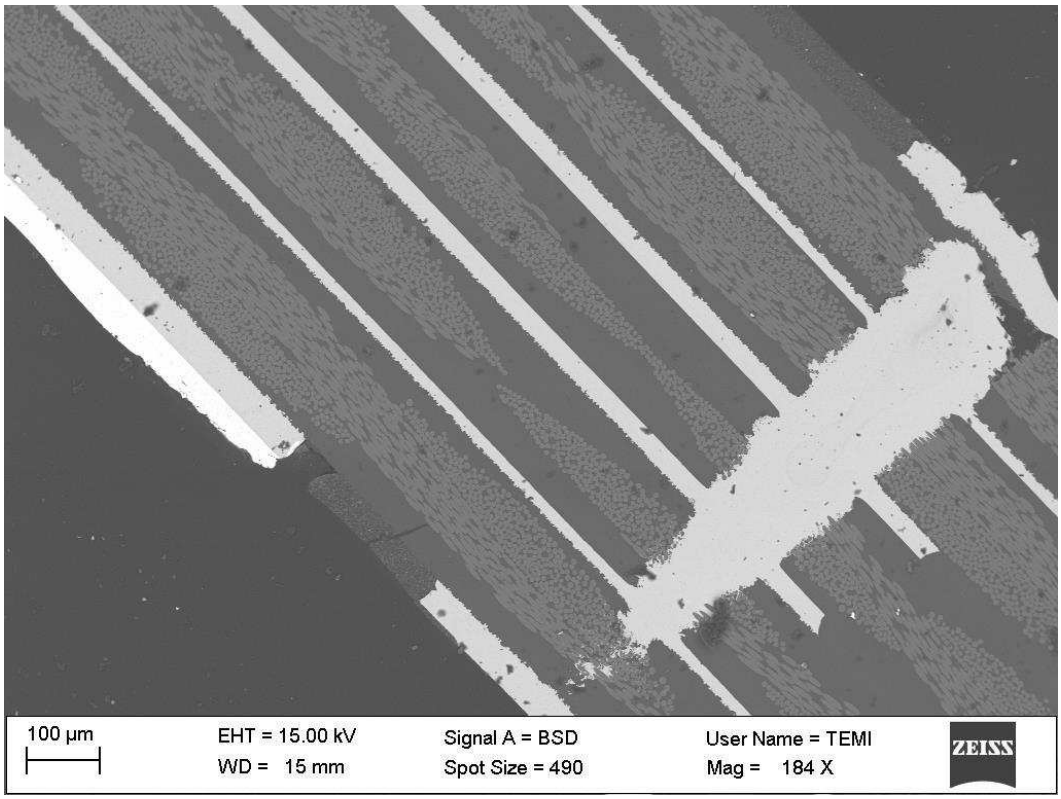

SEM Image, Molten PCB Scrap